Title

THE ANALYSIS OF THE NUCLEAR MAGNETIC RESONANCE SPECTRA OF FOUR-MEMBERED RING COMPOUNDS OF THE TYPE A2B4 USING BOTH COMPUTER AND DOUBLE-IRRADIATION TECHNIQUES

Author

Ferretti, James A.

Publication Date

1965-08-01

UCRL-16349

University of California

Ernest O. Lawrence Radiation Laboratory

THE ANALYSIS OF THE NUCLEAR MAGNETIC RESONANCE SPECTRA OF FOUR-MEMBERED RING COMPOUNDS OF THE TYPE A_2B_4 USING BOTH COMPUTER AND DOUBLE-IRRADIATION TECHNIQUES

Berkeley, California

DISCLAIMER

UCRL-16349

UNIVERSITY OF CALIFORNIA

Lawrence Radiation Laboratory
Berkeley, California

AEC Contract W-7405-eng-48

THE ANALYSIS OF THE NUCLEAR MAGNETIC RESONANCE SPECTRA OF FOUR-MEMBERED RING COMPOUNDS OF THE TYPE A_2B_4 USING BOTH COMPUTER AND DOUBLE-IRRADIATION TECHNIQUES

James A. Ferretti

(Ph.D. Thesis)

August 1965

TABLE OF CONTENTS

THE ANALYSIS OF THE NUCLEAR MAGNETIC RESONANCE SPECTRA OF FOUR-MEMBERED RING COMPOUNDS OF THE TYPE A_2B_4 USING BOTH COMPUTER AND DOUBLE-IRRADIATION TECHNIQUES

James A. Ferretti

Inorganic Materials Research Division of
Lawrence Radiation Laboratory and Department of Chemistry
University of California, Berkeley, California

ABSTRACT

August 1965

The Nuclear Magnetic Resonance spectra of a series of four-membered ring molecules have been analyzed using both computer and double-irradiation techniques. The molecules, trimethylene oxide, trimethylene imine, trimethylene sulfide, and 1,1-dimethylcyclocutanedicarboxylate, were analyzed as A_2B_4 systems. The chemical shifts, and vicinal and long range coupling constants were found to be quite normal. Current theories concerning substituent effects on geminal proton coupling constants are presented and the substitutive trends observed in the above series are interpreted in the light of these theories. The effects of bond hybridization on substituent effects was also found to be interpretable in terms of the theory.

Nuclear Magnetic Double Resonance spectra were observed both by sweeping the observing rf field ν_1 and also by sweeping the perturbing field ν_2. When ν_1 is set on a non-degenerate transition frequency and ν_2 subsequently swept to perturb the other lines in the spectrum, intensity changes are observed when any transition which is perturbed by ν_2 has an energy level in common with the line being observed by ν_1. An intensity

increase is observed when the energy levels are ordered in a progressive manner and a decrease in intensity is observed when the energy levels are ordered in a regressive manner. This procedure has been used to establish the ordering of the energy levels of the ABC system of protons in 2-chlorothiophene.

Pulse experiments were carried out in order to gain a fuller understanding of the phenomena observed in the above double-resonance experiments. These experiments indicate that the observed phenomena are caused by population inversion due to adiabatic rapid passage.

A detailed description of the field-frequency spectrometer constructed and used in the above work is presented.

I. INTRODUCTION

Small-ring molecules are currently the subject of considerable interest in a number of fields of spectroscopy, nuclear magnetic resonance (NMR) being no exception. A great deal of this interest stems from the inherent simplicity of these systems which in many cases allows a number of properties of these molecules to be interpreted in terms of their molecular structure and geometry.

The NMR spectra of three-membered ring compounds have been studied in considerable detail by a number of investigators.[1-4] The molecular structures of some of these compounds have been accurately determined by microwave spectroscopy[5] thereby making it possible to experimentally determine which structural factors, if any, contribute to the coupling constants. Hutton and Schaefer[6] have shown in three-membered rings that the geminal proton nuclear spin-spin coupling constants are dependent in approximately a linear fashion on the electronegativities of the substituents in positions α to the CH_2 group. Mortimer[7] has measured the geminal proton coupling constants in ethylene oxide, ethylene imine, and ethylene sulfide to be 5.5 cps, 2.0 cps, and $< \pm 0.4$ cps, respectively; the signs of the coupling constants being measured on a relative basis only.

Knowledge of the structural features of these small-ring compounds makes it possible to compare experimental data with theoretical calculations of the coupling constants. An early study by Gutowsky, et al.[8] using a valence bond method predicted a positive value for the coupling constant in methane which should decrease (become more negative) as the H-C-H bond angle opened out. Subsequent experimental data such as that cited above have established the opposite trend for hydrocarbons

and, in molecules with substituents, there appears to be very little correlation with the H-C-H bond angle.

As has been noted above, the NMR spectra of three-membered ring molecules have been studied in considerable detail. However, the literature has been notably lacking in similar studies on four-membered ring compounds, only a few highly substituted systems having been reported.[9-11] Probably the chief reason for this lack of NMR spectral data on four-membered ring molecules is the complexity of the spectra involved. These highly complex non-first order spectra did not lend themselves to simple analysis by the usual methods.[12,13]

This study of four-membered ring systems was undertaken in order to determine if trends similar to those observed in three-membered ring compounds exist, and also to what extent analogies can be drawn between the two systems. As in the three-membered rings the geometries of the four-membered ring molecules studied in this dissertation are well defined since their molecular structures have been determined exactly in a few cases.[14-16] Analogous trends were observed although the effect of substituents was found to be considerably less pronounced in the four-membered ring series.

Pople and Bothner-By[17] have recently presented a paper in which they demonstrated that a molecular orbital treatment of the electrons in a methylene group leads to a theory of the effect of substitution on the geminal proton-proton coupling constants. The theory still does not lead to a satisfactory calculation of the absolute magnitudes of the coupling constants. However, it does provide an interpretation of the substitutive trends previously noted in the literature. Furthermore, the theory leads to a number of predictions about algebraic increases

and decreases in the geminal coupling constants and does properly predict the trends noted above for both the three-membered ring and four-membered ring series. Finally, it will be shown that the theory can be extended to predict the effects of different types of hybridization on the substituent effects of the electronegative groups α to the H-C-H group. Experimental data will be discussed in the light of the rules suggested by this theory.

The determination of the chemical shielding parameters and the nuclear spin-spin coupling constants in the A_2B_4 four-membered ring molecules trimethylene oxide, trimethylene imine, trimethylene sulfide, and 1,1-dimethylcyclobutanedicarboxylate was accomplished both by means of a high-speed computer and also through the use of nuclear magnetic double resonance, where the NMR spectra are observed in the presence of a second radio-frequency field.

The computer program used in these analyses is the iterative program developed by Swalen and Reilly.[19] In this scheme a theoretical spectrum is first calculated from a trial set of parameters. These parameters are then readjusted in order to reproduce the experimental spectrum as well as possible from the experimental data which are in the form of transition frequencies and intensities. The chief steps in this analysis are first to correctly assign the observed transition frequencies to those calculated from the trial parameters and, secondly, to convert these frequencies into a set of correctly ordered energy levels. This procedure is strictly a trial and error method and in the four-membered ring molecules of interest did not prove to be feasable. The lack of feasability of this method resulted from the fact that it was not possible to correctly assign a sufficient number of transition frequencies starting

from an arbitrary set of trial parameters.

Improvement of the analysis procedure was possible using the additional experimental data obtained from double-resonance spectra. A simple technique for obtaining proton double resonance spectra has recently been developed[20] by which the magnetic resonance of one nucleus or group of nuclei (Group A) may be observed by means of a rf field H_1 at frequency ν_1, while a second nucleus or group of nuclei (Group B) is irradiated with a field H_2 at frequency ν_2. The frequencies ν_1 and ν_2 are related to the field strength H_o by the Larmor resonance conditions for Groups A and B, and in order to scan through the spectrum at least one of these three quantities must be varied. The following cases can be distinguished:

(a) Field sweep: $(\nu_1-\nu_2)$ constant, H_o variable. Either the magnetic field H_o is swept or the two rf fields are swept simultaneously to observe the spectrum.

(b) ν_1 frequency sweep: ν_2 is applied at a fixed position and ν_1 is swept to observe the spectrum.

(c) ν_2 frequency sweep: ν_1 is applied at a fixed position and ν_2 is swept through the various lines in the spectrum.

In the past case (b) has been the most common method used to observe double resonance spectra. In this dissertation it will be shown that case (c) also provides a very good method by which spectra can be observed. Experimental data will be presented and discussed in terms of this method and will be compared with the methods of case (a) and case (b).

II. THEORY

A. Electron Coupled Nuclear Spin-Spin Interactions

1. The Hamiltonian and General Formulas

A complete general theory of the interactions of nuclear spins in a molecule was first given by Ramsey[29] who showed that they arise by three distinct mechanisms. In this section a brief outline of Ramsey's derivation of the general equations for the spin and orbital contributions to the nuclear spin coupling is presented along with some changes in notation and formulation.

The Hamiltonian for a molecular system in a magnetic field is given by

$$\mathcal{H} = \mathcal{H}_1 + \mathcal{H}_2 + \mathcal{H}_3 + \mathcal{H}_4 \tag{1}$$

where

$$\mathcal{H}_1 = \sum_k [\tfrac{1}{2} m_k][\frac{\hbar}{i} \nabla_k + \frac{e}{c} \left\{ \sum_N \hbar \gamma_N \vec{I}_N \times \vec{r}_{kN} / r_{kN}^3 + \tfrac{1}{2} H \times r_k \right\}]^2$$

$$+ V + \mathcal{H}_{LL} + \mathcal{H}_{LS} + \mathcal{H}_{SS} + \mathcal{H}_{SH} \tag{2}$$

$$\mathcal{H}_2 = \gamma_e \hbar^2 \sum_{kN} \gamma_N \left\{ 3\left(\vec{S}_k \cdot \vec{r}_{kN}\right)\left(\vec{I}_N \cdot \vec{r}_{kN}\right) r_{kN}^{-5} - \vec{S}_k \cdot \vec{I}_N \, r_{kN}^{-3} \right\} \tag{3}$$

$$H_3 = \left(\frac{8\pi\gamma_e\hbar^2}{3}\right) \sum_{kN} \gamma_N \, \delta\left(\vec{r}_{kN}\right) \vec{S}_k \cdot \vec{I}_N \tag{4}$$

$$\mathcal{H}_4 = -\hbar_2 \sum_{NN'} \gamma_N \gamma_{N'} \left\{ 3\left(\vec{I}_N \cdot \vec{r}_{NN'}\right)\left(I_{N'} \cdot \vec{r}_{NN'}\right) r_{NN'}^{-5} - \vec{I}_N \cdot \vec{I}_N \cdot r_{NN'}^{-3} \right\} \tag{5}$$

γ_e is the gyromagnetic ratio of the electron, γ_N is the gyromagnetic ratio of nucleus N and $\vec{I}_N$ is the nuclear angular momentum in units of $\hbar$.

$\vec{r}_{kN}$ is used to represent the difference $\vec{r}_k - \vec{r}_N$, where $\vec{r}_k$ designates the coordinate of the k'th electron. The first part of the squared term in $\mathcal{H}_1$ gives the total electronic kinetic energy and the remainder of the term follows directly from the equations of motion of a charged particle in a magnetic field and represents the magnetic interactions between electronic orbital motions and nuclear moments. $\mathcal{H}_{LL}$, $\mathcal{H}_{LS}$, $\mathcal{H}_{SS}$, and $\mathcal{H}_{SH}$ designate, respectively, the contributions to the Hamiltonian of the electron orbital-orbital, spin-orbital, electron spin-spin, and the electron spin-external field interactions. For singlet molecular states the effects of these terms on the quantities of interest are of 2nd or higher order.

$\mathcal{H}_2$ gives the magnetic dipolar interactions between electrons in non-s orbits and nuclear spins. $\mathcal{H}_3$ gives the Fermi contact interactions between electron spins in s orbits and nuclear spins. $\mathcal{H}_4$ is the term for the direct magnetic interaction of the nuclei with each other. To first order $\mathcal{H}_4$ averages to zero in experiments such as high-resolution nuclear magnetic resonance of liquids in which frequent collisions average the molecule over all orientations.

The only term that shall be considered in detail is $\mathcal{H}_3$, the Fermi contact term, since it is well known that in most cases it is the only term which contributes significantly to proton-proton coupling constants in liquids.[22] Considering, therefore, an electron-nuclear coupling involving only two nuclei of spins $\vec{I}_A$ and I_B, one gets the following expression for $\mathcal{H}_3$:

$$\mathcal{H}_3 = \left(\frac{8\pi\gamma_e\hbar^2}{3}\right)\left[\gamma_A\vec{I}_A \cdot \sum_k \vec{s}_k\delta(\vec{r}_{kA}) + \gamma_B I_B \cdot \sum_j \vec{s}_j \cdot \delta(\vec{r}_{jB})\right] \quad (6)$$

$$\mathcal{H}_3 = \mathcal{H}_A + \mathcal{H}_B$$

where the nuclei differ with gyromagnetic ratios γ_A and γ_B, and spins I_A and I_B. The formula for the coupling of nuclear spins by electron spins is then obtained as follows: The operator $\mathcal{H}_3$ gives no first-order perturbation of the energy of the molecular ground state. Second-order perturbations will mix the ground singlet state with excited triplet electronic states. If E' then represents the total second-order nuclear-spin electron-spin perturbation energy, then one gets

$$E' = \sum_{n\neq 0} \frac{\langle 0|\mathcal{H}_3|n\rangle\langle n|\mathcal{H}_3|0\rangle}{E_o - E_n} \tag{7}$$

$$E' = -\sum_{n\neq 0} \frac{\langle 0|\mathcal{H}_A + \mathcal{H}_B|n\rangle\langle n|\mathcal{H}_A + \mathcal{H}_B|0\rangle}{E_n - E_o} \tag{8}$$

$$E' = -\sum_{n\neq 0} \left(\frac{1}{E_o - E_n}\right)\Big(\langle 0|\mathcal{H}_A|n\rangle\langle n|\mathcal{H}_A|0\rangle + \langle 0|\mathcal{H}_B|n\rangle\langle n|\mathcal{H}_B|0\rangle$$

$$+ \langle 0|\mathcal{H}_A|n\rangle\langle n|\mathcal{H}_B|0\rangle + \langle 0|\mathcal{H}_B|n\rangle\langle n|\mathcal{H}_A|0\rangle\Big) \tag{9}$$

The first two terms represent the extra energy one would obtain if only one of the nuclei were present. The last two terms represent the extra energy one obtains when both nuclei are present. This represents an energy of interaction and is the quantity to be calculated. Therefore, considering the last two terms of Eq. (9) and the fact that $\mathcal{H}_A$ and $\mathcal{H}_B$ are Hermitian, one gets

$$E = -2 \sum_{n\neq 0} \frac{\langle 0|\mathcal{H}_A|n\rangle\langle n|\mathcal{H}_B|0\rangle}{E_n - E_o} \tag{10}$$

$$E = -2\left(\frac{8\pi\gamma_e\hbar^2}{3}\right)^2 \gamma_A\gamma_B \sum_{jkn\neq 0} \frac{\langle 0|\delta(\vec{r}_{kA})\vec{S}_k\cdot\vec{I}_1|n\rangle\langle n|\delta(\vec{r}_{jB})S_j\cdot I_2|0\rangle}{E_n-E_o} \quad (11)$$

It can then be shown that this term can be written in the form

$$E = -2\left(\frac{8\pi\gamma_e\hbar^2}{3}\right)^2 \gamma_A\gamma_B \sum_{jkn\neq 0} I_1\cdot\frac{\langle 0|\delta(\vec{r}_{kA})\vec{S}_k|n\rangle\langle n|\delta(\vec{r}_{jB})\vec{S}_j|0\rangle}{E_n-E_o}\cdot I_2 \quad (12)$$

In the liquid state, frequent collisions will average the molecular orientations over all directions so that one then obtains

$$E = -\frac{1}{3}\left(\vec{I}_A\cdot\vec{I}_B\right)\left[2\left(\frac{8\pi\gamma_e\hbar^2}{3}\right)^2 \gamma_A\gamma_B \sum_{jkn\neq 0} \frac{\langle 0|\delta(\vec{r}_{kA})\vec{S}_k|n\rangle\cdot\langle n|\delta(\vec{r}_{jB})\vec{S}_j|0\rangle}{E_n-E_o}\right. \quad (13)$$

Equation (13) can then be written in the usual form where

$$E = J_{AB}\,\vec{I}_A\cdot\vec{I}_B \quad (14)$$

and

$$J_{AB} = -\frac{2}{3}\left(\frac{8\pi\gamma_e\hbar^2}{3}\right)^2 \gamma_A\gamma_B \sum_{jkn\neq 0} \frac{\langle 0|\delta(\vec{r}_{kA})\vec{S}_k|n\rangle\langle n|\delta(\vec{r}_{jB})\vec{S}_j|0\rangle}{E_n-E_o} \quad (15)$$

J being termed the nuclear spin-spin coupling constant.

One difficulty with the formula in Eq. (15) is that the summation extends over all triplet states, of which there may be an infinite number and, moreover, the triplet wave functions are generally not known. One common approximation[23] has been to replace the differences (E_n-E_o) with an average excitation energy ΔE. When this is done it becomes possible to substitute Ψ_o for all the Ψ_n and eliminate the summation over n. For polyelectronic molecules, a summation is extended over all possible pairs, k, j, of electrons and Eq. (15) becomes

$$J_{AB} = -\frac{2}{3}\left(\frac{8\pi\gamma_e\hbar^2}{3}\right)^2 \gamma_A\gamma_B \frac{1}{\Delta E} \langle 0|\delta(\vec{r}_{kA})\delta(\vec{r}_{jB})\vec{S}_k \cdot \vec{S}_j|0\rangle \qquad (16)$$

Within the limits of this "average energy approximation", the problem of calculating J_{AB} is now the substitution of a suitable expression for the ground state wave function. However, it will be shown in later sections that this approximation in some instances not only leads to an incorrect prediction of the magnitude of the coupling constants, but, in fact predicts the sign of the coupling constants incorrectly.

2. Molecular Orbital Theory of Nuclear Spin Coupling Constants Between Geminal Hydrogen Atoms

A number of experimental values now exist for nuclear spin coupling constants between geminal hydrogen atoms with an intermediate carbon atom. One observes the following trends among these coupling constants:

a. In simple hydrocarbons the geminal coupling constants are very sensitive to the hybridization on the carbon atom. This can be seen from the values of the geminal coupling constants in the following systems:

	Molecule	Geminal Coupling Constant	
1)	CH_4	-12.4 cps	24
2)	$CH_2=CH_2$	2.5 cps	25
3)	Cyclopropane	ca. + 4 cps	26
4)	Cyclobutane	ca. -11 cps	27

b. Substitution of an electronegative atom in a position α to the CH_2 group produces a positive shift in the geminal coupling constant. This has now been observed in a large number of widely differing systems.

Until recently no satisfactory theory had been developed to provide an explanation of the trends observed. An early study by Gutowsky et al,[8]

predicted a positive geminal coupling constant which should decrease with increasing bond angle. As one can see from the above trends, any such change in the geminal coupling constant with bond angle would be, in fact, quite difficult to observe. More recently a molecular orbital treatment by Pople and Bothner-By[17] in which they considered only the electrons in a CH_2 group was found to give quite a satisfactory prediction of the effect of an electronegative substituent α to the methylene group without actually predicting the absolute magnitudes of the coupling constants. It is therefore basically a treatment along these same lines that will be presented in this section.

According to the molecular orbital theory of closed shell molecules,[28] the 2N-electron antisymmetrical product ground state wave function is given by

$$\Psi_o = \left[(2n)!\right]^{-\frac{1}{2}} \begin{vmatrix} \Psi_1(1)\alpha(1)\Psi_1(1)\beta(1)\Psi_2(1)\alpha(1) \cdots \\ \Psi_1(2)\alpha(2) \cdots \\ \cdots \\ \cdots \Psi_N(2N)\beta(2N) \end{vmatrix} \tag{17}$$

or in the shorter conventional notation by

$$\Psi_o = \left| \Psi_1\Psi_1\Psi_2\Psi_2 \cdots \Psi_N\overline{\Psi}_N \right| \tag{18}$$

In this theory the only excited states that will be considered are those formed by the excitation of a single electron from an unoccupied MO Ψ_j. Approximate wave functions are obtained by replacing one MO of the ground-state antisymmetrized product by a new MO which has to be orthogonal to all the ground-state MO's, in particular to the one it replaces. One then gets four wave functions corresponding to a singlet and triplet state:

$$
{}^1\Psi_{i\to j} = \frac{1}{\sqrt{2}} \begin{vmatrix} \Psi_1 \cdots \Psi_i \bar{\Psi}_j \cdots \end{vmatrix} + \begin{vmatrix} \Psi_1 \cdots \Psi_j \bar{\Psi}_i \cdots \end{vmatrix}
$$

$$
{}^3\Psi_{i\to j} = \frac{1}{\sqrt{2}} \begin{vmatrix} \Psi_1 \cdots \Psi_i \bar{\Psi}_j \cdots \end{vmatrix} - \begin{vmatrix} \Psi_1 \cdots \Psi_j \bar{\Psi}_i \cdots \end{vmatrix} \qquad (19)
$$

The corresponding excitation energies are ${}^1\Delta E_{i\to j}$ and ${}^3\Delta E_{i\to j}$.

The only states which need to be considered are the triplet states, since they are the only states which mix with the ground state in Eq. (15). The problem then becomes one of evaluating the many-electron matrix elements. Equation (15) is first simplified by making the appropriate substitutions for $\langle 0|$ and $\langle n|$. Then reducing the many-electron matrix elements in the standard way gives

$$
J_{AB} = -\frac{2}{3}\left(8\pi\gamma_e\hbar^2/3\right)^2 \gamma_A\gamma_B \sum_i^{occ}\sum_j^{unocc} \frac{\langle \Psi_1 | \delta(\vec{r}_A)\vec{S} | \Psi_j S' | \delta(\vec{r}_B)\vec{S} | \Psi_i S\rangle}{{}^3\Delta E_{i\to j}} \qquad (20)
$$

where the Ψ and S refer to the space and spin parts of the molecular orbitals respectively. The operators $\delta(\vec{r}_A)\vec{S}$ and $\delta(\vec{r}_B)\vec{S}$ can be dealt with according to the method of McConnell[23] and one then obtains

$$
J_{AB} = -\frac{64\pi^2\gamma_e{}^2\hbar^4}{9} \gamma_A\gamma_B \sum_i^{occ}\sum_j^{unocc} \frac{\langle \Psi_i | \delta(\vec{r}_A) | \Psi_j\rangle\langle \Psi_j | \delta(\vec{r}_B) | \Psi_i\rangle}{{}^3\Delta E_{i\to j}} \qquad (21)
$$

where the elements $\langle \Psi_i | \delta(\vec{r}_A) | \Psi_j\rangle\langle \Psi_j | \delta(\vec{r}_B)\Psi_i\rangle$ are now one-electron integrals and i and j are summed over occupied and unoccupied molecular orbitals respectively.

If the LCAO approximation

$$\Psi_i = \sum_\alpha C_{i\alpha}\Phi_\alpha \tag{22}$$

in which each molecular orbital is written as a linear combination of a set of atomic orbitals Φ_α is used, one then gets

$$J_{AB} = -\frac{64\pi^2\gamma_e^2\hbar^4}{9}\gamma_A\gamma_B \sum_i^{occ}\sum_j^{unocc} ({}^3\Delta E_{i\to j})^{-1} \sum_{\lambda\mu\nu\sigma} C_{i\lambda}C_{j\mu}C_{j\nu}C_{i\sigma}$$

$$\langle\Phi_\lambda|\delta(\bar{r}_k)|\Phi_\mu\rangle\langle\Phi_\nu|\delta(\bar{r}_B)|\Phi_\sigma\rangle \tag{23}$$

The approximation in which only one-center integrals are retained shall now be used which means that Φ_λ, Φ_μ must both be s-orbitals on atom A and Φ_ν, Φ_σ must be s-orbitals on atom B. Further, since inner-shells take only little part in the formation of bonding MO's, the most important terms will be those involving the valence-shell s-functions. These functions are the 1s-function for hydrogen and the 2s-function for carbon. They are the only functions that shall be considered at this time and they will be written as s_A and s_B so that:

$$J_{AB} = -\frac{64\pi^2\gamma_e^2\hbar^4}{9}\gamma_A\gamma_B \langle s_A|\delta(\vec{r}_A)|s_A\rangle\langle s_B|\delta|\vec{r}_B|s_B\rangle \tag{24}$$

$$\times \sum_i^{occ}\sum_j^{unocc} ({}^3\Delta E_{i\to j})^{-1} C_{is_A}C_{js_A}C_{js_B}C_{is_B}$$

If the approximation of considering an independent-electron molecular orbital model is used in which the molecular orbitals are determined as eigenfunctions of a one-electron Hamiltonian, ${}^3\Delta E_{i\to j}$ can be written as the difference of one-electron energies $(\epsilon_j-\epsilon_i)$. Making this substitution in Eq. (24) one obtains

$$J_{AB} = \frac{16\pi^2\gamma_e^2\hbar^4}{9}\gamma_A\gamma_B\langle s_A|\delta(\vec{r}_A)|s_A\rangle\langle s_B|\delta(\vec{r}_B)|s_B\rangle\pi_{SA,SB} \qquad (25)$$

where $\pi_{SA,SB}$ represents the "mutual polarizability" of the orbitals s_A and s_B.

$$\Pi_{SA,SB} = 4\sum_{i}^{occ}\sum_{j}^{unocc}(\epsilon_i-\epsilon_j)^{-1}C_{is_A}C_{js_A}C_{js_B}C_{is_B} \qquad (26)$$

Equation (25) is essentially the same as that obtained by Pople and Bothner-By.[17]

At this point this author feels that some comment concerning the "average energy approximation" is in order. If all the $^3\Delta E_{i\rightarrow j}$ are replaced by an average value ΔE in Eq. (24), one gets the following relation:

$$J_{AB} = \frac{16\pi^2\gamma_e^2\hbar^4}{9\Delta E}\gamma_A\gamma_B\langle s_A|\delta(r_A)s_A\rangle\langle s_B|\delta(\vec{r}_B)|s_B\rangle\left(4C_{s_A}^2C_{s_B}^2\right) \qquad (27)$$

This equation is identical to the one derived by McConnell[23] where he made the "average energy approximation" before reducing the many-electron matrix elements. Equation (27) requires that J_{AB} be positive whereas this fact does not directly follow from Eq. (24). In fact it has been shown in numerous examples that geminal coupling constants are in many cases indeed negative. Further comments concerning this matter will be made in later sections.

An isolated CH_2 group will be considered as the model used in the calculations. It will be considered in terms of four delocalized MO's within the valence shell, two of which are bonding and occupied and the other two being unoccupied and antibonding. If one now considers the case of sp^2 hybridization and chooses for the molecular orbitals the

appropriate linear combination of atomic orbitals which form bases for irreducible representations of the C_{2v} point group, one gets

$$\Psi_\sigma = 1/\sqrt{2}\ (1S_A + 1S_B) \tag{28}$$

$$\Psi_y = 1/\sqrt{2}\ (1S_A - 1S_B) \tag{29}$$

for the σ and π_y molecular orbitals respectively. The coefficients for Ψ_σ and Ψ_y are given by

$$C_{i\sigma} = 1/\sqrt{2}\ (C_{iS_A} + C_{iS_B}) \tag{30}$$

$$C_{iy} = 1/\sqrt{2}\ (C_{iS_A} - C_{iS_B}) \tag{31}$$

so that one obtains the following expression for π_{S_A,S_B}:

$$\pi_{S_A,S_B} = \sum_i^{occ} \sum_j^{unocc} (\epsilon_j - \epsilon_i)^{-1} (C_{iy}^2 C_{j\sigma}^2 + C_{i\sigma}^2 C_{jy}^2 - C_{i\sigma}^2 C_{j\sigma}^2 - C_{iy}^2 C_{jy}^2) \tag{32}$$

Considering then Pople's approximation of using mean triplet excitation energies described in terms of the following notation: ϵ_σ, unoccupied σ orbitals; ϵ_y, occupied π_y orbitals; ϵ_σ^*, unoccupied σ orbitals; ϵ_y^*, unoccupied π_y orbitals; one then gets the following expression for π_{S_A,S_B}:

$$\pi_{S_A,S_B} = \sum_i^{occ} \sum_j^{unocc} \left(\frac{C_{iy}^2 C_{j\sigma}^2}{\epsilon_\sigma^* - \epsilon_y} + \frac{C_{i\sigma}^2 C_{jy}^2}{\epsilon_y^* - \epsilon_\sigma} - \frac{C_{i\sigma}^2 C_{j\sigma}^2}{\epsilon_\sigma^* - \epsilon_\sigma} - \frac{C_{iy}^2 C_{jy}^2}{\epsilon_y^* - \epsilon_y} \right) \tag{33}$$

Expressing Eq. (33) then in terms of electron population, $P_{\sigma\sigma}$ and P_{yy}, of the delocalized hydrogen group functions Ψ_σ and Ψ_y, and then differentiating with respect to $P_{\sigma\sigma}$ and P_{YY}, the following relationship is obtained for ΔJ_{AB}:

$$\Delta J_{AB}^{sp^2} = k(\Delta P_{yy} - \Delta P_{\sigma\sigma}) \tag{34}$$

where k is given by

$$k = \frac{1}{4}\left(\frac{16\pi^2\gamma_e^2\hbar^4}{9}\right)\gamma_A\gamma_B \langle S_A|\delta(\vec{r}_A)|S_A\rangle\langle S_B|\delta(\vec{r}_B)S_B\rangle\left(\frac{1}{\epsilon_\sigma^* - \epsilon_y} - \frac{1}{\epsilon_y^* - \epsilon_\sigma}\right) \tag{35}$$

In the context of this simplified theory, it is then possible to expand the above calculations to the case of sp^3 hybridization using molecular orbitals which form bases for irreducible representations of the C_{3V} point group,

$$\Psi_\sigma = 1/\sqrt{3}\ (1S_A + 1S_B + X)$$
$$\Psi_x = 1/\sqrt{2}\ (1S_A - 1S_B)$$
$$\Psi_y = 1/\sqrt{6}\ (1S_A\ \ 1S_B - 2X)$$

X being an appropriate valence orbital. (Strictly for the use of C_{3V} symmetry is incorrect, but it turns out to be quite reasonable for a simplified analysis of the type being considered here.)[17] The following relationship is then obtained by the same procedure as that outlined above for the case of sp^2 hybridization.

$$\Delta J_{AB}^{sp^3} = \frac{4}{9}k\left(\Delta P_{yy} - \Delta P_{\sigma\sigma}\right)$$

This section can be concluded by stating that the theory predicts that geminal coupling constants will be dependent upon substituents α to the CH_2 group. Furthermore, electronegative substituents (withdrawal of σ electrons thereby producing a negative value for $P_{\sigma\sigma}$) should produce a positive shift in the coupling constants. Finally, it is extremely interesting to note that the theory predicts that substituents should have about twice as large an effect in sp^2 hybridization as in sp^3 hybridization.

3. Nuclear Spin-Spin Coupling Constants in Saturated Systems Between Protons Separated by Three or More Bonds

Nuclear spin-spin coupling constants between protons in saturated systems separated by three or more bonds can be broken down into two general classifications; vicinal coupling constants (i.e., coupling constants between protons separated by exactly three bonds, for example, between protons on adjacent carbon atoms) and "long range" coupling constants where the protons are separated by more than three bonds.

The theory concerning the origin of vicinal spin-spin coupling constants has been the subject of investigation of a number of workers. Probably the most famous of these studies is the calculation of Karplus[29] of the relationship of the dihedral angle between two protons on vicinal carbon atoms and the coupling constant. The six-electron system

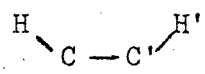

is used as the model on which these calculations are based. Valence-bond type wave functions are used throughout this calculation. With a ground state wave function of the form

$$\Psi = \sum_j C_j \Psi_j \qquad (40)$$

where the Ψ_j are the non-polar valence-bond structures and the C_j are the corresponding constant coefficients, Karplus and Anderson[30] have used the Hamiltonian of Ramsey to show that the contact contribution to the electron-coupled nuclear spin-spin coupling interaction between nonbonded protons can be written in the form

$$J_{AB} = \frac{1.395\times10^3}{\Delta E} \sum_j \sum_\ell C_j C_\ell \left(2^{n-i_{j,\ell}}\right)^{-1} [1+2f_{j,\ell}(P_{AB})] \qquad (41)$$

where ΔE denotes the average excitation energy (the "average energy approximation"), and in the superposition diagram of Ψ_j and Ψ_ℓ, $i_{j,\ell}$ is the number of islands and $f_{j,\ell}$ (P_{AB}) is the coefficient of the exchange integral between the A and B protons.

In all of the molecules of interest in this dissertation, the singlet and triplet eigenfunctions of interest can be represented in terms of a localized bond description; that is, in the valence-bond approach the only structure that contributes significantly to the ground state is the perfect-pairing structure. Correspondingly, the triplet states can be expressed as functions which differ from the perfect-pairing structure only by having the spins of one electron pair coupled to give a triplet instead of a singlet bond function. In this sense, Karplus[31] has shown that the average energy approximation is valid for those calculations of coupling constants which are applied to systems in which the deviations from perfect-pairing are small.

It is easy to show that the perfect-pairing structure and valence bond structures which do not involve any bonds between chemically bonded atoms do not contribute appreciably to the nuclear spin coupling constant. Thus, the measurements of a non zero coupling constant implies that significant deviations from perfect-pairing to occur, the magnitude of the deviation being directly related to the numerical value of the coupling constant. However, these deviations are small when compared to the contribution of the perfect-pairing structure to the electronic structure of the molecule. In fact, only the cross terms between the wavefunctions for one valence bond between chemically bonded pairs of atoms need be included in the calculations. Karplus has shown that structures with no valence bonds between chemically bonded pairs do not yield significant contributions

to the coupling constants. Therefore, cross terms which involve these structures and the perfect-pairing structure will also not contribute to the coupling constants.

It is well known that exchange integrals which involve only carbon orbitals can be expressed as functions of the dihedral angle between the two carbon atoms. The coupling constant J_{AB} can therefore be expressed as a function of the dihedral angle. The calculations then predict the interesting result that the coupling constant will depend in a sensitive fashion on the dihedral angle, such that the coupling constant is maximal at dihedral angles of 0 and 180°; the magnitude of the coupling constant at 0° being 8.0 cps and the magnitude of the coupling constant at 180° being 9.2 cps. The minimal value of the coupling occurs near 90° with a corresponding magnitude of -0.27 cps.

A similar calculation using molecular orbital wave functions and again using the Hamiltonian derived by Ramsey was carried out. It is rather interesting to point out that these calculations demonstrate a generally excellent agreement with the valence bond calculations of Karplus. A limited number of experimental studies have demonstrated a general qualitative agreement with the predictions of these theories.

More recently a number of studies have demonstrated that vicinal coupling constants depend not only on the dihedral angle between the protons but also on the substituents present on neighboring carbon atoms. The exact nature of the substituent dependence is as yet unclear but it does not appear to follow the same trends as is observed for geminal coupling constants. A number of investigators have suggested various forms of linear relationships between the electronegativities of the substituents and the coupling constants in substituted acyclic hydrocarbons.

However, similar studies on strained ring systems have not shown such linear dependences. Hutton and Schaefer[32] have studied the effect of substituents on vicinal coupling constants in a series of three-membered ring systems, but were not able to determine any definite relationship between the coupling constant changes and the substituents electronegativities. It has also been suggested that strained ring systems possess some π character. However, it appears that the π character, if present, does not contribute appreciably to the vicinal coupling constants, since if it did contribute, one might expect a large substituent electronegativity effect in ethylenic type compounds. Such a large effect is not observed.

In view of this evidence it appears that it would be quite hazardous, as Karplus[33] has recently pointed out, to use these calculations for structural determinations, especially when trying to compare two quite dissimilar systems such as systems which possess different substituents of widely varying electronegativities. One might expect a generally good agreement with the theory within a given system where the only change is the bond angle. For example, in the cases of trimethylene oxide and trimethylene sulfide; it would be expected that the cis and trans vicinal coupling constants in either of these molecules would follow the Karplus relationship but that attempting to compare the cis coupling constants between these molecules might prove to be difficult.

A large number of nuclear spin-spin coupling constants across four or more bonds have been observed in high-resolution nuclear magnetic resonance spectra. Recently, the interest has centered around the stereospecificity of these coupling constants. The magnitudes of these couplings have been generally observed to be less than about 2 cps although some

notable exceptions do exist, but depending on the relative orientation of the two carbon-hydrogen bonds containing the coupled protons, both positive and negative coupling constants have been observed.

Until recently no calculations have been reported on coupling constants across four bonds, probably because of the inherent difficulty involved due to the extremely small magnitude of the coupling constants and also probably because of the unavailability of the suitable exchange integrals required in valence-bond types of calculations. The only treatment to appear to date is that of Barfield[34] wherein a model of the type

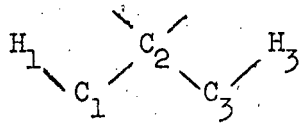

was used as a basis for the calculations. In these calculations Barfield used the formulation developed by Karplus, et al., and a limited set of valence-bond wave functions in addition to the perfect-pairing structure; those which involve the breaking of C_1-H_1 and/or C_3-H_3, since these should be the structures which would contribute most to the coupling constant. The assumption of the use of a limited set of non-perfect pairing structures is certainly a perilous one at best. With this approximation it can only be hoped that the calculations will predict the approximate function of the coupling constants on the dihedral angles of the C_1-H_1 and C_3-H_3 bonds and that no critical significance can be attributed to the magnitude of the values calculated.

Barfield's calculations lead to explicit expressions for the two possible coupling mechanisms; the "direct" ("through space") contribution and the "indirect" ("through the bond") contribution. The expressions for the "direct" and "indirect" contributions respectively are as follows:

$$\mathrm{Dir}_{J_{HH'}} = \frac{1.395\times10^{3}}{\Delta E}\,\frac{3}{4K(C,H)}\,[K(H_1,H_3) + K(C_1,C_3) - K(C_1,H_3) - K(C_3,H_1)] \qquad (42)$$

$$\mathrm{Indir}_{J_{HH'}} = \frac{1.395\times10^{3}}{\Delta E}\,\frac{3}{8}\sum_{j}\,\frac{\{K(C_1,\gamma_j')-K[C_1,\gamma_j(C_2)]\}\{K(C_3,\gamma_j')-K[C_3,\gamma_j(C_2)]\}}{\{K(C,H) + K[\gamma_j', \gamma_j(C_2)]\}^2} \qquad (43)$$

where $\gamma_j(C_2)$ denotes the jth orbital on C_2, which is directed toward orbital γ_j'; where the summation index j in Eq. (43) extends over all hybrid orbitals on C_2, and K(A,B) are the appropriate exchange integrals. For the "indirect" effect, Barfield estimated the exchange integrals from a number of experimental values. From this author's point of view, it appears that this method has the inherent disadvantage, at least to a certain extent, of presuming the answers beforehand and thereby does not provide a true test of the theory.

In any event, Barfield's theory predicts that the maximum coupling constant across four bonds (if it is positive in sign) should correspond to a planar zigzag arrangement; that is, it corresponds to the situation where H_1 and H_3 are in the same plane, and the absolute minimum should occur for the case where H_1 and H_3 are in perpendicular planes. From his calculations, Barfield also concluded that the contribution from the "direct" or "through space" effect should be negligible, and the "indirect" effect provides the only contribution to the coupling constant, at least in saturated systems and also probably in unsaturated systems. A certain amount of experimental evidence has indicated that the trends predicted by this theory are in agreement with observed values for nuclear spin coupling constants across four bonds.

However, in view of the fact that substituent effects are almost sure to be important, and that detailed information regarding the ...

substituent effects on spin coupling constants across four or more bonds is lacking (due, of course, to the very small magnitude of the coupling constants), it appears that it would be extremely dangerous to use these calculations to draw conclusions concerning molecular geometries, and that any such conclusions could possibly lead to erroneous results. Such difficulties which arise from neglecting substituent effects, incorrect assumptions concerning hybridization, and using incorrect bond lengths would certainly be expected to make themselves apparent in strained ring systems such as the four-membered ring systems of interest in this dissertation.

B. Nuclear Magnetic Double Resonance

1. The Hamiltonian and General Formulas.

Double resonance refers to the general type of spectroscopic experiment in which a system is simultaneously irradiated at two different frequencies,[37] which is applicable to two groups of nuclei of arbitrary spin, either in situations involving different nuclear species or in situations where the chemical shift is large compared to the nuclear spin-spin coupling constant. More recently this theory was extended to include the case of strongly coupled spin systems (i.e., situations wherein the chemical shift may be of the same order of magnitude as the nuclear spin coupling constant).[38] Such situations are in fact quite common in nuclear magnetic resonance. In this section a general outline of the theory of double resonance will be presented with specific applications being directed to systems of interest in this dissertation.

It has been shown that high-resolution nuclear magnetic resonance spectra can be completely described in terms of a Hamiltonian of the form[39]

$$\mathcal{H}^{\circ} = \sum_i \nu_i I_i^z + \sum_{i<j} J_{ij} \vec{I}_i \vec{I}_j \qquad (44)$$

with

$$\nu_i = -\left(\gamma_i/2\pi\right)\left(1-\sigma_i\right)\mathcal{H}_o \qquad (45)$$

σ_i is the magnetic shielding parameter, γ_i is the gyromagnetic ratio of the i'th nucleus in the absence of any spin coupling and I is the nuclear spin angular momentum operator with Z component I_i^z. The quantity J_{ij} is the nuclear spin coupling constant between the i'th and j'th nuclei measured in cycles per second.

In the experiments to be described the nuclear spin system will be assumed to be in a static magnetic field, $\vec{H}_o = kH_o$, which is in the positive Z direction. In addition, the spin system interacts with the two radio-frequency fields H_1, the radio-frequency field used to observe the spectrum, and H_2, the perturbing rf field, both of which lie along the X axis. H_1 and H_2 are given by the following expressions:

$$\begin{aligned} \vec{H}_1 &= \hat{i}\, 2\, H_1 \cos \omega_1 t \\ \vec{H}_2 &= \hat{i}\, 2\, H_2 \cos \omega_2 t \end{aligned} \qquad (46)$$

It is assumed that each oscillating field can be described as a pair of counter-rotating fields, and that only the component rotating with either the frequency$(-\omega_1)$, or$(-\omega_2)$, is effective in inducing transitions. The error involved in this assumption is negligible provided that the oscillatory fields are small compared to H_o.[40] With this assumption one obtains for H_1 and H_2

$$\begin{aligned} \vec{H}_1 &= H_1 \left(\hat{i} \cos \omega_1 t - \hat{j} \sin \omega_1 t \right) \\ \vec{H}_2 &= H_2 \left(\hat{i} \cos \omega_2 t - \hat{j} \sin \omega_2 t \right) \end{aligned} \qquad (47)$$

so that effective magnetic field $\vec{H}_{eff}$ is given by

$$\bar{H}_{eff} = \hat{k} H_o + H_1(\hat{i} \cos \omega_1 t - \hat{j} \sin \omega_1 t) + H_2(\hat{i} \cos \omega_2 t - \hat{j} \sin \omega_2 t)$$

The Hamiltonian for a molecule in the liquid state in the field H_{eff} in the laboratory coordinate frame is given by

$$\mathcal{H} = \mathcal{H}^\circ + \mathcal{H}(t) \tag{49}$$

where $\mathcal{H}(t)$ is expressed in the following manner:

$$\mathcal{H}(t) = -\frac{H_1}{2\pi} \sum_i \gamma_i (I_i^x \cos \omega_1 t - I_i^y \sin \omega_1 t) - \frac{H_2}{2\pi} \sum_i \gamma_i (I_i^x \cos \omega_2 t - I_i^y \sin \omega_2 t) \tag{50}$$

$$\mathcal{H}(t) = \mathcal{H}'''(t) + \mathcal{H}''(t)$$

The H_1 field is only used to observe the resonant frequencies of the system and it will therefore be assumed to be sufficiently small so that it does not appreciably perturb the system. In this approximation the system will be completely describable in terms of the time-dependent Hamiltonian $\mathcal{H}'$ where

$$\mathcal{H}' = \mathcal{H}^\circ + \mathcal{H}''(t) \tag{51}$$

The Hamiltonian is given in units of cycles per second and the summations are carried out over all the spins i and j in the molecule.

Since the Hamiltonian is time dependent, it is not possible to obtain time-independent solutions to Eq. (51). However, the time-dependent terms in H_2 can be removed if the Hamiltonian is transformed to a coordinate system rotating with angular velocity-ω_2. The operator for a finite rotation-$k\omega_2 t$ can be written:

$$T = \exp\left[-i\omega_2 t \textstyle\sum_i I_i^z\right] \tag{52}$$

The transformed Hamiltonian $\mathcal{H}_T$ can then be given by the following expression:

$$\mathcal{H}_T = -\sum_i (\nu_i - \nu_2) I_i^z + \sum_{i<j} J_{ij} \vec{I}_i \cdot \vec{I}_j - \frac{H_2}{2\pi} \sum_i \gamma_i^x \qquad (53)$$

At this point it is instructive to consider a typical example of the calculations involved. The example to be considered will be a two spin system, the AB system. The Hamiltonian in the rotating coordinate system for an AB molecule where the nuclei A and B both have spin $\frac{1}{2}$ is given by

$$\mathcal{H}_{T_{AB}} = (\nu_2 - \nu_A) I_z(a) + (\nu_2 - \nu_B) I_z(b) + J_{AB} \vec{I}(a) \cdot \vec{I}(b) - \frac{H_2}{2\pi} \left(\gamma_A I_x(a) + \gamma_B I_x(b) \right) \qquad (54)$$

The complete Hamiltonian matrix, using the spin functions $\alpha\alpha$, $\alpha\beta$, $\beta\alpha$, and $\beta\beta$ as the basic product functions for the system, is given by

$$\begin{pmatrix} \mathcal{H}_{T_{11}} & -\gamma_B H_2/4\pi & -\gamma_A H_2/4\pi & 0 \\ -\gamma_B H_2/4\pi & \mathcal{H}_{T_{22}} & \frac{1}{2} J_{AB} & -\gamma_A H_2/4\pi \\ -\gamma_A H_2/4\pi & \frac{1}{2} J_{AB} & \mathcal{H}_{T_{33}} & -\gamma_B H_2/4\pi \\ 0 & -\gamma_A H_2/4\pi & -\gamma_B H_2/4\pi & \mathcal{H}_{T_{44}} \end{pmatrix}$$

with diagonal matrix elements

$$\mathcal{H}_{T_{11}} = -\frac{1}{2}(\nu_A + \nu_B) + \nu_2 + \frac{1}{4} J_{AB}$$

$$\mathcal{H}_{T_{22}} = -\frac{1}{2}(\nu_A - \nu_B) - \frac{1}{4} J_{AB}$$

$$\mathcal{H}_{T_{33}} = \frac{1}{2}(\nu_A - \nu_B) - \frac{1}{4} J_{AB}$$

$$\mathcal{H}_{T_{44}} = \frac{1}{2}(\nu_A + \nu_B) - \nu_2 + \frac{1}{4} J_{AB}$$

If this case is then considered in the AX approximation, that is, the

approximation of considering the chemical shift to be large compared to the coupling constant and, if it is further assumed that the X nucleus is being irradiated by H_2 so that ν_2 is approximately equal to ν_x, then the problem becomes greatly simplified. In this approximation the difference between $\mathcal{H}_{T_{11}}$ and $\mathcal{H}_{T_{33}}$ is much greater than the connecting off-diagonal element $-\gamma_A H_2/4\pi$ and the difference between $\mathcal{H}_{T_{22}}$ and $\mathcal{H}_{T_{33}}$ is much greater than $\frac{1}{2} J_{AB}$ so that these off-diagonal elements may also be neglected. With these approximations the secular determinant may be factored into two 2×2 determinants which are readily evaluated. The results of this evaluation will be considered in detail in the next section.

2. Graphical Presentation and Discussion

The results of the evaluation of the determinant in the previous section for various values of ν_1, ν_2, and two values of H_2 are presented in graphical form in Fig. 1 and Fig. 2, where two quantities, Δ and Ω have been defined as follows:[38]

$$\Delta = (\nu_2 - \nu_x)/|J|$$
$$\Omega = (\nu_1 - \nu_A)/|J| \qquad (56)$$

In ordinary nuclear magnetic resonance experiments, spectra may be observed either by sweeping the radio-frequency ν_1 while holding the magnetic field H_o constant or by sweeping the main magnetic field while holding the radio-frequency constant. Experimental details of these procedures along with additional remarks concerning the relative advantages of each method will be considered in later sections of this dissertation. However, the spectra obtained in both cells are identical. In nuclear magnetic double resonance where the additional perturbing field

H_2 has been introduced such is not the case. In addition to this complication the variable ν_2 has been introduced permitting an additional degree of freedom. In the ordinary frequency-sweep experiment ν_2 and H_o are held constant and ν_1 is swept to observe the spectrum. The resulting spectrum may be predicted by drawing a vertical line through the graph at a prescribed value of Δ. The more common experiment is the field sweep wherein H_o is varied (corresponding to varying ν_1-ν_2 at a constant rate) which is equivalent to varying Δ and Ω simultaneously. On the graphs in Figs. 1 and 2 this corresponds to a line drawn with a slope γ_A/γ_x and an intercept on the Δ axis which may be called Δ' corresponding to the deviation from the resonance condition of ν_2 when $\nu_1 = \nu_A$. For proton-proton double resonance the slope of the line is very nearly 45° and

$$\Delta' = \left[(\nu_A - \nu_x) - (\nu_1 - \nu_2)\right]/|J| \qquad (57)$$

that is, the discrepancy between the chemical shift and the frequency difference between ν_1 and ν_2. In the other type of frequency-sweep experiment where ν_2 is varied while ν_1 and H_o are held constant, it should be possible to predict the spectrum by drawing a horizontal line through the graphs in Figs. 1 and 2 at a prescribed value of Ω. However, sweeping a strong rf field through a spectrum in this manner introduces a number of other complications which will be discussed in greater detail in a later part of this section. The intensities are proportional to the square of the I^x matrix elements in the representation where $\mathcal{H}_T$ is diagonal.

The theory previously developed in this section can easily be extended to include the case of the strongly coupled spin system by considering the experiment wherein the perturbing rf field H_2 is close to a single non-degenerate transition and sufficiently far from other transitions so that

they are not appreciably perturbed. With these restrictions a relatively simple situation ensues.

The schematic representation of a two-spin system is shown in Fig. 3. It is evident that two different arrangements of the energy levels are possible. These two possible arrangements are shown in Figs. 4a and 4b. In Fig. 4a the energy level common to both transitions is E_r. The other two levels then have the same magnetic quantum number. This situation will be denoted by the term regressive ($\Delta m = 0$). In Fig. 4b, E_s is the energy level common to both transitions. The other two energy levels differ in spin quantum number by two units. This situation is denoted by the term progressive ($\Delta m = 2$). These two possible arrangements of the energy levels must be distinguished since they lead to extremely important differences in the double resonance spectra.

The experimental conditions will be the same as in the case of the weakly coupled spin system. The A nucleus will be observed by the weak rf field H_1 while the B nucleus is being perturbed by the strong radio-frequency field H_2. Since this analysis is restricted to the condition that the perturbing rf field be near a single non-degenerate transition frequency, it will also be applicable to any system of n spins since only transitions with energy levels in common with the perturbed levels will be affected. The theory may also be extended to include the situation where two transition frequencies are close together but have no energy level in common. Examples of degenerate transition frequencies are more likely to occur in weakly coupled spin systems in which case the results of the previous derivations will be applicable.

Because the radio-frequency field H_2 is near a single non-degenerate transition frequency, $-\gamma_x H_2/4\pi$ may be safely neglected as being small

compared to $\nu_A - \nu_2$, just as in the AX approximation for weakly coupled spin systems. The single non-degenerate transition ν_{rs} is defined by the energy eigenvalues E_r and E_s. From the solution of the resulting 2×2 eigenvalue problem one obtains the result that only the states defined by Ψ_r and Ψ_s are appreciably perturbed. This leads to eigenvalues ϵ_r and ϵ_s and the following eigenfunctions:

$$\Psi_r = C_{11}\,\psi_r + C_{12}\,\psi_S \tag{58}$$

$$\Psi_s = C_{21}\,\psi_r + C_{22}\,\psi_S \tag{59}$$

For either the case $\Delta m = 0$ or the case where $\Delta m = 2$; in the absence of ν_2 the transition ν_{rp} is permitted by a nonzero value of $\langle\Psi_p|I^x|\Psi_r\rangle^2$. If ν_2 is turned on near ν_{rs}, the new mixed states Ψ_r and Ψ_S are obtained. When ν_2 is on $\langle\Psi_p|I^x|\Psi_r\rangle^2$ and $\langle\Psi_p|I^x|\Psi_s\rangle^2$ can both be different from zero. Freeman and Anderson[38] have shown that the two allowed transitions will occur at

$$\nu_1 = \nu_{rp} + \frac{1}{2}(\nu_2-\nu_{rs}) \pm \frac{1}{4}\left[(\nu_2-\nu_{rs})^2 + \frac{4\gamma_i^2 H_2^2 \lambda_{rs}^2}{\pi^2}\right]^{\frac{1}{2}} \tag{60}$$

for the p and s levels with spin M and r level with spin M-1 (see Fig. 4a) or

$$\nu_1 = \nu_{rp} - \frac{1}{2}(\nu_r-\nu_{rs}) \pm \frac{1}{4}\left[(\nu_2-\nu_{rs})^2 + \frac{4\gamma_i^2 H_2^2 \lambda_{rs}^2}{\pi^2}\right]^{\frac{1}{2}} \tag{61}$$

for s level with spin M, r level with spin M-1 or M+1 where λ_{rs} is given by the expression

$$\lambda_{rs} = \langle\Psi_s|I^x|\Psi_r\rangle \tag{62}$$

If ν_2 is equal to ν_{rs}, then both of these expressions (Eqs. 60 and 61) reduce to the following expression:

$$\nu_1 = \nu_{rp} \pm \gamma_1 H_2 |\lambda_{rs}| \tag{63}$$

This relationship indicates that the splitting in this case is proportional to the strength of the perturbing field H_2 and also to the square root of the intensity of the line being irradiated. This means that if one is exactly on resonance, then two equally intense peaks should be observed but, if ν_2 is slightly different from ν_{rs}, then one component will be stronger than the other.

The results of these two cases are most conveniently presented in graphical form by considering the appropriate portions of the graphs in Figs. 1 and 2. This is best illustrated in Fig. 5 for the experiment where ν_1 is varied holding ν_2 and H_o constant. By drawing a vertical line through the graph at the appropriate value of Δ, it then becomes possible to predict the frequencies and intensities of the double resonance spectrum.

The problem then becomes one of distinguishing between the two cases; $\Delta m = 0$ and $\Delta m = 2$. This information can be extremely useful when attempting to trace out energy level diagrams for complex systems. Perhaps one way of differentiating between the two cases would be to study the way in which the relative intensities of the two components of the doublet change when ν_2 is increased. From Fig. 1 one can verify that one component grows and the other component gets weaker and the sense is opposite in the two cases $\Delta m = 0$ and $\Delta m = 2$. However, it will be shown that there are two other preferable methods by which the two cases may be distinguished.

In conventional nuclear magnetic resonance experiments at high resolution, the profile of the observed lines usually represents the

distribution of the magnetic field over the effective volume of the sample, for the standard practice is to remove dissolved oxygen and to keep the viscosity low, so that natural linewidths are hidden by the broadening due to the inhomogeneity of the magnetic field H_o. In double resonance the situation is quite complex and depends very much on whether the main magnetic field or one of the radio frequencies, ν_1 or ν_2, is swept to display the spectrum.

Although the field-sweep experiments constitute the least satisfactory method of displaying double-resonance spectra, it will be considered first because it provides a convenient way of introducing the reader to the phenomena which occur in double-resonance. A magnetic field sweep corresponds to a simultaneous variation of ν_1 and ν_2 in Fig. 5 (see Fig. 6) along a straight line of slope $|\gamma_A/\gamma_x|$. If $|\gamma_A/\gamma_x| > 1$ each branch of the curve is cut just once, but if $|\gamma_A/\gamma_x| < 1$, one branch of the curve may be cut twice during a single sweep. Under certain conditions a field sweep diagonal may avoid both branches entirely, which introduces the interesting possibility that lines may 'disappear' in some field sweep double-resonance spectra. Proton-proton and fluorine-fluorine double resonance spectra, where $|\gamma_A/\gamma_x| = 1$, represent a limiting case where such an effect could occur, and, in fact, has been observed. In all of these cases the magnetic field inhomogeneity broadens each line in the same way except that the natural linewidth intervenes when a branch of the curve is cut at an acute angle. This might be visualized by giving the branches of the curves a "thickness" corresponding to the natural linewidth of the sample, then a section through the curve at a sufficiently acute angle would produce a broadening which exceeds the field inhomogeneity width. The effective sweep rate for this line is correspondingly

reduced and the ideal slow passage condition more nearly approached, giving an unusual appearance to the observed line. One should certainly be able to visualize that these effects would only serve to make field-sweep double-resonance spectra inordinantly complex. This method then unnecessarily introduces complexities into the spectra rather than aiding in building up an energy level scheme.

The interpretation of double-resonance spectra obtained by sweeping the observing radio-frequency ν_1 is considerably simpler than attempting to interpret spectra obtained by sweeping the main magnetic field H_o. If the magnetic field inhomogeneity determines the width of lines in a spectrum, the lines observed by means of a ν_1 frequency sweep double-resonance experiment may be either broader or narrower than those observed in the usual single-resonance experiment. The observed nuclear resonance signal is made up from the contributions of all parts of the sample which are located in a range of values of the magnetic field. The diagram in Fig. 6 shows how the line profiles are calculated for frequency-sweep double-resonance experiments. The bold line has a slope of $|\gamma_A/\gamma_x|$ and represents the width at half-height of the magnetic field distribution over the effective sample volume. The center of the field distribution has coordinates Δ_o and Ω_o.

Lines 1 and 2 in Figs. 1 and 2 represent the situation obtained where $\Delta m = 0$ and lines 3 and 4 the situation where $\Delta m = 2$. The line-width in a conventional high-resolution spectrum, or in a double-resonance experiment when ν_2 is far from resonance, is given by the amount by which Ω (or ν_1) must be swept to drive the bold line of Fig. 6 through a horizontal portion of the curve. The discussion will now be limited to cases of similar nuclei such as protons or fluorines, where the slope

of γ_A/γ_x is very nearly unity. If the case is now considered where the frequency of ν_2 is exactly equal to the resonance frequency of a single transition (i.e., where the slopes of lines 1 and 2 are equal and the slopes of lines 3 and 4 are equal), it becomes apparent that both lines 1 and 2 will appear sharper than lines observed in a single-resonance spectrum, since the slopes of both lines 1 and 2 and the bold line representing the magnetic field inhomogeneity have the same sense. One can observe from Fig. 6 that the bold line will pass through lines 1 and 2 at a relatively acute angle.

For lines 3 and 4, the situation obtained is quite different. In this case the slopes of lines 3 and 4 are of opposite sense compared to the slope of the bold line. This means that the bold line will pass through lines 3 and 4 at quite a large angle. From this fact one concludes that these lines will appear to be broader than the lines observed in a corresponding single-resonance experiment. In addition to this another important facit makes itself apparent for low values of H_2 in that the bold line may straddle both lines 3 and 4 simultaneously. In the experiment where ν_1 is swept, this appears as an unresolved doublet.

The situation wherein H_o is held constant and ν_1 set equal to ν_{rs} (see Fig. 4) while sweeping ν_2 through the spectrum can lead to differing effects depending upon the experimental conditions. If this situation is considered where ν_2 is swept through ν_{rp} in a time which is short in comparison with the spin relaxation times, T_1 and T_2, of the spin system, the irradiated levels will acquire equal populations while the populations of the nonirradiated levels, given by the Boltzmann distribution, remain unchanged.

The intensity I_{sr} for a line corresponding to a transition between

the levels r and s is expressed as

$$I_{sr} = \gamma^2 H_1^2 |L_{sr}|^2 (N_s - N_r)\, g(\nu) \qquad (64)$$

where I_{sr} is the transition matrix element, (N_s-N_r) is the excess population of Level s over Level r and $g(\nu)$ is a shape function. Only the quantity (N_s-N_r) is affected by a saturation of a transition of the form described above.

The case of the non-degenerate transition frequencies using the levels depicted in Fig. 4 can be considered as an illustration. It may be deduced that dynamic saturation of the transition ν_{rp} causes intensity changes for lines having an energy level in common with the level being irradiated. The intensity of the transition ν_{rs} will be reduced for the case where $\Delta m = 0$ and will be enhanced for the case where $\Delta m = 2$ due to the non-equilibrium condition generated by the saturation of the transition ν_{rp}. This observation of intensity changes is termed the nuclear Overhauser effect.[41]

The same intensity changes would also be observed under the conditions where the adiabatic fast passage inequality,

$$\frac{d\nu_2}{dt} << \frac{1}{2\pi} (\gamma H_2)^2 \qquad (65)$$

is met. The phenomenon of adiabatic passage is discussed in detail by Abragam.[42] Under this condition or under the conditions in which the Overhauser effect could occur, one would expect, when ν_2 sweeps through a transition frequency which has an energy level in common with the line being monitored by ν_1, for the recorder pen to show a rise in the absorption signal for the case $\Delta m = 2$ but a dip in the signal for the case $\Delta m = 0$.

In addition to the two possibilities outlined above, it is also necessary to consider the situation where neither of the necessary conditions for either effect are met, but where the intensity H_2 of the perturbing frequency ν_2 is sufficiently large so that, when the bold line representing the field inhomogeneity is swept through a horizontal portion of the graph in Fig. 7, the situation where it will not be overlapping either of the lines will occur both for the case $\Delta m = 0$ and also the case where $\Delta m = 2$. This corresponds to what might be termed the 'normal double-irradiation experiment.' In this case the recorder pen will show dips in the absorption for both $\Delta m = 0$ and $\Delta m = 2$, but the dip will be sharp for $\Delta m = 0$ and broad for the case $\Delta m = 2$ for essentially the same reasons as those discussed above for the ν_1 sweep situation.

III. EXPERIMENTAL

A. Sample Preparation

Trimethylene imine was synthesized according to the method of Vaughan, et al.[43] The sample was purified by repeated distillations in vacuo. The sample, containing a small amount of TMS as an internal reference and a lock signal for the field-frequency control spectrometer, was degassed by the freeze thaw method taking care to prevent exposure of the sample to the atmosphere. The sample tube was then sealed.

1,1-dimethylcyclobutanedicarboxylate was prepared by esterification of 1,1-cyclobutanedicarboxylic acid obtained from Aldrich Chemical Company, and was purified by distillation under vacuum. The sample which contained a small amount of TMS was sealed in a sample tube after repeated degassing by the freeze thaw technique.

Trimethylene sulfide, trimethylene oxide, and cyclobutanone were obtained commercially from Aldrich Chemical Company, and were purified by vapor phase chromatography. The samples were estimated to be greater than 99% pure. Small amounts of TMS were added to each sample. The samples were then degassed and the sample tubes sealed.

B. Instrumentation

1. Construction of a Field-Frequency Lock Spectrometer

It was pointed out in the previous section that conventional high-resolution nuclear magnetic resonance spectra may be recorded either by sweeping the radio-frequency υ_1 or by sweeping the main magnetic field H_o. In both instances the spectra obtained are identical. The magnetic field-sweep experiment is more common mainly because most commercially

available spectrometers operate in the field-sweep mode. Also, sweeping the main magnetic field allows the radio-frequency to be held constant thereby permitting phase sensitive detection at a single frequency. Phase sensitive detection at one frequency is highly desirable from an instrumental point of view since phase shifts and changes in system gains usually accompany frequency changes and would have to be eliminated in a system operating in a frequency mode.

As was also pointed out in the previous section, the frequency-sweep and not the field-sweep technique is the logical method to use for spectral display when performing double-resonance experiments. A spectrum of N lines would require N separate frequency-sweep experiments but N^2-N field-sweep experiments. The required number of field-sweep experiments must be reduced by the number of repeated spacings in the spectrum, but the advantage will still be well on the side of the frequency-sweep method. In consideration of the advantages to be had by using the frequency-sweep method, it was chosen and used exclusively in this work and is therefore described in detail below.

The frequency-sweep experiment requires that the main magnetic field H_o (and ν_2 if also performing double-irradiation experiments) be held constant during the time of one complete scan. Instrumentally, this is not a simple problem. The electro-magnets used in this work are equipped with flux stabilizers[44] which reduce the rapid field fluctuations to an acceptable level for field-sweep experiments (about 1 cps or less). However, the flux stabilizer, in general, will always leave a very slow magnetic field drift. This drift is totally untolerable when operating in a frequency-sweep mode and must therefore be eliminated. Thus, it is necessary to develop a stabilization system capable of elim-

inating both magnetic field fluctuations and also long-term field drifts. Such a system was constructed and developed and is subsequently described.

The stabilization method used in this investigation is one which was originally described by Freeman and Whiffen.[45] The standard Varian Associates spectrometers, the HR-60 and the HR-100, and their associated equipment were used as the basic spectrometers in this work, the additional equipment required having been built up around one or the other of these units depending on whether 60 Mc/sec or 100 Mc/sec spectra were required. The flux stabilizer is an integral part of this system since it may be conveniently adapted to provide the necessary magnetic field control which is required. The flux stabilizer operates in part through a pair of sweep coils, the so-called pickup-coils and the buckout-coils, which are placed on the pole faces on the electromagnetic field. This voltage produces a current through the galvanometer in the flux stabilizer, which in turn results in a dc unbalance. This unbalance is amplified which subsequently causes a change in the dc amplifier current flowing through the buckout coils. In this manner the magnetic field is held constant by the compensating current in the buckout coils. A magnetic field-sweep may be generated by applying a dc voltage to the end of the galvanometer input coil on the flux stabilizer. The field control system will then produce a change in the current in the buckout coils in order to equalize the voltages at the ends of the galvanometer input coils thereby generating a magnetic field sweep; the direction of the field sweep being determined by the sign of the voltage applied to the galvanometer.

To generate a field-frequency servo loop, a dispersion mode signal from an internal reference compound inside the sample instead of a constant dc voltage is fed as an 'error signal' to the galvanometer input

coil. The galvanometer will integrate this signal and a correction to the magnetic field will be generated. Providing that the proper sense of the dispersion mode signal is chosen, random field fluctuations which would cause the reference sample to deviate from the resonance condition will generate a dc signal which, when applied to the buckout coils, will correct the magnetic field so as to maintain the internal reference sample exactly on resonance.

A block diagram of the field-frequency lock spectrometer is given in Fig. (8). The control loop was driven by a single sharp line in the high-resolution spectrum, usually from chloroform or tetramethylsilane (TMS). In order to be able to observe the NMR spectrum in the standard absorption mode, the error signal was excited by a 1000 cps field modulation sideband. This procedure allows the phase of the centerband and the phase of the sideband to be controlled and detected completely independent of each other. This error signal was separated from other audio-frequencies at the output J314 of the Varian Associates V4311 Transmitter[46] unit by means of a synchronous or phase-sensitive detector. The audio frequency sideband signal was generated by a Hewlett-Packard #100D Low Frequency Standard. This low frequency standard was found to possess the required degree of stability which was found to be greater than one part in 10^7. Since the output impedance of the 100D is quite high, its output signal was passed through an audio amplifier with a low output impedance before being fed to the sweep coils of the probe and to the reference channel of the phase-sensitive detector. Before being fed to the sweep coils on the Varian Associates model V4331A[47] probe, the signal was attenuated by means of a 500k one-turn pot. This attenuation is necessary in order to maintain

the non-saturation condition in the sideband resonance. The phase-sensitive detector employed in this control loop was a Princeton Applied Research Co. model #JB-4 Lock-In Amplifier. The #JB-4 was equipped with both a meter and a monitor output jack so that the amplified lock signal of the internal reference sample could be observed either as a dc level on the meter or as a sine wave on an oscilloscope. Because the impedance of the galvanometer input coil on the flux stabilizer is rather low, the output from the #JB-4 was fed to a Philbrick UPA-2 dc operational amplifier with a gain set at about 1:1 and an output impedance of less than 100 Ω . The dc signal was then filtered just sufficiently to remove modulation frequency components. The filtered signal was then applied to the flux stabilizer through the Varian Associates #V3507 Slow Sweep Unit with the unit operating in the Fast X 100 position. With the switch in this position, only a 15k resistor is placed between the filtered output of the dc amplifier and the galvanometer input coil. A separate 10k ten-turn pot was placed after the filtered output in order to control the output gain to the flux stabilizer. It is extremely important to maintain the overall control loop gain sufficiently low in order to prevent the loop from going into oscillation.

It was previously stated that the flux stabilizer operates in part through the buckout coils of the electromagnet. These coils have a time constant which is of the order of 0.5 sec. Therefore in this field-frequency lock mode of operation there is a distinct tendency from the system to 'hunt' at a frequency determined by this time constant. This 'hunting' makes itself apparent as a slight oscillation in the control loop sine wave signal. It has been found that this stability can be eliminated if the high-frequency response is improved by feeding the

error signal not only to the flux stabilizer but also to the "modulation" terminals of the V4311 transmitter unit. A signal fed into these terminals is first filtered and then applied to a negatively biased solid-state diode. The error signal will pull the solid-state diode in such a way as to cause it to change the oscillator frequency in a manner which will restore the resonance condition for the internal reference sample.

The overall resulting situation is rather complex where fast perturbations of the magnetic field, caused for example by the rapid movement of magnetic objects, are compensated for initially by a rapid change in the radio frequency caused by slightly varying the bias on the solid-state diode, and then by slower magnetic field changes with a simultaneous return of the radio-frequency to its normal value. The flux stabilizer part of the control loop is quite indespensible because of its very much wider range of control, but the system will operate without the frequency control. When the frequency control loop is being used, it is extremely important to avoid modulation frequency components in the error signal fed to the rf unit since they generate frequency modulation sidebands which are, in general, out of phase with the field modulation sidebands. The output for this control loop was taken from the same dc operational amplifier and filter network. However, a separate pot was provided to control the gain of this loop completely independently of the gain of the loop involving the flux stabilizer. It was found that this field-frequency lock maintains the Larmor, ω-1000 = $\gamma_{TMS}H_{TMS}$ condition within a range of about 0.1 cps or about ±1 part in 109 for a period of several days. In fact, the system controlled the field or frequency to better than 0.01 cps or about ±1-2 parts in 10^{10} for periods of up to hours at a time. Probably the most

important factor here is the stability of the low frequency standard. It was found that the oscillator performed quite well if protected from drafts, allowed to warm up sufficiently, connected to well regulated power sources, and kept in good repair.

In order to excite and observe proton resonance spectra, a variable frequency audio oscillator operating in the range of 400 to 1000 cps is required. This oscillator will produce a second set of sidebands by which all proton resonances may be observed. This second set of sidebands by which all proton resonances may be observed. This second set of audio frequency sidebands were generated by means of a Quan Tech model #304 Wave Analyzer which was capable of sweeping ranges from 50 cps to 5000 cps at rates of 18 sec., 180 sec., or 1800 sec. at a linear rate. Frequency control and sweep is affected by means of a voltage-controlled oscillator (VCO) in the #304. The VCO is electronically also available at an output jack for operating an X-Y recorder. This allows the recorder to be swept simultaneously with the frequency which has the highly desirable advantage of automatically providing precalibrated spectra with essentially no effort. This oscillator not only met the stringent stability requirements, but also provided a three-way single/auto/reset scan switch for producing single or repetitive scans.

It is then necessary to separate out the signals excited by the variable frequency oscillator from all other audio frequency signals. This problem becomes somewhat involved because, in general, electronic equipment such as amplifiers and other phase sensitive equipment, etc., show phase shifts as functions of the audio frequency. It is also necessary to insure that amplifier gains remain constant over the region of frequency which is of interest or at least over the frequency region

of a given scan. Therefore, a lock-in amplifier was designed and constructed to accomodate these requirements as well as possible. A schematic circuit diagram of this lock-in amplifier is given in Fig. (9). In this lock-in amplifier the reference signal from the #304 wave analyzer is fed into the reference audio amplifier. The signal is then amplified and fed to the NMR probe and also to the phase shift curcuit and finally to the reference channel of the phase-sensitive detector. In the phase shift network the resistance of the 50CK resistor and the capacitive inpedance of the $0.01_{\mu f}$ capacitor are maintained in at least a 10:1 ratio to reduce any frequency dependent phase shifts to a minimum. The signal from the spectrometer (J314) in addition to being fed to the signal channel of the #JB-4 is also fed to the signal channel of this lock-in amplifier. The signal is first passed through an audio amplifier which contains a feed-back network which is designed to maintain wide flat audio frequency response throughout the frequency range of interest. The amplified signal is than fed into the signal channel of the phase-sensitive detector. The dc phase-sensitive detected signal from this lock-in amplifier is then fed to a second Philbrick UPA-2 dc operational amplifier. This amplifier has its gain set at about 18:1 and an output impedance of approximately 1000 Ω . This impedance is sufficiently low to drive any X-Y recorder. Before feeding the signal to the X-Y recorder the amplified dc output was passed through a filter network where it was possible to filter the signal at 0.1 cps, 0.25 cps, 0.5 cps, 1.0 cps, and 2.0 cps. This filter network is quite similar to that used in the Varian Associates #V3521A Integrator/Spin Decoupler and is described in the corresponding Varian Instruction Manual.

The perturbing field H_2 was then provided by a third field modula-

tion. For this an extremely stable oscillator is required, especially when scanning very small segments of the spectrum. A Hewlett-Packard oscillator model #204B was found to have the required stability and a conveniently fine frequency vernier for adjustment of ν_2. The stability of this oscillator was better than 0.001 cps or about 1 part in 10^6. Since the #204B is a battery powered oscillator, it has an extremely low current output. It was, therefore, found necessary to increase the output by passing the signal through an audio amplifier before feeding the signal to the sweep coils. An output balanced at 600 Ω above ground was used in order to avoid "ground loops".

Should it be desirable to do multiple irratiation experiments, the apparatus should require no modification other than the addition of extra oscillators. The additional field modulations should be impressed at higher modulation indices on the sweep coils. Such additions and changes will probably necessitate some adjustments in the phases and gains in the system, but no other changes would be anticipated.

2. Spectral Data

The majority of the spectra to be described in the following sections were taken on either the HR-60 or the HR-100 spectrometers modified as discussed in the previous section. The operation of a field-frequency lock spectrometer is in no way a simple task. In this respect the author feels it would be well worth while to discuss some of the operational aspects of the spectrometer.

The spectrometer is 'locked' to a TMS sideband signal by properly centering the signal on a scope and then switching on the control loops. For a given phase adjustment, only one of the two sideband responses

is in the correct sense for regulation, and this was always chosen to be the low-field sideband. The spectrometer invariably locked on to the TMS signal, which was evidenced by the appearance of the 1kc signal at the signal monitor output of the #JB-4 lock-in amplifier and also by an appreciable reading on the voltmeter of the #JB-4.

One of the adjustment problems in this system is to get the phase of the locking loops adjusted correctly. The control loop through the V4311 was adjusted easily by observing the locking signal on the oscilloscope and maximizing this signal with the rf phase control adjustment of the V4311 unit when only this control loop was connected. The control loop through the flux stabilizer can then be adjusted by first turning on the loop and then adjusting the phase control on the #JB-4 to a maximum signal on the scope.

By monitoring the signal from J314 before it entered the phase detector of the #JB-4 but after it passed through its narrow-band preamplifier, it was possible to detect rather small changes in the homogeneity of the magnetic field of the order of 1-2 parts in 10^{10}. If a small drop in the intensity of the signal on the scope due to a slight degradation of the field resulted, it was quite easy to optimize the homogeneity again with the 10-turn pot for the HR-60 or the fine control for the HR-100 of the magnetic field Y-gradient control even while recording a spectrum.

In the field-frequency mode of operation it is quite important to prevent interference between the sidebands and also to avoid saturation of the sideband responses. This was accomplished by setting the rf centerband power far above its normal value in the HR mode of operation and keeping only a very small amount of power in the sidebands. Doing

this sets the modulation indeces very low thereby preventing saturation, loop oscillation, and sideband interference. Signals were taken from J314 at the wide-line phase-dector output with the receiver gain set at 3 or 4, a low impednace point with a response extending to high audio frequencies (i.e., ahead of the filter circuits).

As has been previously pointed out, there are two types of frequency-sweep experiment that one can perform when doing double-resonance with a frequency-field lock spectrometer. The equipment involved in both experiments is identical although the use of the equipment is slightly different and the procedures involved for the two types of experiment are vastly different. Therefore the procedures for each experiment will be discussed separately.

The perturbing field is set somewhat higher in modulation index than the observing field H_1 so that the condition $\frac{1}{2\pi}\gamma H_2 \approx \Delta\nu$ is met, where $\Delta\nu$ is the width of the line to be observed. The procedure for irradiating a single non-degenerate transition is to sweep the frequency up to the line and stop exactly on the line. The irradiating field H_2 is then turned on at a frequency near ν_1 and the beat frequency between ν_1 and ν_2 minimized as much as possible by tuning ν_2. After a single scan of the spectrum, ν_2 could be adjusted so as to make the intensities of the two components of the doublet equal. Spectra are then run in the normal manner just as is done when the perturbing field H_2 is absent.

In order to perform the experiment wherein the perturbing frequency ν_2 is swept while observing a single transition with ν_1, the function of the #304 wave analyzer's oscillator and the HP #204B oscillator must be reversed. This first involves connecting the output of the #204B to the reference channel input of the wide-band lock-in amplifier and subsequently

connecting the output of the #304 to the sweep coils of the probe through an audio amplifier with an output balanced at 600 Ω above ground.

Once the peak to be observed during a single scan was determined, the frequency having first been accurately determined from a precalibrated spectrum, ν_1 (now generated from the #204B instead of the #304) was swept as close to the center of the line as possible. The frequency of the oscillator was always continuously monitored on a frequency counter. Once ν_1 was found to be sufficiently close the fine control of the #204B could then be adjusted until a maximum deflection of the recorder pen was observed. Due to the extremely narrow linewidths (of the order of magnitude of 0.2 cps full width at one-half peak height), it was found to be generally necessary to sweep back and forth through the peak several times, each time adjusting ν_1 very slightly in order to determine the maximum amplitude and consequently the best setting. In these experiments the perturbing field was always swept at a rate of 50 cps/1800 sec (ca. 0.03 cps/sec) using a filter bandwidth of 0.1 cps. It was also found to be quite important to have ν_1 sitting exactly on the center of the resonant line. The #204B oscillator was sufficiently stable so that only a very small oscillation about the height of the peak could be observed. Also, essentially no drift of the frequency ν_1 during the time of a single scan (1800 sec) could be observed.

In addition to the experiment where ν_2 is swept, studies were carried out by pulsing H_2 at the frequency ν_2, while ν_1 was monitoring a line with an energy level in common with the line being perturbed by the pulse. If the amplitude H_2 is fairly large and the duration of the pulse t_w is short, relaxation effects during the on period will be negligible and the total effect will be to rotate the macroscopic mag-

nteization vector M through an angle α given by the expression

$$\alpha = \gamma H_2 L_{ab} t_w \qquad (66)$$

where L_{ab} is the appropriate transition moment. An excellent description of the pulse experiment may be found in Pople, et al.[48] Pulses for which $\gamma H_2 L_{ab} t_w = \pi$ are referred to as 180° or π pulses and have the effect of completely reversing the direction of M. Abragam[49] has shown that under the proper experimental conditions adiabatic rapid passage and pulse experiments yield the same results. The π pulses used in these experiments were generated first by setting t_w = ca 0.5 sec and then emperically adjusting H_2 for a maximum response.

In addition to the HR-60 and the HR-100 spectra, some spectra were run on a Varian A-60 chiefly for calibration pruposes.

IV. RESULTS

A. Complete Analysis of the Nuclear Magnetic Resonance Spectra of Trimethylene Sulfide, Trimethylene Imine, Trimethylene Oxide, and 1,1-Dimethylcyclobutane Dicarboxylate

In this section the results of the analyses of the NMR spectra of a series of four-membered ring compounds of the type A_2B_4 are presented. Analyses of the spectra of this type have never been studied in detail before because of a number of reasons. Probably the most critical of these reasons is that although there are six protons on a molecule, there are only two 'chemically' different types. For the purposes of this dissertation a set of nuclei will be considered to be chemically equivalent if each nucleus of the set possesses the same electronic environment. It is possible for a set of nuclei to be chemically equivalent without all the nuclei in the set being magnetically equivalent, magnetic equivalence implying that each nucleus in the set couples to all other nuclei in the same identical manner. Thus, in methane, for example, all protons are in the same electronic environment and all possible coupling constants are identical. Therefore, the protons in methane are said to be both chemically and magnetically equivalent. However, in $CH_2 = CF_2$[50] the two hydrogen atoms form one chemically equivalent set and the two fluorine atoms another. Although the fluorine atoms and hydrogen atoms each form a chemically equivalent set, the spin coupling constants between hydrogen and fluorine are different for the cis and trans positions. Therefore, the two hydrogens are said to be magnetically inequivalent and, likewise, the two fluorine atoms, although being chemically equivalent do not possess magnetic equivalence. In this terminology magnetic equivalence presupposes chemical equivalence, the converse not being true; chemical equivalence does not presuppose magnetic equivalence.

This distinction between chemical and magnetic equivalence is a critical one in terms of the analysis of the A_2B_4 four-membered ring system. It is well known in NMR that the spectrum due to two magnetic equivalent sets of nuclei will be completely independent of the coupling constants within the sets. The two groups of nuclei, A and B, each constitute a set of chemically equivalent nuclei. However, the two A protons are not magnetically equivalent since the cis and trans coupling constants, in general, will be different. The four B protons will also not be magnetically equivalent for the same reason. In addition the two possible long range coupling constants, if significant, would not be expected to be equal. It can then be seen that, since these two sets of protons are not magnetically equivalent, one would expect some transitions in the spectra of these molecules to depend on the geminal coupling constants, J_{12} and J_{56} (See Fig. 10), and also on the cross ring or "long range" coupling constants. This means that the spectra should be a function of all the parameters (i.e., chemical shifts and coupling constants) in the molecules. This type of parameter dependency involving chemically equivalent groups has been demonstrated in the past for two sets of two chemically equivalent protons, the A_2B_2 case.[51] Analyses of these systems, in general, should also yield the relative signs of the coupling constants, a matter which until quite recently was a subject of considerable controversy.

The ability to observe the coupling constants between chemically equivalent protons in these A_2B_4 systems will be determined to a large part by the magnitude of the chemical shift, ν_{AB}, between the A and B protons. Generally, in systems of this sort it is the presence of the so-called "higher order effects" which allow the transitions between

chemically equivalent protons to be observed. The "higher order effects" become important in complex spin systems when the chemical shifts between different nuclei are of the same order of magnitude as the coupling constants between the different nuclei. In these situations, the resulting spectra cannot be completely explained solely in terms of first-order perturbation theory. Complete analyses of such spectra can only be affected by a solution of the resulting secular equations. In considering these "higher order effects", say by considering second-order perturbation theory, account is taken of the mixing of states between which there are off-diagonal matrix elements. This has the effect of both removing degeneracies and also of allowing other additional transitions whose intensities would otherwise be identically zero. In the four-membered ring A_2B_4 systems of interest, it will be the observation of these additional transitions which will yield the geminal and cross-ring coupling constants, since they will be the transitions that possess geminal and cross-ring coupling constant dependency.

In order for the statements of the previous paragraph to be more fully understood, it is necessary to consider in detail the appropriate basis functions and Hamiltonian matrix for the A_2B_4 system. It would be possible to take as a set of basis functions, the simple product functions and classify them according to their total spin component F_z. However, it will be more convenient to choose as basis functions, those functions which form irreducible representations of the appropriate point group for the molecules. With the exception of trimethylene imine,[52] the point group for these molecules will be D_2, where $D_2 = C_{2V} \otimes C_i$. However the symmetrized spin functions can be calculated using the C_{2V} point group since C_i will not provide any new information as concerns the NMR spectra. The basis functions for this case

are listed in Table I, in the C_{2V} representation. These basis functions will be helpful in understanding some features of these A_2B_4 systems and also the double-irradiation experiments to be described.

From the listing of the A_2B_4 symmetrized spin functions it is evident that there will be only four transitions in an entire spectrum for which analytical expressions can be obtained. These transitions will belong to the A_1 element and will result from considering the 1×1 and 2×2 elements for $F_z = \pm 3$ and ± 2, the 2×2 submatrix diagonalizations being a trivial process. The Hamiltonian used to calculate these elements is the standard NMR Hamiltonian given in Eq. (44).

The part of the Hamiltonian matrix for $F_z = \pm 2$ and ± 3 then takes the form

$$M_a = \begin{pmatrix} \mathcal{H}_{11} & 0 & 0 \\ 0 & \mathcal{H}_{22} & \mathcal{H}_{23} \\ 0 & \mathcal{H}_{23} & \mathcal{H}_{23} \end{pmatrix} \qquad M_b = \begin{pmatrix} \mathcal{H}_{24\ 24} & 0 & 0 \\ 0 & \mathcal{H}_{23\ 23} & \mathcal{H}_{22\ 23} \\ 0 & \mathcal{H}_{22\ 23} & \mathcal{H}_{22\ 22} \end{pmatrix}$$

$F_z = +3$ and $+2$ $\qquad$ $F_z = -3$ and -2

where

$$\mathcal{H}_{11} = \langle \alpha\alpha\alpha\alpha\alpha\alpha \,|\mathcal{H}|\, \alpha\alpha\alpha\alpha\alpha\alpha \rangle$$

$$\mathcal{H}_{11} = \nu_A + 2\nu_B + \frac{1}{4} J_{gem} + J_{vic} + J'_{vic} + \frac{1}{2} J'_{gem} + \frac{1}{2}(J_{diag} + J'_{diag}) \tag{67}$$

$$\mathcal{H}_{22} = \frac{1}{4} \langle \alpha\alpha\alpha\alpha\alpha\beta + \alpha\beta\alpha\alpha\alpha\alpha + \alpha\alpha\alpha\alpha\beta\alpha + \beta\alpha\alpha\alpha\alpha\alpha \,|\mathcal{H}|\, \alpha\alpha\alpha\alpha\alpha\beta + \alpha\beta\alpha\alpha\alpha\alpha + \alpha\alpha\alpha\alpha\beta\alpha + \beta\alpha\alpha\alpha\alpha\alpha \rangle$$

$$\mathcal{H}_{22} = \nu_A + \nu_B + \frac{1}{4} J_{gem} + \frac{1}{2}(J_{diag} + J'_{diag}) + \frac{1}{2}(J_{vic} + J'_{vic}) \tag{68}$$

$$\mathcal{H}_{33} = \frac{1}{2}\langle \alpha\alpha\alpha\beta\alpha\alpha + \alpha\alpha\beta\alpha\alpha\alpha \,|\mathcal{H}|\, \alpha\alpha\alpha\beta\alpha\alpha + \alpha\alpha\beta\alpha\alpha\alpha\rangle$$

$$\mathcal{H}_{33} = 2\nu_B + \frac{1}{4}J_{gem} + \frac{1}{2}J'_{gem} + \frac{1}{2}(J_{diag} + J'_{diag}) \qquad (69)$$

$$\mathcal{H}_{23} = \mathcal{H}_{22\ 23} = \frac{1}{4}\sqrt{2}\,\langle \alpha\alpha\alpha\beta\alpha\alpha + \alpha\alpha\beta\alpha\alpha\alpha \,|\mathcal{H}|\, \alpha\alpha\alpha\alpha\alpha\beta + \alpha\beta\alpha\alpha\alpha\alpha + \alpha\alpha\alpha\alpha\beta\alpha + \beta\alpha\alpha\alpha\alpha\alpha\rangle = \frac{1}{2}\sqrt{2}\,(J_{vic} + J'_{vic}) \qquad (70)$$

$$\mathcal{H}_{22\ 22} = \frac{1}{2}\langle \beta\beta\alpha\beta\beta\beta + \beta\beta\beta\alpha\beta\beta \,|\mathcal{H}|\, \beta\beta\alpha\beta\beta\beta + \beta\beta\beta\alpha\beta\beta\rangle$$

$$= -2\nu_B + \frac{1}{4}J_{gem} + \frac{1}{2}J'_{gem} + \frac{1}{2}(J_{vic} + J'_{vic}) \qquad (71)$$

$$\mathcal{H}_{23\ 23} = \frac{1}{4}\langle \beta\beta\beta\beta\beta\alpha + \beta\alpha\beta\beta\beta\beta + \beta\beta\beta\beta\alpha\beta + \alpha\beta\beta\beta\beta\beta \,|\mathcal{H}|\, \beta\beta\beta\beta\beta\alpha + \beta\alpha\beta\beta\beta\beta + \beta\beta\beta\beta\alpha\beta + \alpha\beta\beta\beta\beta\beta\rangle = -\nu_A - \nu_B + \frac{1}{4}J_{gem} + \frac{1}{2}(J_{vic} + J'_{vic}) + (J_{diag} + J'_{diag}) \qquad (72)$$

$$\mathcal{H}_{24\ 24} = \langle \beta\beta\beta\beta\beta\beta \,|\mathcal{H}|\, \beta\beta\beta\beta\beta\beta\rangle = -\nu_A - 2\nu_B + \frac{1}{4}J_{gem} + J_{vic} + J'_{vic} + \frac{1}{2}J'_{gem} + \frac{1}{2}(J_{diag} + J'_{diag}) \qquad (73)$$

where

$$J_{vic} = J_{13} = J_{35} = J_{24} = J_{46}$$
$$J'_{vic} = J_{14} = J_{45} = J_{23} = J_{36}$$
$$J_{gem} = J_{34}$$
$$J'_{gem} = J_{12} = J_{56}$$
$$J_{diag} = J_{15} = J_{26}$$
$$J'_{diag} = J_{16} = J_{25} \qquad (74)$$

Table I

A_1 Basic Symmetry Functions for Six Nuclei A_2B_4

			F_z
$1\ (A_1)_3$	$\alpha\alpha\alpha\alpha\alpha\alpha$	1×1	3
$1\ (A_1)_2$	$\frac{1}{2}(\alpha\alpha\alpha\alpha\alpha\beta + \alpha\beta\alpha\alpha\alpha\alpha + \alpha\alpha\alpha\alpha\beta\alpha + \beta\alpha\alpha\alpha\alpha\alpha)$	2×2	2
$2\ (A_1)_2$	$\frac{1}{\sqrt{2}}(\alpha\alpha\alpha\beta\alpha\alpha + \alpha\alpha\beta\alpha\alpha\alpha)$		
$1\ (A_1)_1$	$\frac{1}{\sqrt{2}}(\alpha\alpha\alpha\alpha\beta\beta + \beta\beta\alpha\alpha\alpha\alpha)$		
$2\ (A_1)_1$	$\frac{1}{2}(\alpha\alpha\alpha\beta\alpha\beta + \alpha\beta\beta\alpha\alpha\alpha + \alpha\alpha\beta\alpha\beta\alpha + \beta\alpha\alpha\beta\alpha\alpha)$		
$3\ (A_1)_1$	$\frac{1}{\sqrt{2}}(\beta\alpha\alpha\alpha\alpha\beta + \alpha\beta\alpha\alpha\beta\alpha)$	6×6	1
$4\ (A_1)_1$	$\frac{1}{2}(\alpha\alpha\alpha\beta\beta\alpha + \beta\alpha\beta\alpha\alpha\alpha + \alpha\alpha\beta\alpha\alpha\beta + \alpha\beta\alpha\beta\alpha\alpha)$		
$5\ (A_1)_1$	$\frac{1}{\sqrt{2}}(\beta\alpha\alpha\alpha\beta\alpha + \alpha\beta\alpha\alpha\alpha\beta)$		
$6\ (A_1)_1$	$\alpha\alpha\beta\beta\alpha\alpha$		
$1\ (A_1)_0$	$\frac{1}{2}(\beta\beta\beta\alpha\alpha\alpha + \alpha\alpha\alpha\beta\beta\beta + \alpha\alpha\beta\alpha\beta\beta + \beta\beta\alpha\beta\alpha\alpha)$		
$2\ (A_1)_0$	$\frac{1}{2}(\alpha\beta\alpha\alpha\beta\beta + \beta\beta\alpha\alpha\alpha\beta + \beta\alpha\alpha\alpha\beta\beta + \beta\beta\alpha\alpha\beta\alpha)$		
$3\ (A_1)_0$	$\frac{1}{2}(\alpha\alpha\beta\beta\beta\alpha + \beta\alpha\beta\beta\alpha\alpha + \alpha\alpha\beta\beta\alpha\beta + \alpha\beta\beta\beta\alpha\alpha)$	6×6	0
$4\ (A_1)_0$	$\frac{1}{\sqrt{2}}(\alpha\beta\alpha\beta\beta\alpha + \beta\alpha\beta\alpha\alpha\beta)$		
$5\ (A_1)_0$	$\frac{1}{2}(\beta\alpha\alpha\beta\beta\alpha + \beta\alpha\beta\alpha\beta\alpha + \alpha\beta\beta\alpha\alpha\beta + \alpha\beta\alpha\beta\alpha\beta)$		
$6\ (A_1)_0$	$\frac{1}{\sqrt{2}}(\beta\alpha\alpha\beta\alpha\beta + \alpha\beta\beta\alpha\beta\alpha)$		
$1\ (A_1)_{-1}$	$\frac{1}{\sqrt{2}}(\alpha\alpha\beta\beta\beta\beta + \beta\beta\beta\beta\alpha\alpha)$		
$2\ (A_1)_{-1}$	$\frac{1}{2}(\alpha\beta\alpha\beta\beta\beta + \beta\beta\beta\alpha\alpha\beta + \beta\alpha\beta\alpha\beta\beta + \beta\beta\alpha\beta\beta\alpha)$		
$3\ (A_1)_{-1}$	$\frac{1}{2}(\beta\alpha\alpha\beta\beta\beta + \beta\beta\beta\alpha\beta\alpha + \alpha\beta\beta\alpha\beta\beta + \beta\beta\alpha\beta\alpha\beta)$	6×6	-1
$4\ (A_1)_{-1}$	$\frac{1}{2}(\alpha\beta\beta\beta\alpha\beta + \beta\alpha\beta\beta\beta\alpha)$		
$5\ (A_1)_{-1}$	$\frac{1}{2}(\beta\alpha\beta\beta\alpha\beta + \alpha\beta\beta\beta\beta\alpha)$		
$6\ (A_1)_{-1}$	$\beta\beta\alpha\alpha\beta\beta$		

Table I. (Continued)

			F_z
$1\ (A_1)_{-2}$	$\frac{1}{2}(\beta\beta\beta\beta\beta\alpha + \beta\alpha\beta\beta\beta\beta + \beta\beta\beta\beta\alpha\beta + \alpha\beta\beta\beta\beta\beta)$	2×2	-2
$2\ (A_1)_{-2}$	$\frac{1}{\sqrt{2}}(\beta\beta\alpha\beta\beta\beta + \beta\beta\beta\alpha\beta\beta)$		
$1\ (A_1)_{-3}$	$\beta\beta\beta\beta\beta\beta$	1×1	-3

A_2 Basic Symmetry Functions for Six Nuclei A_2B_4

			F_z
$1\ (A_2)_2$	$\frac{1}{2}(\alpha\alpha\alpha\alpha\alpha\beta + \alpha\beta\alpha\alpha\alpha\alpha - \alpha\alpha\alpha\alpha\beta - \beta\alpha\alpha\alpha\alpha\alpha)$	1×1	2
$1\ (A_2')_1$	$\frac{1}{2}(\alpha\alpha\alpha\beta\alpha\beta + \alpha\beta\beta\alpha\alpha\alpha - \alpha\alpha\beta\alpha\beta\alpha - \beta\alpha\alpha\beta\alpha\alpha)$		
$2\ (A_2')_1$	$\frac{1}{2}(\alpha\alpha\beta\alpha\alpha\beta + \alpha\beta\alpha\beta\alpha\alpha - \alpha\alpha\alpha\beta\beta\alpha - \beta\alpha\beta\alpha\alpha\alpha)$	3×3	1
$3\ (A_2)_1$	$\frac{1}{\sqrt{2}}(\alpha\beta\alpha\alpha\alpha\beta - \beta\alpha\alpha\alpha\beta\alpha)$		
$1\ (A_2)_0$	$\frac{1}{2}(\alpha\alpha\alpha\beta\beta\beta + \beta\beta\beta\alpha\alpha\alpha - \alpha\alpha\beta\alpha\beta\beta - \beta\beta\alpha\beta\alpha\alpha)$		
$2\ (A_2)_0$	$\frac{1}{2}(\alpha\beta\alpha\alpha\beta\beta + \beta\beta\alpha\alpha\alpha\beta - \beta\alpha\alpha\alpha\beta\beta - \beta\beta\alpha\alpha\beta\alpha)$	4×4	0
$3\ (A_2)_0$	$\frac{1}{2}(\alpha\alpha\beta\beta\beta\alpha + \beta\alpha\beta\beta\alpha\alpha - \alpha\alpha\beta\beta\alpha\beta - \alpha\beta\beta\beta\alpha\alpha)$		
$4\ (A_2)_0$	$\frac{1}{2}(\beta\alpha\alpha\beta\beta\alpha + \beta\alpha\beta\alpha\beta\alpha - \alpha\beta\beta\alpha\alpha\beta - \alpha\beta\alpha\beta\alpha\beta)$		
$1\ (A_2)_{-1}$	$\frac{1}{2}(\alpha\beta\alpha\beta\beta\beta + \beta\beta\beta\alpha\alpha\beta - \beta\alpha\beta\alpha\beta\beta - \beta\beta\alpha\beta\beta\alpha)$		
$2\ (A_2)_{-1}$	$\frac{1}{2}(\beta\alpha\alpha\beta\beta\beta + \beta\beta\beta\alpha\beta\alpha - \alpha\beta\beta\alpha\beta\beta - \beta\beta\alpha\beta\alpha\beta)$	3×3	-1
$3\ (A_2)_{-1}$	$\frac{1}{\sqrt{2}}(\alpha\beta\beta\beta\alpha\beta - \beta\alpha\beta\beta\beta\alpha)$		
$1\ (A_2)_{-2}$	$\frac{1}{2}(\beta\beta\beta\beta\beta\alpha + \beta\alpha\beta\beta\beta\beta - \beta\beta\beta\beta\alpha\beta - \alpha\beta\beta\beta\beta\beta)$	1×1	-2

B_1 Basic Symmetry Functions for Six Nuclei A_2B_4

			F_z
1 $(B_1)_2$	$\frac{1}{2}(\alpha\alpha\alpha\alpha\alpha\beta - \alpha\beta\alpha\alpha\alpha\alpha - \alpha\alpha\alpha\alpha\beta\alpha + \beta\alpha\alpha\alpha\alpha\alpha)$	2×2	2
2 $(B_1)_2$	$\frac{1}{2}(\alpha\alpha\alpha\beta\alpha\alpha - \alpha\alpha\beta\alpha\alpha\alpha)$		
1 $(B_1)_1$	$\frac{1}{2}(\alpha\alpha\alpha\beta\alpha\beta - \alpha\beta\beta\alpha\alpha\alpha - \alpha\alpha\beta\alpha\beta\alpha + \beta\alpha\alpha\beta\alpha\alpha)$		
2 $(B_1)_1$	$\frac{1}{2}(\alpha\alpha\beta\alpha\alpha\beta - \alpha\beta\alpha\beta\alpha\alpha - \alpha\alpha\alpha\beta\beta\alpha + \beta\alpha\beta\alpha\alpha\alpha)$	3×3	1
3 $(B_1)_1$	$\frac{1}{\sqrt{2}}(\beta\alpha\alpha\alpha\alpha\beta - \alpha\beta\alpha\alpha\beta\alpha)$		
1 $(B_1)_0$	$\frac{1}{2}(\alpha\alpha\alpha\beta\beta\beta - \beta\beta\beta\alpha\alpha\alpha - \alpha\alpha\beta\alpha\beta\beta + \beta\beta\alpha\beta\alpha\alpha)$		
2 $(B_1)_0$	$\frac{1}{2}(\alpha\beta\alpha\alpha\beta\beta - \beta\beta\alpha\alpha\alpha\beta - \beta\alpha\alpha\alpha\beta\beta + \beta\beta\alpha\alpha\beta\alpha)$		
3 $(B_1)_0$	$\frac{1}{2}(\alpha\alpha\beta\beta\beta\alpha - \beta\alpha\beta\beta\alpha\alpha - \alpha\alpha\beta\beta\alpha\beta + \alpha\beta\beta\beta\alpha\alpha)$	6×6	0
4 $(B_1)_0$	$\frac{1}{\sqrt{2}}(\alpha\beta\alpha\beta\beta\alpha - \beta\alpha\beta\alpha\alpha\beta)$		
5 $(B_1)_0$	$\frac{1}{2}(\beta\alpha\alpha\beta\beta\alpha - \beta\alpha\beta\alpha\beta\alpha - \alpha\beta\beta\alpha\alpha\beta + \alpha\beta\alpha\beta\alpha\beta)$		
6 $(B_1)_0$	$\frac{1}{\sqrt{2}}(\beta\alpha\alpha\beta\alpha\beta - \alpha\beta\beta\alpha\beta\alpha)$		
1 $(B_1)_{-1}$	$\frac{1}{2}(\alpha\beta\alpha\beta\beta\beta - \beta\beta\beta\alpha\alpha\beta - \beta\alpha\beta\alpha\beta\beta + \beta\beta\alpha\beta\beta\alpha)$		
2 $(B_1)_{-1}$	$\frac{1}{2}(\beta\alpha\alpha\beta\beta\beta - \beta\beta\beta\alpha\alpha\beta - \beta\alpha\beta\alpha\beta\beta + \beta\beta\alpha\beta\beta\alpha)$	3×3	-1
3 $(B_1)_{-1}$	$\frac{1}{\sqrt{2}}(\beta\alpha\beta\beta\alpha\beta - \alpha\beta\beta\beta\beta\alpha)$		
1 $(B_1)_{-2}$	$\frac{1}{2}(\beta\beta\beta\beta\beta\alpha - \beta\alpha\beta\beta\beta\beta - \beta\beta\beta\beta\beta\alpha\beta + \alpha\beta\beta\beta\beta\beta)$	2×2	-2
2 $(B_1)_{-2}$	$\frac{1}{\sqrt{2}}(\beta\beta\beta\alpha\beta\beta - \beta\beta\alpha\beta\beta\beta)$		

B_2 Basic Symmetry Functions for Six Nuclei A_2B_4

			F_z
$(B_2)_2$	$\frac{1}{2}(\alpha\alpha\alpha\alpha\alpha\beta - \alpha\beta\alpha\alpha\alpha\alpha + \alpha\alpha\alpha\alpha\beta\alpha - \beta\alpha\alpha\alpha\alpha\alpha)$	1×1	2

Table I. (Continued)

			F_z
$(B_2)_1$	$\frac{1}{\sqrt{2}}(\alpha\alpha\alpha\alpha\beta\beta - \beta\beta\alpha\alpha\alpha\alpha)$		
$(B_2)_1$	$\frac{1}{2}(\alpha\alpha\alpha\beta\alpha\beta - \alpha\beta\beta\alpha\alpha\alpha + \alpha\alpha\beta\alpha\beta\alpha - \beta\alpha\alpha\beta\alpha\alpha)$	3×3	1
$(B_2)_1$	$\frac{1}{2}(\alpha\alpha\beta\alpha\alpha\beta - \alpha\beta\alpha\beta\alpha\alpha + \alpha\alpha\alpha\beta\beta\alpha - \beta\alpha\beta\alpha\alpha\alpha)$		
$(B_2)_0$	$\frac{1}{2}(\alpha\alpha\alpha\beta\beta\beta - \beta\beta\beta\alpha\alpha\alpha + \alpha\alpha\beta\alpha\beta\beta - \beta\beta\alpha\beta\alpha\alpha)$		
$(B_2)_0$	$\frac{1}{2}(\alpha\beta\alpha\alpha\beta\beta - \beta\beta\alpha\alpha\alpha\beta + \beta\alpha\alpha\alpha\beta\beta - \beta\beta\alpha\alpha\beta\alpha)$	4×4	0
$(B_2)_0$	$\frac{1}{2}(\alpha\alpha\beta\beta\beta\alpha - \beta\alpha\beta\beta\alpha\alpha + \alpha\alpha\beta\beta\alpha\beta - \alpha\beta\beta\beta\alpha\alpha)$		
$(B_2)_0$	$\frac{1}{2}(\beta\alpha\alpha\beta\beta\alpha - \beta\alpha\beta\alpha\beta\alpha + \alpha\beta\beta\alpha\alpha\beta - \alpha\beta\alpha\beta\alpha\beta)$		
$(B_2)_{-1}$	$\frac{1}{\sqrt{2}}(\alpha\alpha\beta\beta\beta\beta - \beta\beta\beta\beta\alpha\alpha)$		
$(B_2)_{-1}$	$\frac{1}{2}(\alpha\beta\alpha\beta\beta\beta - \beta\beta\beta\alpha\alpha\beta + \beta\alpha\beta\alpha\beta\beta - \beta\beta\alpha\beta\beta\alpha)$	3×3	-1
$(B_2)_{-1}$	$\frac{1}{2}(\beta\alpha\alpha\beta\beta\beta - \beta\beta\beta\alpha\beta\alpha + \alpha\beta\beta\alpha\beta\beta - \beta\beta\alpha\beta\alpha\beta)$		
$(B_2)_{-2}$	$\frac{1}{2}(\beta\beta\beta\beta\beta\alpha - \beta\alpha\beta\beta\beta\beta + \beta\beta\beta\beta\alpha\beta - \alpha\beta\beta\beta\beta\beta)$	1×1	-2

In an equivalent shorter notation M_a and M_b can be represented by the following matrices,

$$M_a = \begin{pmatrix} \nu_A + 2\nu_B + \gamma + \epsilon & 0 & 0 \\ 0 & \nu_A + \nu_B + \gamma + \frac{1}{2}\epsilon & \frac{\sqrt{2}}{2}\epsilon \\ 0 & \frac{\sqrt{2}}{2}\epsilon & 2\nu_B + \gamma \end{pmatrix}$$

$$M_b = \begin{pmatrix} -\nu_A - 2\nu_B + \gamma + \epsilon & 0 & 0 \\ 0 & -\nu_A - \nu_B + \gamma + \frac{1}{2}\epsilon & \frac{\sqrt{2}}{2}\epsilon \\ 0 & \frac{\sqrt{2}}{2}\epsilon & -2\nu_B + \gamma \end{pmatrix} \qquad (75)$$

where

$$\gamma = \frac{1}{4} J_{gem} + \frac{1}{2} J'_{gem} + \frac{1}{2} (J_{diag} + J'_{diag}) \qquad (76)$$

$$\epsilon = J_{vic} + J'_{vic} \qquad (77)$$

The problem is now to obtain analytical relationships between the four A_1 transitions, obtained from the solution of the above matrices, and the chemical shifts and/or coupling constants. This can be done by first taking the sum, $M_a + M_b$, of the two matrices. Doing this one obtaines the following matrix:

$$M = M_a + M_b = \begin{pmatrix} 2\gamma + 2\epsilon & 0 & 0 \\ 0 & 2\gamma + \epsilon & \sqrt{2}\epsilon \\ 0 & \sqrt{2}\epsilon & 2\gamma \end{pmatrix} \qquad (78)$$

Diagonalization of M then yields the following eigenvalues:

$$\Lambda_{11} = 2\gamma + 2\epsilon$$

$$\Lambda_{22} = 2\gamma + 2\epsilon$$

$$\Lambda_{33} = 2\gamma - \epsilon \qquad (79)$$

If the sums of the submatrices are considered, then from the trace relations, the following expressions are obtained

$$\Lambda_{11} = \Lambda a_{11} + \Lambda b_{11} = 2\gamma + 2\epsilon \tag{80}$$

$$\Lambda_{22} + \Lambda_{33} = \Lambda a_{22} + \Lambda b_{22} + \Lambda a_{33} + \Lambda b_{33} = 4\gamma + \epsilon \tag{81}$$

Multiplying Eq. (80) by two and then subtracting Eq. (81) from the product one then gets the expression

$$2\Lambda a_{11} + 2\Lambda b_{11} - \Lambda a_{22} - \Lambda b_{22} - \Lambda a_{33} - \Lambda b_{33} = 3\epsilon \tag{82}$$

Defining the four A_1 transitions as

$$\Lambda a_{11} - \Lambda b_{22} = \nu_1$$

$$\Lambda a_{11} - \Lambda b_{33} = \nu_3$$

$$\Lambda b_{11} - \Lambda b_{22} = -\nu_2$$

$$\Lambda b_{11} - \Lambda b_{33} = -\nu_4$$

and then making the appropriate substitutions in Eq. (82), the following expression results,

$$(\nu_1 - \nu_2) + (\nu_3 - \nu_4) = 3(J_{vic} + J'_{vic}) \tag{83}$$

indicating that the sum of the vicinal coupling constants can be determined directly from the spectrum providing that the four transitions, ν_1, ν_2, ν_3, and ν_4 can be identified. In the corresponding first-order pattern consisting of, in the A_2B_4 case, a triplet and a quintet, ν_1 and ν_2 would be the two outer lines of the triplet and ν_3 and ν_4 the two outer lines of the quintet. This hows that the separation between each line of the triplet or quintet would be given by $\frac{1}{2}(J_{vic} + J'_{vic})$. However, picking out these four lines in a couplex spectrum will prove to be considerably more difficult.

The chemical shift in the first-order spectrum will just be the separation between the center of the quintet and the center of the

triplet. Again, in a badly mixed spectrum, determination of the chemical shift will not be a trivial matter.

Assuming that the sum of the vicinal coupling constants can be exactly determined and the chemical shift can be obtained, there still exist an additional five parameters ($J_{vic} - J'_{vic}$, J_{gem}, J'_{gem}, J_{diag}, J'_{diag}) which must be determined in order to complete a spectral analysis. In general, the A_2B_4 systems that are of present concern can yield spectra containing as many as 130-150 lines of observable intensity. It then becomes evident that solution of these problems would be completely intractable without the aid of a high-speed computer. In all of the cases spectral analyses were facilitated by means of the IBM 7094 iterative computer programs,[19] NMRIT and NMREN, which have been described in detail elsewhere. The individual problems encountered in the various analyses will be discussed in more detail under the headings of the individual molecules.

Considerable difficulty was incurred in analyzing the spectra with the use of the iterative program. Essentially this difficulty arose because the program requires a reasonably close approximation to the true parameters before being able to iterate or converge to the exact parameters. The program works by calculating all the transition frequencies from the initial trail parameters and then assigning the experimental transitions to the calculated transitions. After the transitions have been assigned and assuming that they have been assigned correctly the true energy levels of the system may be calculated. The program then uses these energy levels to improve on the original trial parameters. If the initial trial parameters are not close, then it is found to be quite difficult to properly assign the transition frequencies. This occurs

because the spectra are so highly mixed that many of the individual lines are unresolvable, even under optimum experimental conditions. The energy levels of these six spin systems are, in general, greatly over-determined so that some of the transitions need not be assigned or may be assigned incorrectly without causing the program to fail. However, since the systems are so badly mixed and, in general, the initial trial parameters were sufficiently far away from the true parameters that it was for practical purposes impossible to correctly assign a sufficient number of transitions to allow the program to properly cover to the correct answer.

In this connection it was necessary to use spectral data obtained by double-resonance in conjunction with the iterative program in order to eventually obtain the correct parameters. The descriptions of the problems and methods of attack used are discussed below.

1. Trimethylene sulfide.

The A-60 spectrum of trimethylene sulfide on a 500 cps scale using TMS as an internal standard is presented in Fig. 11. The spectrum of trimethylene sulfide on a 50 cps scale was run on the A-60 at the same sweep rate and is presented in Fig. 12. The spectrum was run using the slowest possible sweep speed (0.1 cps/sec) without modification of the instrument. Here it is seen that the ringing seriously hides the true positions of a great number of the lines. Figure 13 shows the spectrum of trimethylene sulfide recorded with the field-frequency lock spectrometer described in the previous section. This spectrum was run at a sweep rate of 0.03 cps/sec and a filter bandwidth of 0.25 cps. Some ringing is still evident, but the positions of many more of the lines can be readily estimated since the ringing is considerably more damped

out in this spectrum. This spectrum should then serve to demonstrate the utility of a slow sweep with this type of spectrometer for spectra wherein there are groupings of lines with very small spacings.

Upon examination of the 60 Mc/sec spectrum one will observe a very badly mixed pattern. In fact, from this spectrum it was not possible to obtain even a reasonable estimate of the chemical shift. The spectrum of trimethylene sulfide was then taken at 100 Mc/sec in order to determine if the increased separation between the A and B proton resonances would be sufficient to allow an approximate value of the chemical shift to be obtained. This 100 Mc/sec spectrum which was run at a sweep rate of 0.1 cps/sec is presented in Fig. 14. One can see that this spectrum does show the remnances of a triplet and quintet pattern, although it is certainly a highly perturbed pattern at best. However, measuring the approximate separation between the apparent centers of the triplet and quintet yielded the value of 27.7 cps for the chemical shift at 100 Mc/sec. Multiplying by the factor 3/5 gave the value of 16.6 cps for the corresponding chemical shift of trimethylene sulfide at 60 Mc/sec.

The above value for the chemical shift at 60 Mc/sec for trimethylene sulfide can be regarded only as a first-order approximation to the true chemical shift. In order to obtain a more precise value it is necessary to consider the $F_z = \pm 3$ and ± 2 submatrices in detail and also the trace relationships for the submatrices using both the 60 Mc/sec and 100 Mc/sec spectra.

An expression for the chemical shift may be obtained by a solution of the Hamiltonian matrices M_a and M_b. Diagonalization of M_a gives the following expressions for the eigenvalues:

$$\Lambda a_{11} = \delta + \gamma + \epsilon$$

$$\Lambda a_{22} = \frac{1}{2}\delta + \frac{1}{4}\epsilon + \frac{1}{2}[(\delta + \frac{1}{2}\epsilon)^2 + 2\epsilon^2]^{1/2} + \gamma$$

$$\Lambda a_{33} = \frac{1}{2}\delta + \frac{1}{4}\epsilon - \frac{1}{2}[(\delta + \frac{1}{2}\epsilon)^2 + 2\epsilon^2]^{1/2} + \gamma \qquad (84)$$

where now δ is given by $\nu_B - \nu_A$. Subsequent diagonalization of M_b produces for the eigenvalues the following expressions:

$$\Lambda b_{11} = -\delta + \gamma + \epsilon$$

$$\Lambda b_{22} = -\frac{1}{2}\delta + \frac{1}{4}\epsilon - \frac{1}{2}[(-\delta + \frac{1}{2}\epsilon)^2 + 2\epsilon^2]^{1/2} + \gamma$$

$$\Lambda b_{33} = -\frac{1}{2}\delta + \frac{1}{4}\epsilon + \frac{1}{2}[(-\delta + \frac{1}{2}\epsilon)^2 + 2\epsilon^2]^{1/2} + \gamma \qquad (85)$$

Taking the appropriate differences between the eigenvalues, one gets the following expressions for $\nu_1 - \nu_3$ and $\nu_2 - \nu_4$:

$$\nu_1 - \nu_3 = \Lambda a_{33} - \Lambda a_{22} = -[(\delta + \frac{1}{2}\epsilon)^2 + 2\epsilon^2]^{1/2} + \gamma \qquad (86)$$

$$\nu_2 - \nu_4 = \Lambda b_{22} - \Lambda b_{33} = [(-\delta + \frac{1}{2}\epsilon)^2 + 2\epsilon^2]^{1/2} + \gamma \qquad (87)$$

Squaring Eqs. (86) and (87) and adding the squares one gets after substituting for ϵ, an equation in δ of the form

$$2\delta^2 = (\nu_1 - \nu_3)^2 + (\nu_2 - \nu_4)^2 - \frac{9}{2}(J_{vic} + J'_{vic})^2 \qquad (88)$$

From Eqs. (84) and (85) and also a detailed consideration of the other Hamiltonian submatrices, one will observe that the two other lines of the spectrum must correspond to two of the four A_1 lines mentioned in the previous paragraph. The outer lines will correspond to either ν_1 and ν_4, or ν_2 and ν_3, depending on what choice of relative sign of the vicinal coupling constants is made; the two vicinal coupling constants being assumed to have the same relative sign. Since NMR spectra are dependent only on the relative signs of the coupling constants positive

signs were assumed for the vicinal coupling constants. The theoretical evidence previously presented[29] does, in fact, indicate that they are positive in an absolute sense. With this choice the low-field outer line becomes ν_1 and the high-field outer line becomes ν_4, with ν_2 and ν_3 being the two inner lines which remain to be determined.

From the arrangements of the energy levels it is observed that ν_1 is associated with ν_3 in a regressive manner ($\Delta m = 0$) and that ν_4 is likewise associated with ν_2. Therefore, irradiating ν_1 in a double-resonance experiment should produce a sharp splitting in ν_3 and similarly irradiating ν_4 should give a sharp doublet for the transition υ_2. In fact, in the respective experiments, ν_3 and ν_2 should be the only lines in which the well-resolved doublets are obtained. With these two experiments it was possible to assign ν_3 and ν_2. The assignments are indicated in Fig. 13. The frequencies of the four lines and the appropriate differences are given in Table II. These values when substituted into the appropriate equations gave the following values for the chemical shift δ and the sum of the vicinal coupling constants:

$$\delta = 16.2 \text{ cps}$$

$$\epsilon = J_{vic} + J'_{vic} = 15.2 \text{ cps}$$

The assignments of the four A_1 transitions is further confirmed by calculating trial spectra using NMRIT.

Additional information may be obtained from the 60 Mc/sec spectra and the 100 Mc/sec spectra using the trace relationships at the two different frequencies for the $F_z = \pm 3$ and ± 2 submatrices. By reasoning similar to that used in the previous paragraph ν_1 at 100 Mc/sec was assigned to the first low field line. ν_3 was assigned by irradiating ν_1 and observing the appearance of a single transition being split into a

well-resolved double. The double-resonance spectrum is shown in Fig. 15. The values for ν_1 and ν_3 at 100 Mc/sec are 332.1 and 303.1 respectively. Again, these values were further confirmed using NMRIT and calculating 100 Mc/sec spectra for a number of reasonable parameters.

The eignevalues at 60 Mc/sec may be represented as Λa_{11}, Λa_{22}, and $\Lambda a_{22} + 23.1$, and the eigenvalues at 100 Mc/sec represented as $\Lambda a'_{11}$, $\Lambda a'_{22}$, and $\Lambda a'_{22} + 29.0$, where

$$\begin{aligned}
&(a) \quad \Lambda a_{11} = \nu_A + 2\nu_B + \gamma + \epsilon \\
&(b) \quad \Lambda a'_{11} = \tfrac{5}{3}\nu_A + \tfrac{10}{3}\nu_B + \gamma + \epsilon \\
&(c) \quad 2\Lambda a_{22} + 23.1 = \nu_A + 3\nu_B + 2\gamma + \tfrac{1}{2}\epsilon \\
&(d) \quad 2\Lambda a'_{22} + 29.0 = \tfrac{5}{3}\nu_A + \tfrac{15}{3}\nu_B + 2\gamma + \tfrac{1}{2}\epsilon \\
&(e) \quad \Lambda a_{11} - \Lambda a_{22} = 206.7 \\
&(f) \quad \Lambda a'_{11} - \Lambda a'_{22} = 332.1
\end{aligned} \tag{89}$$

Subtracting Eq. (89c) from Eq. (89d) and Eq. (89a) from (89b) gives the following results:

$$2(\Lambda a'_{22} - \Lambda a_{22}) + 5.9 = \tfrac{2}{3}(\nu_A + 3\nu_B) \tag{90}$$

$$\Lambda a'_{11} - \Lambda a_{11} = \tfrac{2}{3}(\nu_A + 2\nu_B) \tag{91}$$

With these two expressions and, after making the appropriate substitutions, it becomes possible to solve for the quantity $\nu_A + \nu_B$. Carrying out the calculation produces a value of 367.4 for the sum. With this value and the value of 16.2 cps for the chemical shift (i.e., $\nu_B - \nu_A$) the frequencies of the A and B resonances, respectively, were calculated to be 175.6 cps and 191.8 cps relative to TMS.

From Eq. (89c) and the expression

$$\Lambda a_{22} + 206.7 = \nu_A + 2\nu_B + \gamma + \epsilon \qquad (92)$$

a value of 15.2 cps was calculated for the quantity $J_{vic} + J'_{vic}$. One may note at this point that the same value of 15.2 cps was obtained for this quantity by another completely independent method also using different experimental data. This should, therefore, indicate that the value of 15.2 cps is quite reliable.

Once the chemical shift and the sum of the vicinal coupling constants were obtained, the remainder of the analysis became essentially one of "trial and error" iterative fitting of the remaining parameters. Spectra were calculated with various trial parameters until a satisfactory fit was obtained. Once this satisfactory fit was found the assignment for the various line positions from this computation and the line positions from a calibrated spectrum were compared and a set of eigenvalues calculated using NMREN. The final set of parameters and line positions were then calculated from the above eigenvalues and iterating with NMRIT until satisfactory convergence was attained. The estimated accuracy of the experimental line position measurements was estimated to be about 0.05 cps. The values for the final set of parameters calculated by NMRIT are given in Table III. The errors in the final parameters were estimated by determining what changes in the parameters would cause an unsatisfactory match between the experimental and calculated spectra. A comparison between the experimental and calculated spectra is shown in Fig. 16.

From the NMR data alone in trimethylene sulfide, it is not possible to determine which of the vicinal coupling constants is the larger and,

Table III. Coupling constants and chemical shift for trimethylene sulfide

Coupling constants		Chemical shift
J_{vic}	= 8.9 ± 0.2 cps	16.2 ± 0.05 cps
J'_{vic}	= 6.3 ± 0.2 cps	
J_{gem}	= -11.0 ± 0.2 cps	
J'_{gem}	= -8.0 ± 0.2 cps	
J_{diag}	= 0.6 ± 0.3 cps	
J'_{diag}	= -0.5 ± 0.3 cps	

therefore, also which long range coupling constant is the larger since changing the coupling constants in this instance merely involves relabeling chemically equivalent protons. Previous evidence[53] in the literature has indicated that, in general, the cis coupling constants in four-membered rings are the larger. On this basis the large vicinal coupling constant was assigned to J_{vic} and the small value to J'_{vic}, but it must be borne in mind that this is just a semi-empirical assignment which is yet to be verified.

2. Trimethylene imine.

The complete 60 Mc/sec spectrum of trimethylene imine is presented in Fig. 17. The chemical shift δ is sufficiently large, the spectrum thereby exhibiting the expected triplet and quintet pattern, so that δ may be obtained accurately directly from the spectrum. The factor $\frac{1}{2}(J_{vic} + J'_{vic})$ is also obtained directly from the spectrum; being given by the multiplet separations within the two groups. The values obtained

for δ and $\frac{1}{2}(J_{vic} + J'_{vic})$ are 77.2 cps and 7.2 cps, respectively. The values for the α and β resonances relative to TMS are 134.2 cps and 211.4 cps, respectively.

The N-H proton resonance was not observed because of the line broadening due to the quardrupole moment of the nitrogen. Couplings between the nitrogen or the N-H proton with the α methylene protons were not observed because of the rapid relaxation induced by the quadrupole moment of the nitrogen.

High-resolution spectra of the triplet and quintet portions of the trimethylene imine spectra were run at a sweep rate of 0.03 cps/sec. These spectra were analyzed using a procedure quite similar to that used in the trimethylene sulfide analysis. Once the chemical shift and $\frac{1}{2}(J_{vic} + J'_{vic})$ were determined, a trial and error iterative procedure was used until a satisfactory fit to the observed spectra was obtained. Once this was accomplished the observed and calculated transition frequencies were compared and a set of energy levels calculated. The final set of parameters and line positions were then calculated from these energy levels by iterating with NMRIT. The estimated accuracy of the experimental line position measurements was 0.1 cps. The final parameters calculated by NMRIT for trimethylene imine are given in Table IV. As in trimethylene sulfide the errors in the final parameters were estimated by experimentally determining what changes in the parameters would cause an unsatisfactory match between the calculated and experimental spectra. Comparisons between the experimental and calculated spectra for both the triplet and quintet are shown in Fig. 18 and Fig. 19, respectively.

Table IV. Coupling constants and chemical shift for trimethylene imine

Coupling constants		Chemical shift
J_{vic}	= 8.4 ± 0.2 cps	77.2 ± 0.2 cps
J'_{vic}	= 6.0 ± 0.2 cps	
J_{gem}	= -11.0 ± 0.3 cps	
J'_{gem}	= -6.7 ± 0.3 cps	
J_{diag}	= 0.9 ± 0.5 cps	
J'_{diag}	= -0.3 ± 0.5 cps	

3. Trimethylene oxide.

The procedure involved in the analysis of the spectrum of trimethylene oxide was almost identical to that used in the trimethylene imine analysis. The only major difference was that the chemical shift in trimethylene oxide is considerably larger than that of trimethylene imine, giving a more first-order appearance to the spectrum.

The complete 60 Mc/sec spectrum of trimethylene oxide is shown in Fig. 20. The chemical shift δ was observed to be 119.0 cps. A value of 7.8 cps was observed for the quantity $\frac{1}{2}(J_{vic} + J'_{vic})$. The values for the α and β resonances relative to TMS were observed to be 137.0 cps and 256.0 cps, respectively.

The high-resolution 60 Mc/sec spectra taken with the field-frequency lock spectrometer were run at a sweep rate of 0.03 cps/sec. Upon iteration the parameters given in Table V were obtained. The calculated spectra obtained with these parameters along with the experimental spectra

are presented in Figs. 21 and 22 for the triplet and quintet, respectively. The errors in the final parameters were estimated in a manner identical to that used in trimethylene imine.

Table V. Coupling constants and chemical shift for trimethylene oxide

Coupling constants		Chemical shift
J_{vic}	= 8.9 ± 0.2 cps	121.0 ± 0.2 cps
J'_{vic}	= 6.7 ± 0.2 cps	
J_{gem}	= -11.0 ± 0.3 cps	
J'_{gem}	= -5.8 ± 0.3 cps	
J_{diag}	= -0.4 ± 0.5 cps	
J'_{diag}	= 0.7 ± 0.5 cps	

4. 1,1-Dimethylcyclobutanedicarboxylate.

The spectrum of 1,1-dimethylcyclobutanedicarboxylate on a 500 cps scale is presented in Fig. 23 using TMS as an internal standard. The high-resolution spectrum run at a sweep rate of 0.03 cps/sec is shown in Fig. 24. The spectrum is highly perturbed thereby making it difficult to directly observe the chemical shift and $\frac{1}{2}(J_{vic} + J'_{vic})$. It was therefore necessary to determine these parameters with the use of the equations derived originally for trimethylene sulfide. From Eq. (83) and (88) a value of 33.2 cps was obtained for the chemical shift and a value of 8.25 cps for the quantity $\frac{1}{2}(J_{vic} + J'_{vic})$.

Once these values were obtained the trial and error adjusting of the remaining parameters was affected until a satisfactory fit to the

observed spectrum was obtained. The observed and calculated transition frequencies were then compared and ultimately a set of energy levels calculated with NMREN. The estimated accuracy of the experimental line position measurements was about 0.2 cps. The final parameters were then calculated with NMRIT and are given in Table VI. The errors in the final parameters were estimated in a manner identical to those used for the molecules previously studied. Comparisons between the experimental and calculated spectra are shown in Fig. 25.

Table VI. Coupling constants and chemical shift for 1,1-dimethylcyclobutanedicarboxylate

Coupling constants		Chemical shift
J_{vic}	= 9.9 ± 0.3 cps	33.2 ± 0.1 cps
J'_{vic}	= 6.6 ± 0.3 cps	
J_{gem}	= -11.0 ± 0.3 cps	
J'_{gem}	= -10.0 ± 0.3 cps	
J_{diag}	= 0.7 ± 0.5 cps	
J'_{diag}	= 0.6 ± 0.5 cps	

B. Nuclear Magnetic Double Resonance

Analyses of two- and three-spin systems using ν_1 frequency-sweep nuclear magnetic double-resonance have been carried out and described in considerable detail by Freeman and Anderson.[20] However, complete spectral analysis using the ν_2 frequency-sweep method has not been previously reported. In fact, only a single isolated example of this method exists in the literature.[54]

The purposes of this section will then be twofold. First, experiments will be described demonstrating the value of the ν_2 frequency-sweep method in spectral analysis. Secondly, experiments will be described which were conducted in order to gain a fuller understanding of the 'physics' underlying the phenomena observed in these experiments.

1. Spectral analysis.

The aromatic protons of 2-chlorothiophene have been chosen to demonstrate the application of the ν_2 frequency-sweep technique to the ordering of the energy levels of an unknown strongly coupled ABC system. Figure 26 illustrates the spectrum of the neat, vacuum-degassed liquid at 60 Mc/sec. The spectrum was run at a sweep rate of 0.03 cps/sec using a filter bandwidth of 0.25 cps. In chlorothiophene 14 out of the 15 lines occur with observable intensity. Line 15 was assigned using the frequency sum rule and was also observed indirectly in a double-resonance experiment to be described below.

Suppose ν_1 is set on line 2 and the rest of the spectrum perturbed by ν_2. Perturbing lines which have no energy level in common with line 2 should produce no effect. Lines which are connected by an energy level in a regressive manner ($\Delta m = 0$) when perturbed by ν_2 should cause a decrease in the intensity of line 2. In a similar manner perturbing lines which are connected in progressive manner by a common energy level to line 2 should cause an increase in the intensity of this line.

This situation where line 2 was observed is illustrated in Fig. 27. Note that as ν_2 sweeps through ν_1 a beat frequency is generated as some of the nucelar resonance signal at ν_2 enters the phase sensitive detector operating at ν_1. The beat frequency is rapidly damped out by the output

filter of the phase sensitive detector. In addition to this beat frequency, what appears to be very low frequency ringing is observed on the tails of the peaks. This is actually a saturation phenomenon which is caused by using a rather large H_1. This ringing or saturation was of no significant consequence and could easily be eliminated either by using smaller H_1 or by putting in additional filtering after the phase sensitive detector.

From the spectrum in Fig. 27 it is a simple matter to determine which lines share energy levels in common with line 2 and also whether the lines are connected in a regressive or progressive manner. This is most easily accomplished by superimposing this spectrum on the normal spectrum run at the same sweep rate. The superimposed spectra are shown in Fig. 28. From this superimposed spectrum it can be seen that lines 5 and 10 are connected to line 2 in a regressive manner and lines 7, 13, and 15 are connected to line 2 in a progressive manner. Line 15 represents an interesting situation since under normal conditions it is an extremely weak line and therefore difficult to observe. However, the ν_2 frequency-sweep double resonance spectrum clearly points out the position of the line and also the fact that it shares a common energy level with line 2. This method therefore also represents a new technique by which very weak lines may be indirectly observed.

The results obtained for line 2 are presented in Table VII. Lines 8 and 9 are nearly degenerate and therefore cannot be distinguished on a frequency basis alone.

Table VII. Results of the ν_2 frequency-sweep double-resonance spectrum while observing line 2 of 2-chlorothiophene

Line	Result	Line	Result
1	Unaffected	8 & 9	Unaffected
2	Observed	10	Affected (regressive)
3	Unaffected	11	Unaffected
4	Unaffected	12	Unaffected
5	Affected (regressive)	13	Affected (progressive)
6	Unaffected	14	Unaffected
7	Affected (progressive)	15	Affected (progressive)

Each of the strong single lines in Fig. 26 were observed in a ν_2 frequency-sweep and tables similar to Table VII above were constructed for each of these. In all cases it was quite easy to see which lines were affected and in what manner they were affected. A cross check may be made at once on the results obtained for a single line, for if irradiation of one line causes the line being observed to increase in intensity then the reverse must hold, although this will not necessarily be observable at the same strength of the perturbing rf field if the two lines differ in intensity. This information was then used to construct the energy-level diagram for a three-spin system which has been schematically represented in Fig. 40. This diagram is appropriate to the ABC 2-cholorthiophene system and the assignments of the transitions determined by double-resonance are indicated. The spectra obtained for the remaining strong non-degenerate lines are presented in Fig. 29 through Fig. 37. During the analysis the frequency sum rule provided a useful cross check on the progress of the assignment. The problem is greatly overdetermined

and there was no difficulty in predicting the frequencies of the remaining lines required to complete an analysis of a 15-line ABC system.

In addition to giving the energy-level diagram for 2-chlorothiophene this technique provided a very simple and extremely accurate way of calibrating the high-resolution spectrum. Once the peak height had been accurately determined the frequency was recorded. By this method, the frequencies of the lines were reproducable within 0.05 cps.

Once the transition frequencies were obtained it was a simple matter to obtain the energy levels. The zero of energy was defined by setting the sum of the eigenvalues equal to zero. The energy levels were then fed into NMRIT using an arbitrary set of starting parameters. Given that the energy-level information greatly overdetermines the problem, the program quickly converged to a set of parameters which are presented in Table VIII.

Table VIII. Chemical shifts and coupling constants for 2-chlorothiophene

Coupling constants	Chemical shifts
$J_{12} = 3.44 \pm 0.1$ cps	$\nu_{12} = 4.5 \pm 0.1$ cps
$J_{13} = 5.91 \pm 0.1$ cps	$\nu_{13} = 9.7 \pm 0.1$ cps
$J_{23} = 1.24 \pm 0.1$ cps	$\nu_{23} = 5.2 \pm 0.1$ cps

The errors quoted above are those calculated by NMRIT. A comparison between the experimental and calculated spectra is presented in Fig. 38.

2. Pulse experiments.

The effect of transiently saturating a line while observing the effect of the perturbation on another line where both lines have a common energy level was described. This transient saturation was caused by sweeping the perturbing rf field through the appropriate lines. In this section the results of the experiments wherein the transient saturation was generated by a π pulse instead of a ν_2 frequency-sweep.

In order to produce a π pulse, the conditions of Eq. (66) must be met such that α will be equal to 180°. In practice the π pulse was generated by setting the time of the pulse, t_w, equal to $\frac{1}{2}$ second and then varying the amplitude H_2 of the perturbing rf field until the maximum signal was observed. This procedure is valid because a maximum signal should be observed when the macroscopic magnetization vector has been completely tipped from the positive z direction to the negative z direction, i.e., when $\alpha = 180°$.

The first experiment was performed by turning on H_1 at the frequency of line 2 of 2-chlorothiophene (see Fig. 28) and applying the π pulse to line 13. From Table VII one sees that irradiation of line 13 while observing line 2 should cause an increase in the intensity of line 2. The results of this experiment are presented in Fig. 39.

Similar experiments were carried out by pulsing each of the non-degenerate lines in 2-chlorothiophene. In each case the results were identical to those obtained by the ν_2 frequency-sweep experiment.

It was previously shown that under the proper conditions saturation by ν_2 sweep or by pulse methods are identical. This would then tend to indicate that the phenomena being observed in the ν_2 frequency-sweep are

due to the fact that the condition for adiabatic rapid passage is being met. It was not possible to accurately calibrate H_2 so that a more quantitative statement cannot be made at this time.

V. CONCLUSIONS

The experimental data in Sec. IV.A. have shown that the trends observed in the geminal coupling constants can be explained on the basis of the theory of Sec. II.A. There does appear to be an approximate linear relationship between the geminal coupling constants and the electronegativities of the substituents. However, what is even more interesting to note is that the change in the geminal coupling constant in going from trimethylene sulfide to trimethylene oxide is approximately half as large as the change observed in going from ethylene sulfide to ethylene oxide. This trend, in fact, was predicted quite accurately by this theory assuming nearly sp^2 hybridization for three-membered rings and sp^3 hybridization for four-membered rings. The β geminal coupling constant remained nearly constant in the cases studied indicating that the effect of the substituent over two or more bonds is negligible.

Another point which bears mentioning is the fact that the geminal coupling constants in general have opposite signs to the vicinal coupling constants. Since there is good theoretical evidence indicating that the vicinal coupling constants are positive,[29] it is then to be expected that the geminal coupling constants are negative in absolute magnitude. This is important to note in the light of Gutowsky's[8] original study, using the average energy approximation, which predicted positive geminal coupling constants. As was previously pointed out, use of the average energy approximation insists that the coupling constants be positive whereas this does not necessarily follow from the use of excited state wave functions. It can therefore be concluded that the average energy approximation can and does lead to incorrect conclusions when applied indiscriminantly to second-order perturbation theory calculations.

It appears that it will be considerably more difficult to make any conclusive statements concerning the vicinal coupling constants in four-membered ring compounds. As was pointed out in the previous section, the NMR data alone cannot determine which of the two vicinal coupling constants, cis or trans, is the larger although evidence is available on highly substituted four-membered rings which indicates that the cis coupling constant is the larger. However, in one instance, namely that of 3-chlorothietane,[55] the authors point out that assumption of a larger trans and a smaller cis coupling constant would be more consistent with their observations. In still another example, the cis and trans coupling constants in β-propiolactone were found to be equal within 0.2 cps. In view of the above evidence and the results obtained and previously described it does not appear that there is any direct correlation between the vicinal coupling constant and the electronegativity of the substituent.

In view of the uncertainty of the vicinal coupling constants it is likewise difficult to state any conclusions concerning the long range coupling constants since it is not possible to distinguish between the two possible cross ring coupling constants. However, it is interesting to point out that no large long range coupling constant was observed as opposed to the case of chlorothietane where quite a large cross ring coupling constant was observed. In addition the substituents do not appear to affect the long range coupling constants to any observable extent.

In order to distinguish between the vicinal coupling constants further studies would be necessary. Perhaps substitution in the α position by a group which would not be expected to show a large substituent

effect such as a methyl group or a deuterium atom might provide the necessary information. In addition a complete assessment of the magnitude of the vibrational effects and the corresponding influence on the coupling constants will be necessary. Such a study would require a complete knowledge of the geometry of the molecules; information which is not yet available.

Nuclear magnetic double-resonance spectra recorded by sweeping ν_2 while observing a single non-degenerate transition with ν_1 constitute a very good method by which information concerning the arrangements of the energy levels of complicated spin systems may be derived. Transient saturation experiments where the same information is obtained using a field-sweep mode of operation have been previously described.[56] However, it has been shown that the frequency-sweep technique provides a better method for obtaining the same information. It has been shown that the intensity changes will clearly indicate the energy level arrangement involving two transitions. One of the energy levels is common to both transitions; the other two levels may have either the same quantum number, in which case an intensity decrease will be observed, or quantum numbers which differ by two units, in which case the intensity should increase.

An example of a strongly coupled ABC system was used to indicate that these rules are in fact borne out in practice and can be used in the analysis of unknown systems. Once the energy level assignments were made, the iterative computer program of Swalen and Reilly was used to determine the final parameters. This procedure should be of considerable use in the assignment of energy levels in complex spin systems such as the ones studied in this dissertation. This procedure has in fact been used in the study of one five-spin system.

Finally, pulse experiments were carried out in order to gain a fuller understanding of the theory involved in these experiments. The pulse experiments do tend to indicate that the observed phenomena are caused by population inversion due to adiabatic rapid passage. However, further experimentation will be necessary for an unequivocal proof.

ACKNOWLEDGEMENTS

I would especially like to thank my research director Professor Charles H. Sederholm whose friendship and guidance made this research possible. It was indeed a pleasure and privilege to have worked under his direction.

I am extremely grateful to the staff of the electronic shop of the chemistry department, especially Mr. Steve Smiriga and Mr. Frank Papen for help and discussions concerning the electronics of the spectrometer.

I would like to acknowledge my many fellow graduate students for innumerous helpful discussions. Unfortunately they are too numerous to mention individually and I shall only name a few whose contributions were especially helpful. I would like to thank Mr. T. R. Lusebrink for originally pointing out to me the cause of the intensity changes observed in ν_2 frequency-sweep double-resonance. I would also like to thank Dr. Ernest Lustig, Mr. Richard Millikan and Mr. Warren Keller for many helpful discussions.

I would like to thank Mrs. Mere Gamball for preparing most of the figures presented in this dissertation.

Special thanks go to Mrs. Pat Cookson, Mrs. Judy Purcell and Mrs. Charlotte Machen for typing this manuscript.

Finally I would like to gratefully acknowledge the financial support received from the United States Atomic Energy Commission through the University of California Lawrence Radiation Laboratory.

REFERENCES

1. J. D. Graham and M. T. Rogers, J. Am. Chem. Soc. 84, 2249 (1962).
2. K. B. Wiberg and B. J. Nist, J. Am. Chem. Soc. 85, 2788 (1963).
3. C. A. Reilly and J. D. Swalen, J. Chem. Phys. 34, 980 (1961).
4. H. M. Hutton and T. Schaefer, Can. J. Chem. 41, 2429 (1963).
5. George L. Cunningham, Jr., A. W. Boyd, Rollie J. Myers, William D. Gwinn, and W. K. Le Van, J. Chem. Phys. 19, 676 (1951).
6. H. M. Hutton and T. Schaefer, Can.J. Chem. 41, 684 (1963).
7. F. S. Mortimer, J. Mol. Spectry. 5, 199 (1962).
8. H. S. Gutowsky, Martin Karplus, and D. M. Grant, J. Chem. Phys. 31, 1278 (1959).
9. K. L. Servis and J. D. Roberts, J. Phys. Chem. 67, 2885 (1963).
10. Ernest Lustig, J. Chem. Phys. 37, 2725 (1962).
11. E. Lippert and H. Prigge, Ber. der Buns. Gesell. 67, 415 (1963).
12. See, for example, J. A. Pople, W. G. Schneider, and H. J. Bernstein, High-Resolution Nuclear Magnetic Resonance (McGraw-Hill Book Company, Inc., New York, 1959).
13. C. N. Banwell and H. Primas, J. Mol. Phys. 6, 221 (1963).
14. Sunney I. Chan, John Zinn, and William D. Gwinn, J. Chem. Phys. 34, 1319 (1961).
15. David Owen Harris, Vibration-Rotation Interaction in Trimethylene Sulfide and Pseudorotation in Tetrahydrofuran (Ph.D. Thesis), University of California, Berkeley, June 9, 1965.
16. A. Bauder, F. Tank, and Hs. H. Günthard, Helv. Chim. Acta. 46, 1453 (1963).
17. J. A. Pople and A. A. Bothner-By, J. Chem. Phys. 42, 1339 (1965).
18. John D. Baldeschwieler and Edward W. Randall, Chem. Revs. 81 (1963).

19. J. D. Swalen and C. A. Reilly, J. Chem. Phys. 37, 21 (1962).

20. R. Freeman and W. A. Anderson, J. Chem. Phys. 37, 2053 (1962).

21. Norman F. Ramsey, Phys. Rev. 91, 303 (1953).

22. N. F. Ramsey and E. M. Purcell, Phys. Rev. 85, 143 (1952).

23. H. M. McConnell, J. Chem. Phys. 24, 460 (1956).

24. M. Karplus, D. H. Anderson, T. C. Farrar, and H. S. Gutowsky, J. Chem. Phys. 27, 597 (1957).

25. R. M. Lynden-Bell and N. Sheppard, Proc. Roy. Soc. (London) A269, 385 (1962).

26. The approximate value of the geminal coupling constant in cyclopropane was inferred from the data available on a number of substituted cyclopropanes.

27. The approximate value of the geminal coupling constant in cyclobutane was inferred from the data obtained in the research to be discussed in this dissertation.

28. C. C. J. Roothan, Rev. Mod. Phys. 23, 69 (1951).

29. Martin Karplus, J. Chem. Phys. 30, 11 (1959).

30. Martin Karplus and D. H. Anderson, J. Chem. Phys. 30, 6 (1959).

31. Martin Karplus, J. Chem. Phys. 33, 941 (1960).

32. H. M. Hutton and T. Schaefer, Can. J. Chem. 41, 1623 (1963).

33. Martin Karplus, J. Am. Chem. Soc. 85, 2870 (1963).

34. Michael Barfield, J. Chem. Phys. 41, 3825 (1964).

35. R. Freeman, Mol. Phys. 3, 435 (1960).

36. A. P. Cox, G. W. Flynn, and E. B. Wilson, J. Chem. Phys. 42, 3094 (1965).

37. W. A. Anderson and R. Freeman, J. Chem. Phys. 37, 85 (1962).

38. R. Freeman and W. A. Anderson, J. Chem. Phys. 37, 2053 (1962).

39. See, for example, J. A. Pople, W. G. Schneider, and H. J. Bernstein, High-Resolution Nuclear Magnetic Resonance (McGraw-Hill Book Company, Inc., New York, 1959), pp. 105.

40. F. Bloch and A. Siegert, Phys. Rev. 57, 522 (1940).

41. A. W. Overhauser, Phys. Rev. 92, 411 (1953).

42. A. Abragam, The Principles of Nuclear Magnetism, pp. 34-36 (clarendon Press, Oxford, 1961).

43. Wyman R. Vaughan, Robert S. Klonowski, R. Stanley McElhinney, and Brian B. Millward, J. Org. Chem. 26, 138 (1961). This compound was prepared by Drs. H. L. Strauss and A. G. Robiette.

44. Varian Associates Maintenance Instruction Manual for HR-60, DP-60, and VF-16 Spectrometers (Publication Number 87-100-068).

45. R. Freeman and D. H. Whiffen, Proc. Phys. Soc., 79, 794 (1962).

46. The staff of Varian Associates, NMR and EPR Spectroscopy (Pergamon Press).

47. It was necessary to carefully match impedances when using the V4332 probe (HR-100) since input impedance is only 20 Ω.

48. See, for example, J. A. Pople, W. G. Schneider, and H. J. Bernstein, High-Resolution Nuclear Magnetic Resonance (McGraw-Hill Book Company, Inc., New York, 1959).

49. A. Abragam, The Principles of Nuclear Magnetism, pp. 65-68 (Clarendon Press, Oxford, 1961).

50. E. Bright Wilson, Jr., J. Chem. Phys. 27, 60 (1957).

51. See, for example, J. A. Pople, W. G. Schneider, and H. J. Bernstein, High-Resolution Nuclear Magnetic Resonance (McGraw-Hill Book Company, Inc., New York, 1959), pp. 138.

52. T. R. Borgers (private communication).

53. E. Lustig (private communication).

54. Reinhold Kaiser, J. Chem. Phys. 39, 2435 (1963).

55. Warren Keller, T. R. Lusebrink, and C. H. Sederholm, J. Chem. Phys. (to be published).

56. S. Forsen and R. A. Hoffman, Acta. Chem. Scand. 18, 249 (1964).

FIGURE CAPTIONS

Fig. 1 The transition frequencies Ω and intensities L of the A resonance plotted against the offset parameter Δ for an AX system for $\gamma H_2/2\pi = 0.2J$.

Fig. 2 The transition frequencies Ω and intensities L of the A resonance plotted against the offset parameter Δ for an AX system for $\gamma H_2/2\pi = J$.

Fig. 3 The schematic representation of the energy levels of a two-spin system.

Fig. 4 The schematic representation of regressive (a) and progressive (b) energy levels.

Fig. 5 Enlarged section of Fig. 1 as shown by solid line in Fig. 1.

Fig. 6 Enlarged section of Fig. 1 as shown by solid line in Fig. 1 showing also the distribution of the main magnetic field H_o over the region of the sample.

Fig. 7 Enlarged section of Fig. 1 as shown by dashed line in Fig. 1.

Fig. 8 A block diagram of the field-frequency lock spectrometer.

Fig. 9 A schematic circuit diagram of the variable frequency lock-in amplifier used in the field-frequency lock spectrometer.

Fig. 10 Structure and identification of the six A_2B_4 protons.

Fig. 11 The A-60 spectrum of trimethylene sulfide on a 500 cps scale.

Fig. 12 The A-60 spectrum of trimethylene sulfide on a 50 cps scale.

Fig. 13 The spectrum of trimethylene sulfide (sweep rate = 0.03 cps/sec) recorded with the field-frequency lock spectrometer.

Fig. 14 The 100 Mc/sec spectrum of trimethylene sulfide.

Fig. 15 The 100 Mc/sec spectrum of trimethylene sulfide recorded while irradiating ν_1.

Fig. 16 The observed (a) and calculated (b) spectra of trimethylene sulfide.

Fig. 17 The 60 Mc/sec spectrum of trimethylene imine.

Fig. 18 The observed (a) and calculated (b) spectra for the trimethylene imine triplet.

Fig. 19 The observed (a) and calculated (b) spectra for the trimethylene imine quintet.

Fig. 20 The 60 Mc/sec spectrum of trimethylene oxide.

Fig. 21 The observed (a) and calculated (b) spectra for the trimethylene oxide triplet.

Fig. 22 The observed (a) and calculated (b) spectra for the trimethylene oxide quintet.

Fig. 23 The A-60 spectrum of 1,1-dimethylcyclobutanedicarboxylate on a 500 cps scale.

Fig. 24 The spectrum of 1,1-dimethylcyclobutanedicarboxylate (sweep rate = 0.03 cps/sec) recorded with the field-frequency lock spectrometer.

Fig. 25 The observed (a) and calculated (b) spectra of 1,1-dimethyl-cyclobutanedicarboxylate.

Fig. 26 The high-resolution spectrum of 2-chlorothiophene.

Fig. 27 The ν_2 frequency-sweep double-resonance spectrum of 2-chloro-thiophene observing line 2.

Fig. 28 The super position of the high-resolution spectrum of 2-chloro-thiophene and the ν_2 frequency-sweep double-resonance spectrum observing line 2.

Fig. 29 The super position of the high-resolution spectrum of 2-chloro-thiophene and the ν_2 frequency-sweep double-resonance spectrum observing line 3.

Fig. 30 The super position of the high-resolution spectrum of 2-chlorothiophene and the ν_2 frequency-sweep double-resonance spectrum observing line 4.

Fig. 31 The super position of the high-resolution spectrum of 2-chloro thiophene and the ν_2 frequency-sweep double-resonance spectrum observing line 6.

Fig. 32 The super position of the high-resolution spectrum of 2-chlorothiophene and the ν_2 frequency-sweep double-resonance spectrum observing line 7.

Fig. 33 The super position of the high-resolution spectrum of 2-chlorothiophene and the ν_2 frequency-sweep double-resonance spectrum observing line 10.

Fig. 34 The super position of the high-resolution spectrum of 2-chlorothiophene and the ν_2 frequency-sweep double-resonance spectrum observing line 11.

Fig. 35 The super position of the high-resolution spectrum of 2-chlorothiophene and the ν_2 frequency-sweep double-resonance spectrum observing line 12.

Fig. 36 The super position of the high-resolution spectrum of 2-chlorothiophene and the ν_2 frequency-sweep double-resonance spectrum observing line 13.

Fig. 37 The super position of the high-resolution spectrum of 2-chlorothiophene and the ν_2 frequency-sweep double-resonance spectrum observing line 14.

Fig. 38 The observed (a) and calculated (b) spectra of 2-chlorothiophene.

Fig. 39 Observation of line 13 in 2-chlorothiophene while pulsing line 2.

Fig. 40 The schematic representation of the energy levels of the three-spin system 2-chlorothiophene.

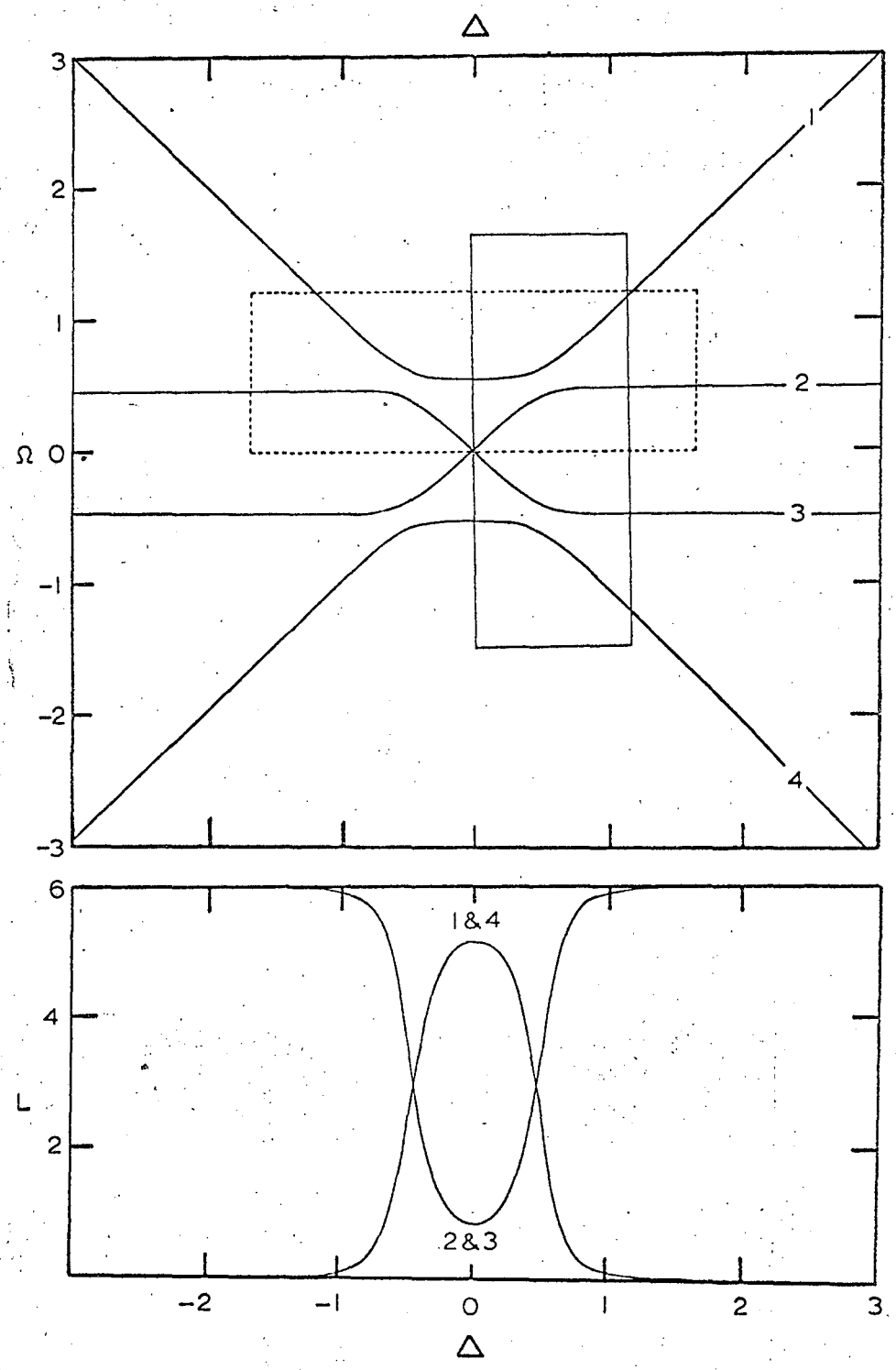

The transition frequencies Ω and intensities L of the A resonance plotted against the offset parameter Δ for an AX system for $\gamma H_2/2\pi = 0.2J$.

Fig. 1

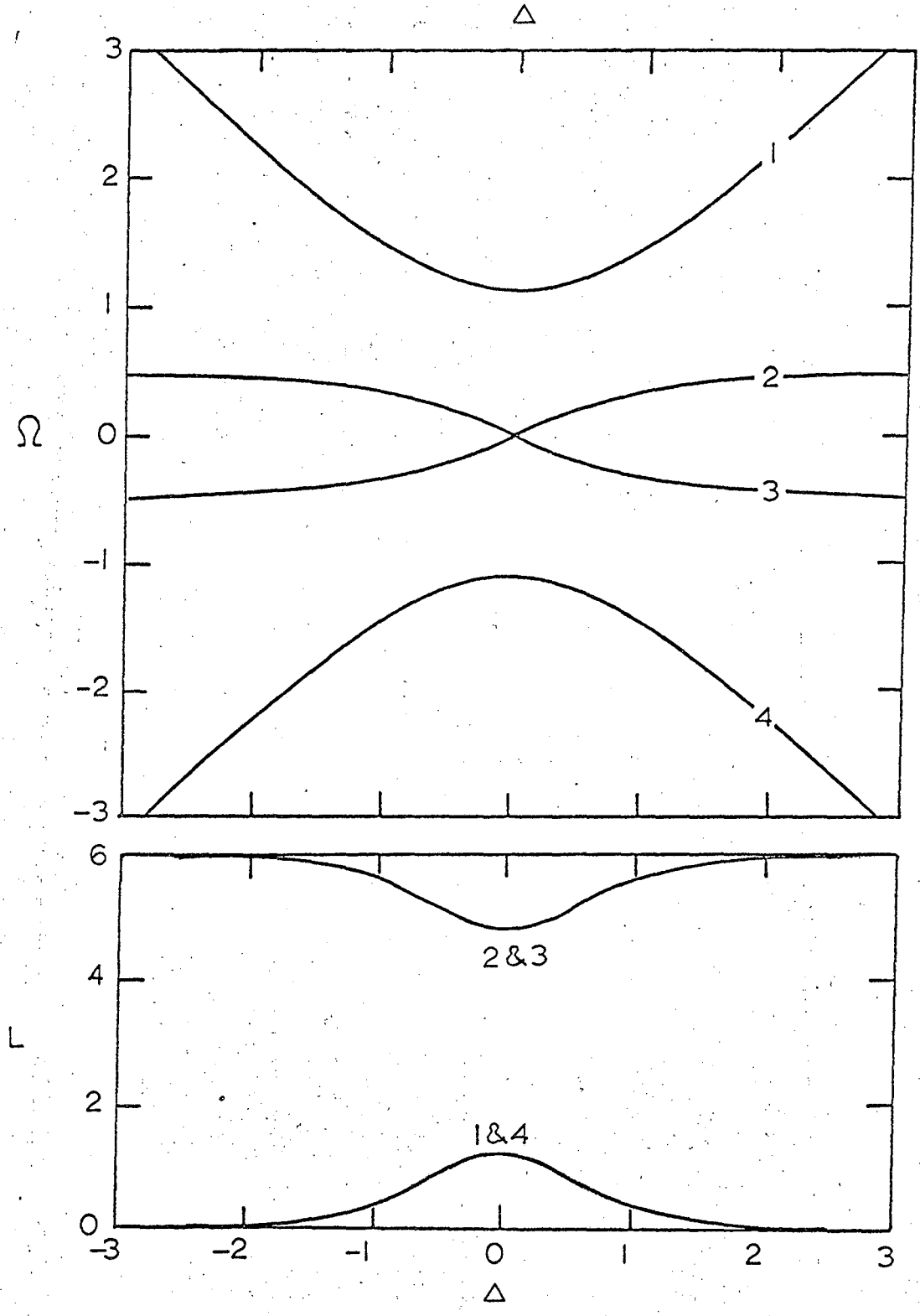

The transition frequencies Ω and intensities L of the A resonance plotted against the offset parameter Δ for an AX system for $\gamma H_2/2\pi = J$.

Fig. 2

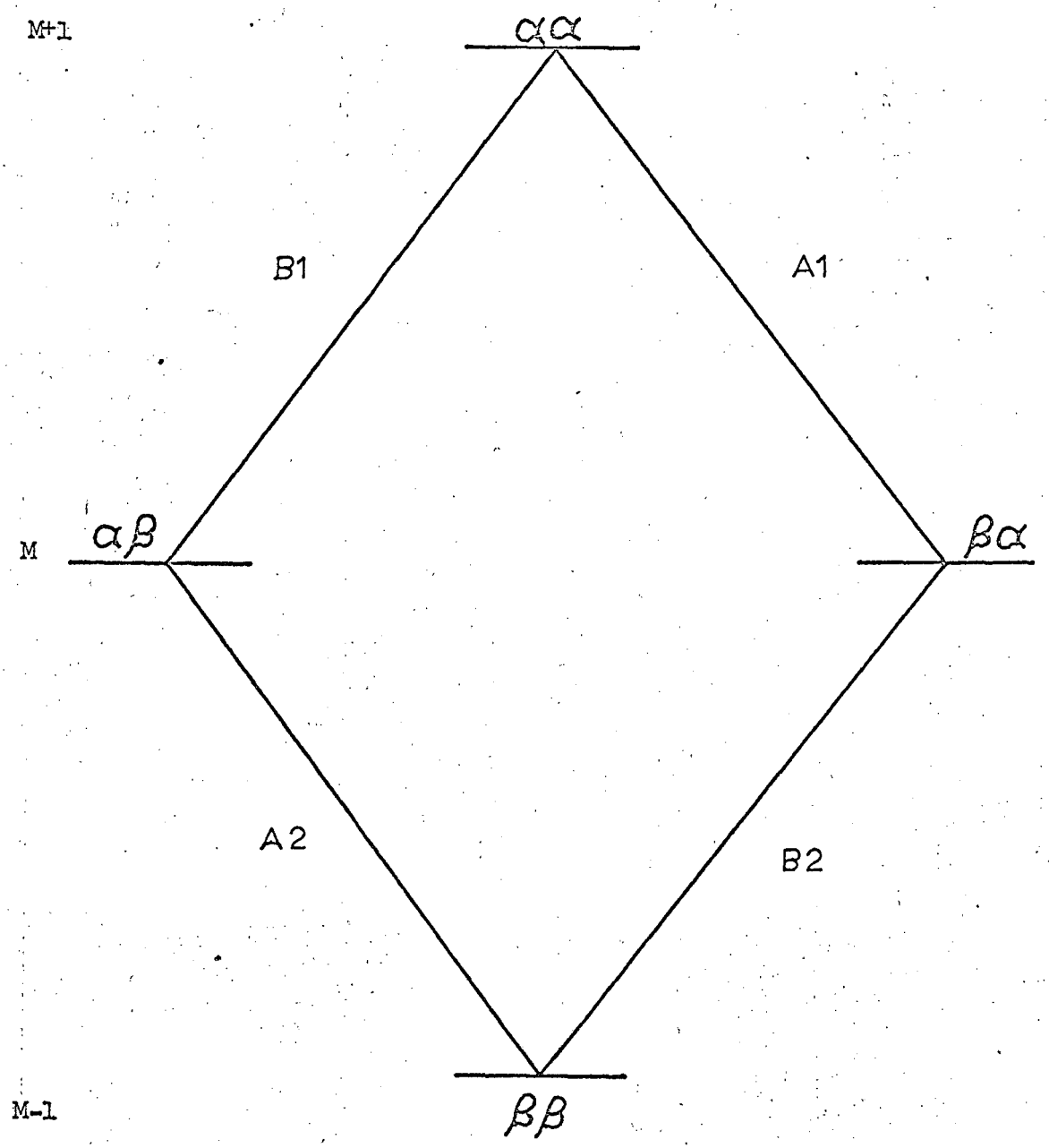

Fig. 3

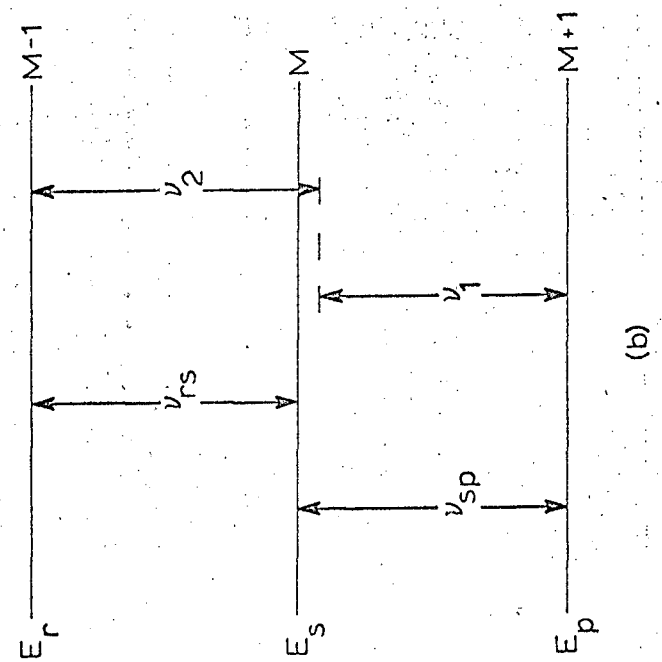
M-1
M
M+1
ν_2
ν_1
ν_{rs}
ν_{sp}
E_r
E_s
E_p
(b)

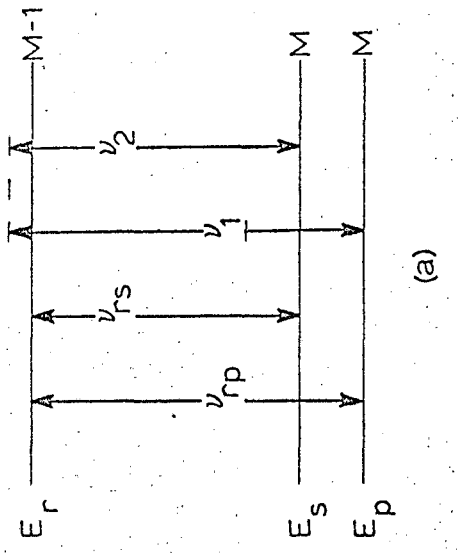
M-1
M
M
ν_2
ν_1
ν_{rs}
ν_{rp}
E_r
E_s
E_p
(a)

Fig. 4

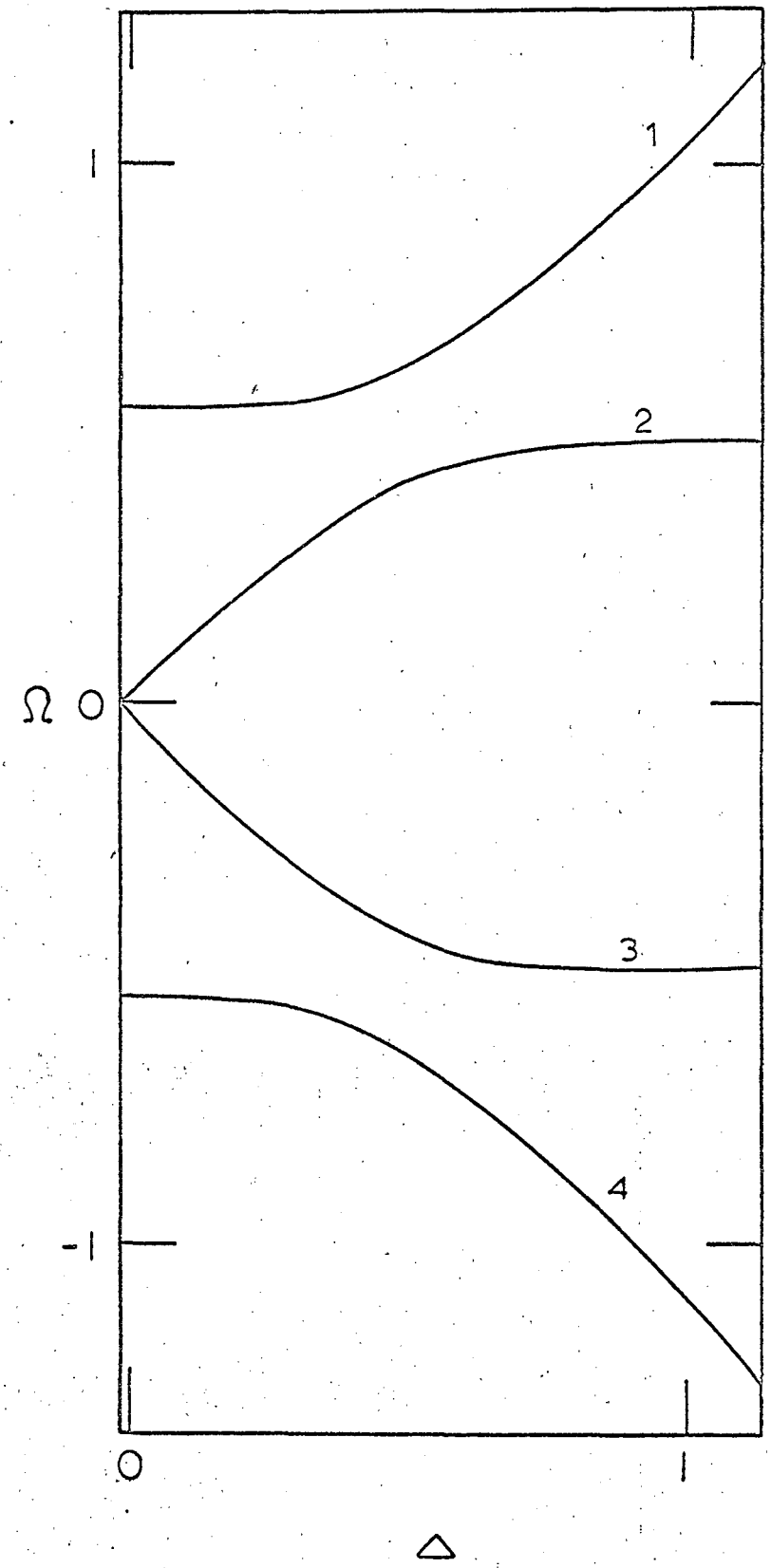

Fig. 5

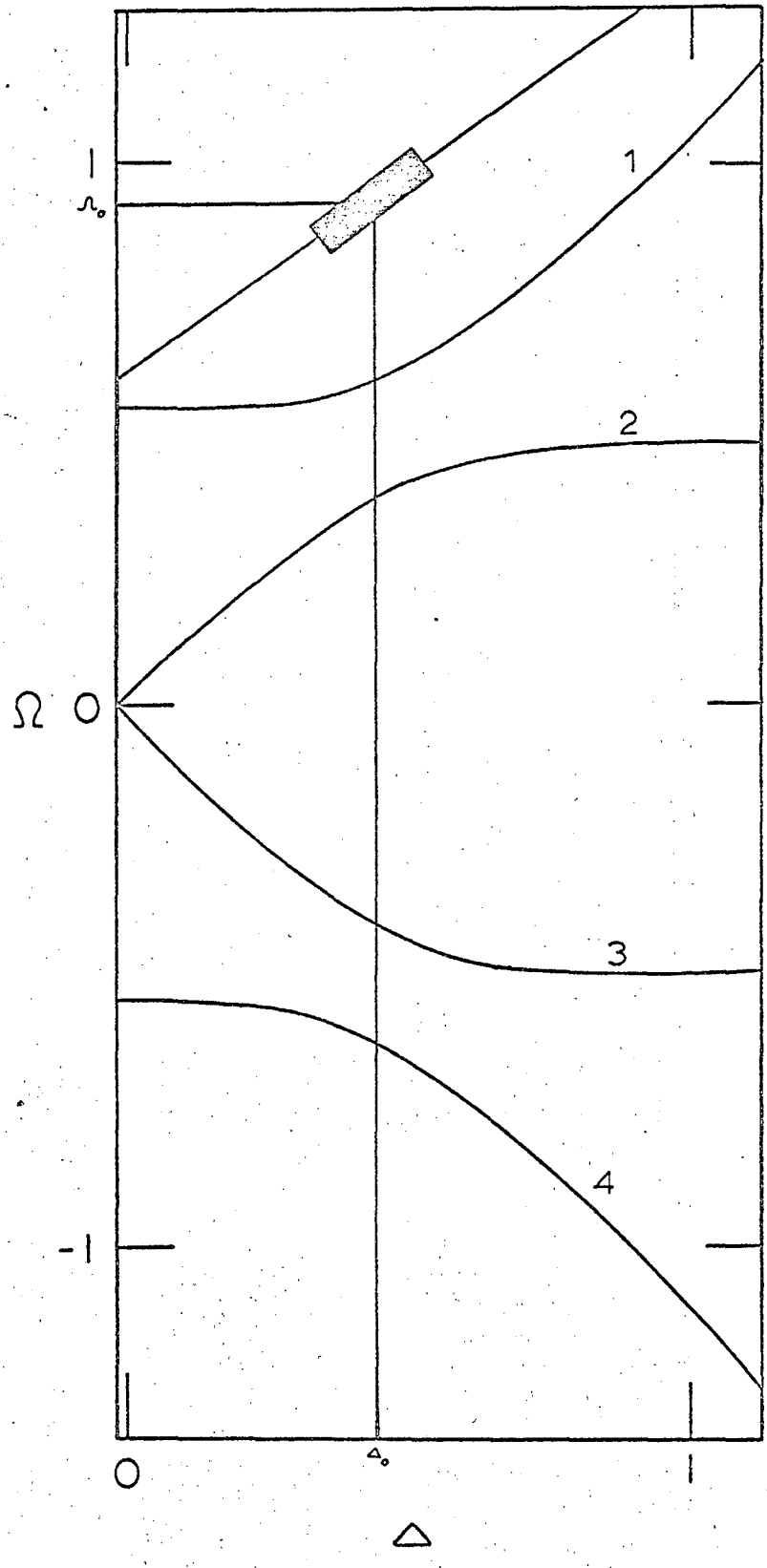

Fig. 6

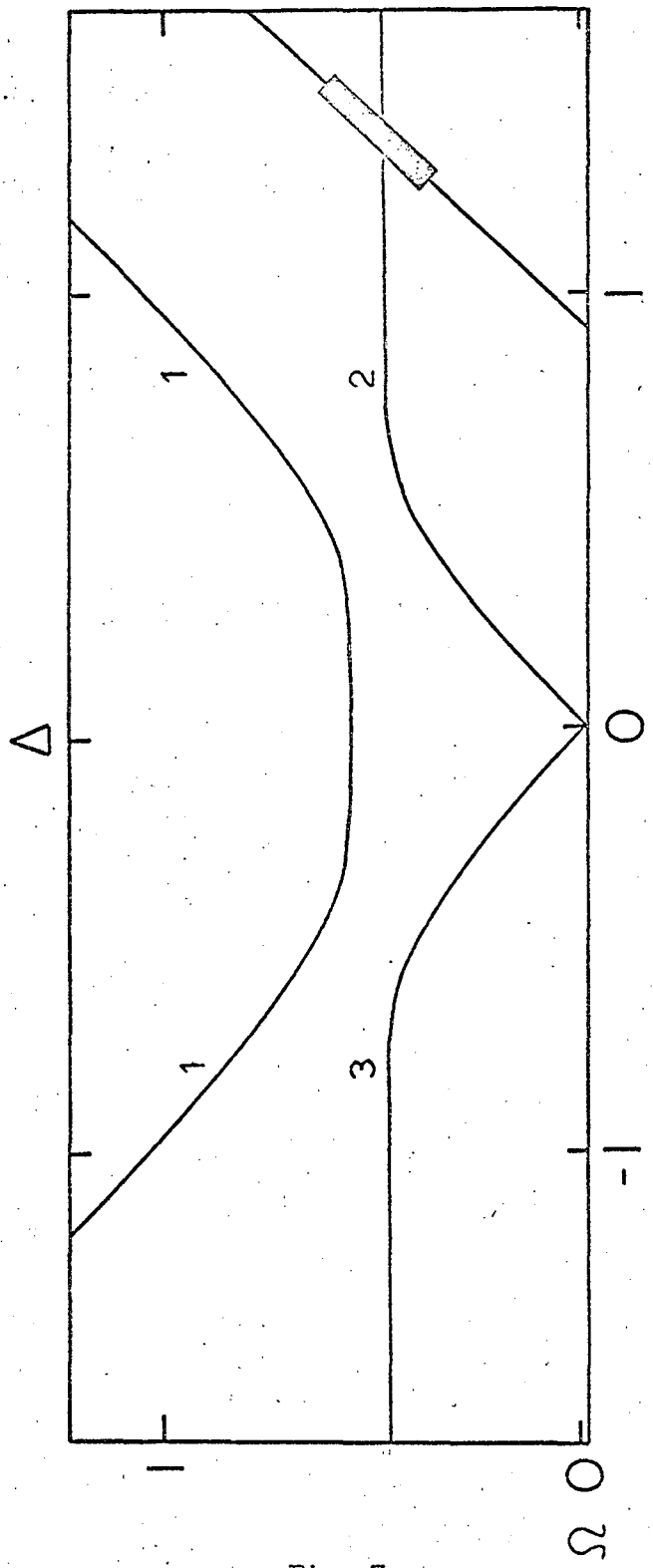

Fig. 7

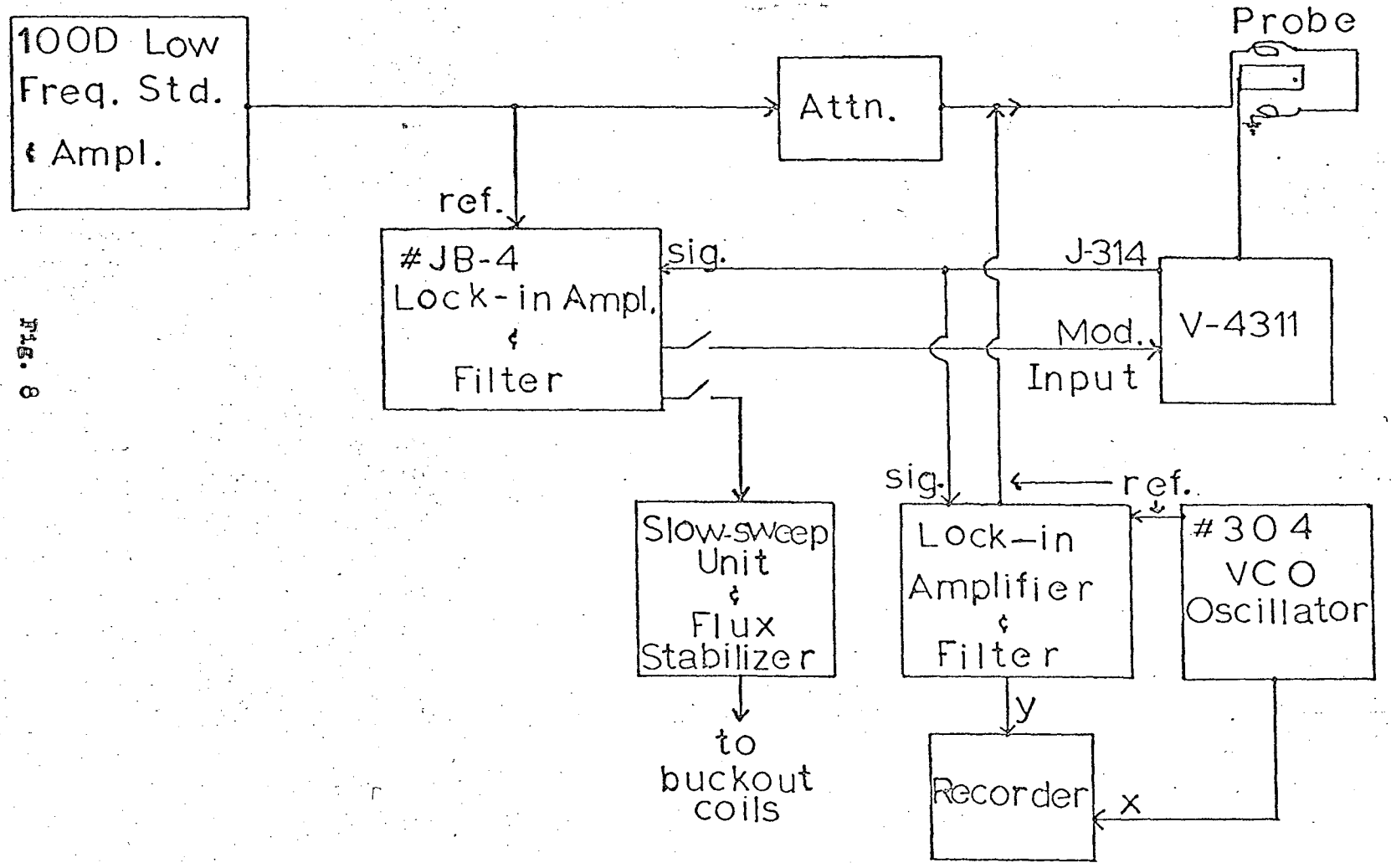
100D Low
Freq. Std.
& Ampl.
Attn.
Probe
ref.
#JB-4
Lock-in Ampl.
&
Filter
sig.
J-314
Mod.
Input
V-4311
Slow-sweep
Unit
&
Flux
Stabilizer
to
buckout
coils
sig.
ref.
Lock-in
Amplifier
&
Filter
#304
VCO
Oscillator
y
Recorder
x

Fig. 8

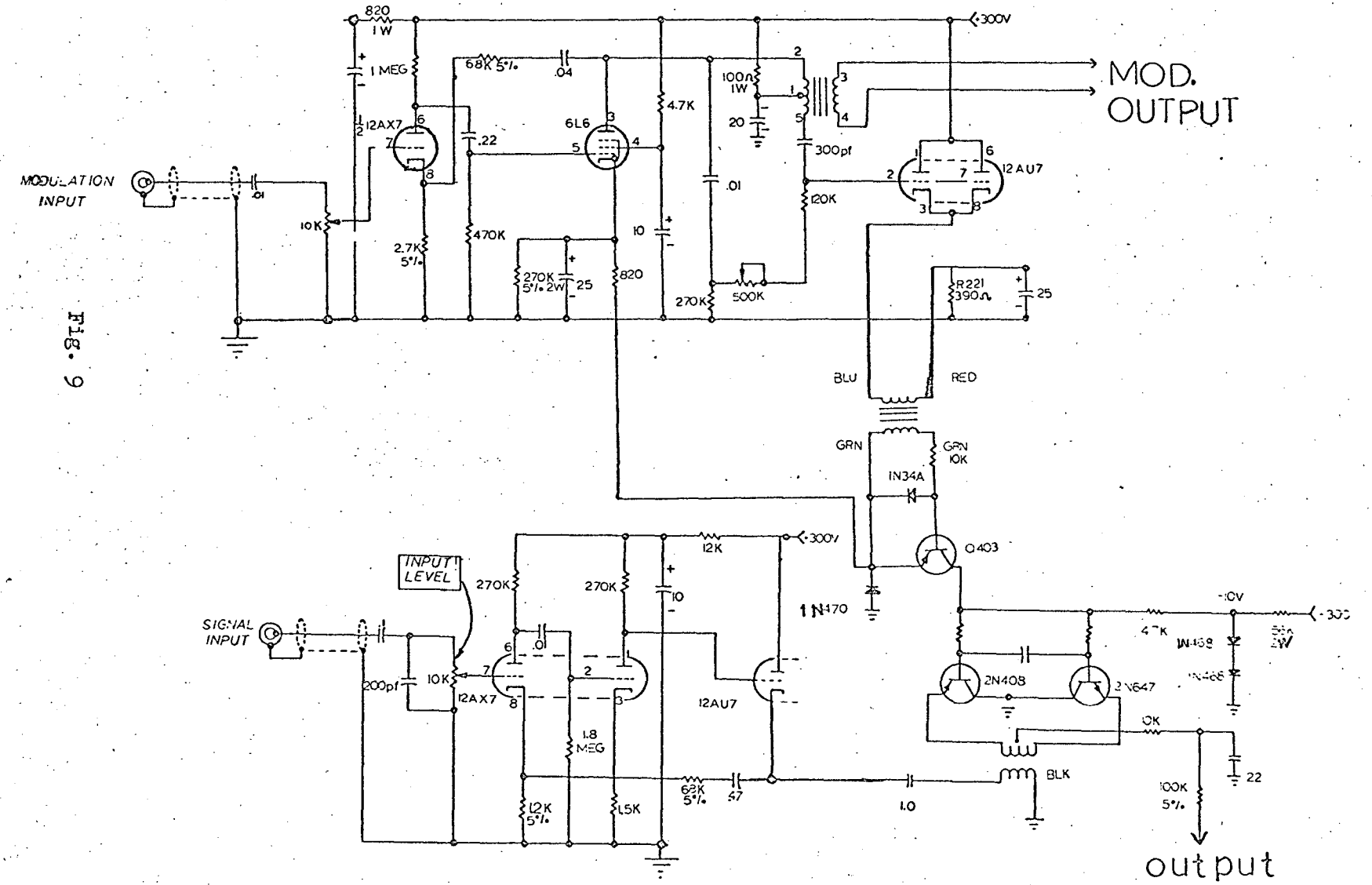
820 1W
1 MEG
68K 5%
.04
12AX7
.22
6L6
4.7K
100Ω 1W
20
300pf
MOD. OUTPUT
+300V
MODULATION INPUT
.01
10K
2.7K 5%
470K
270K 5% 2W
25
820
10
.01
270K
500K
120K
12AU7
R221 390Ω
25
BLU
RED
GRN
GRN 10K
IN34A
Q403
INPUT LEVEL
270K
270K
12K
+300V
10
1N470
SIGNAL INPUT
200pf
10K
12AX7
.01
1.8 MEG
12AU7
-10V
4.7K
IN468
IN468
2N408
2N647
10K
22
BLK
62K 5%
.47
1.0
12K 5%
15K
100K 5%
output

Fig. 9

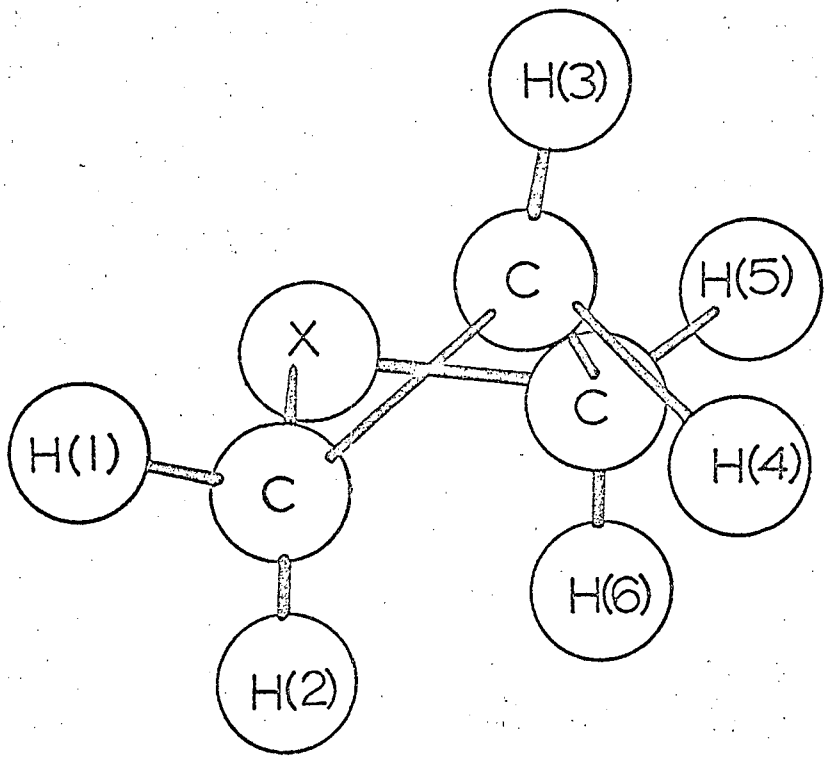

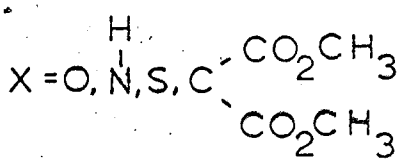

Fig. 10

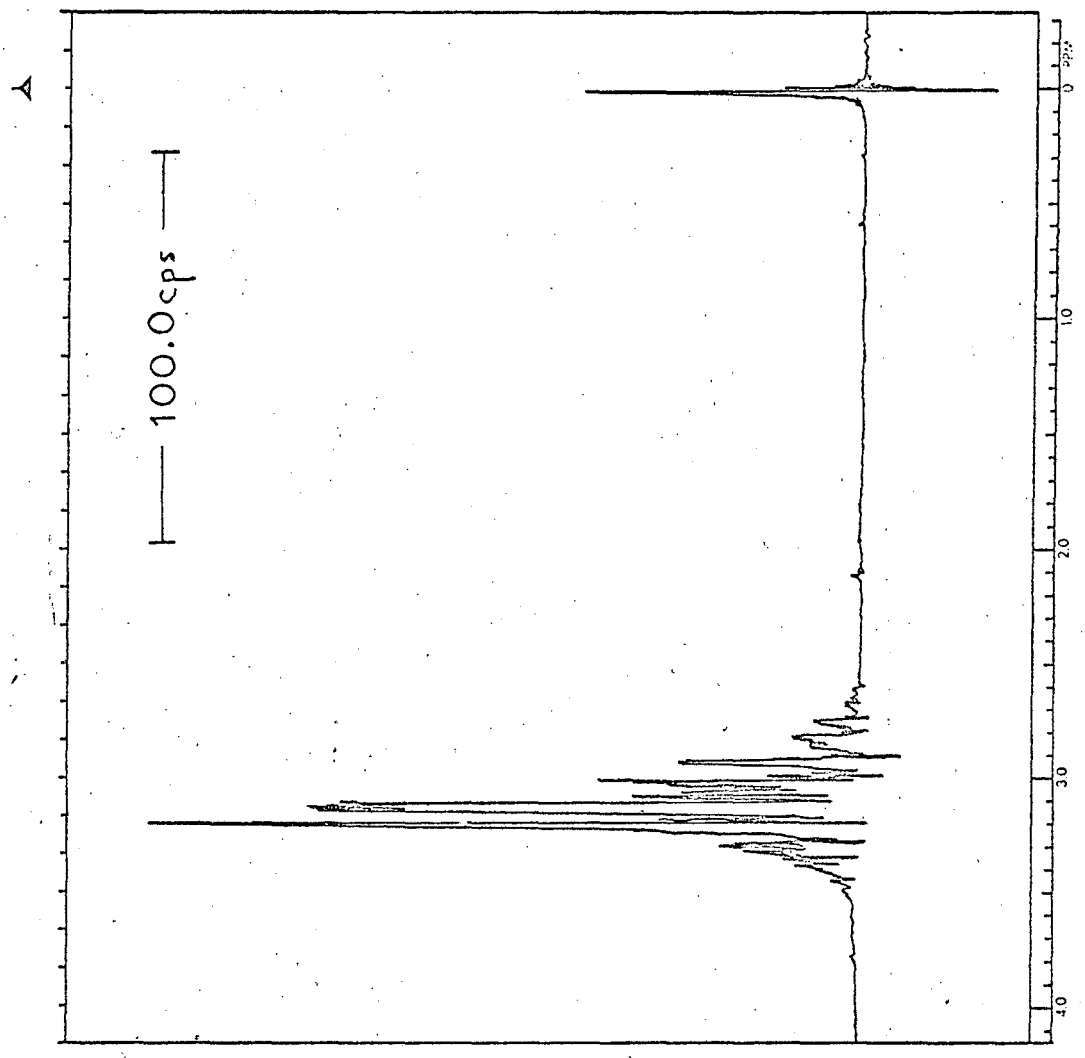

Fig. 11

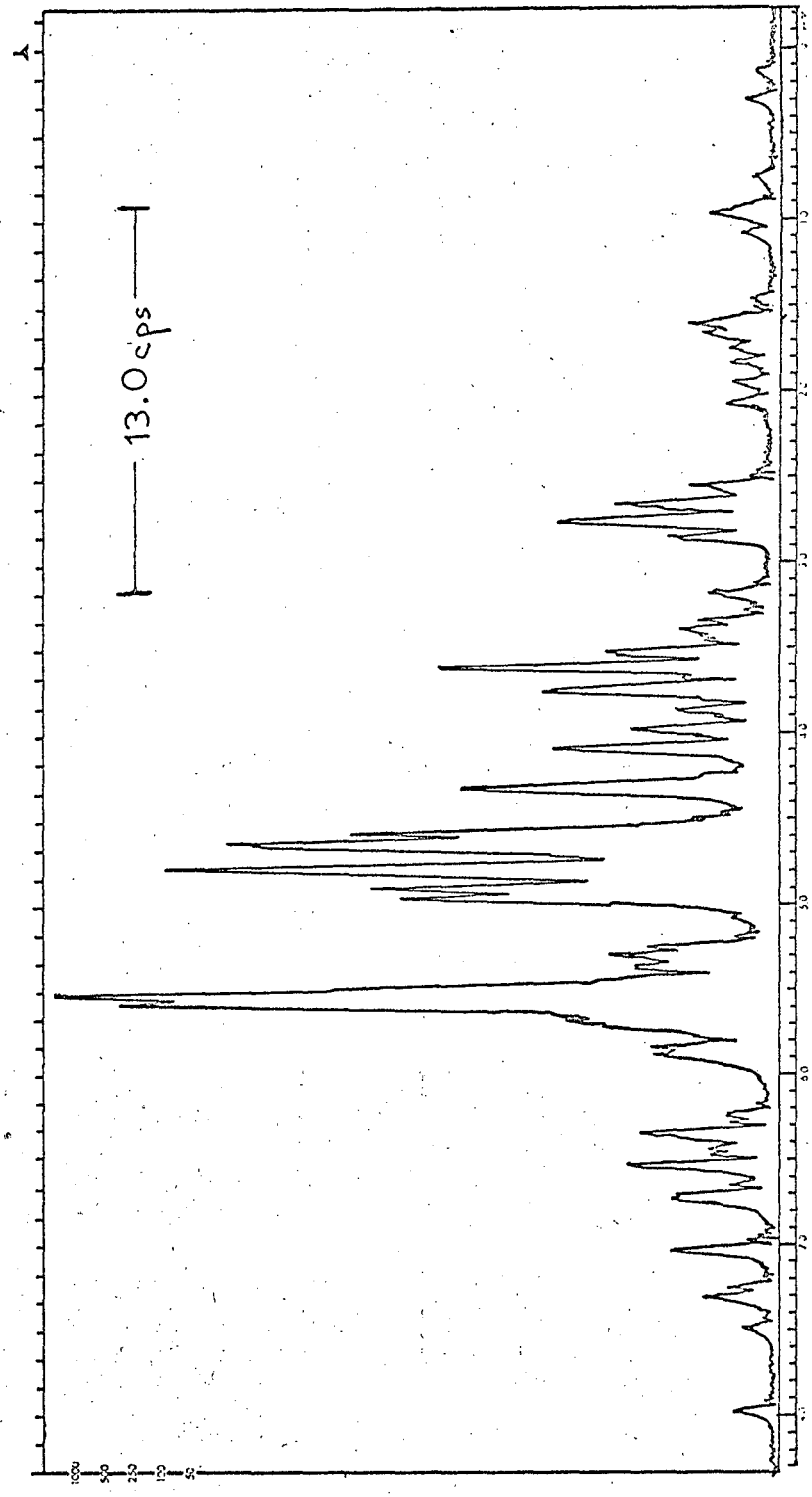

Fig. 12

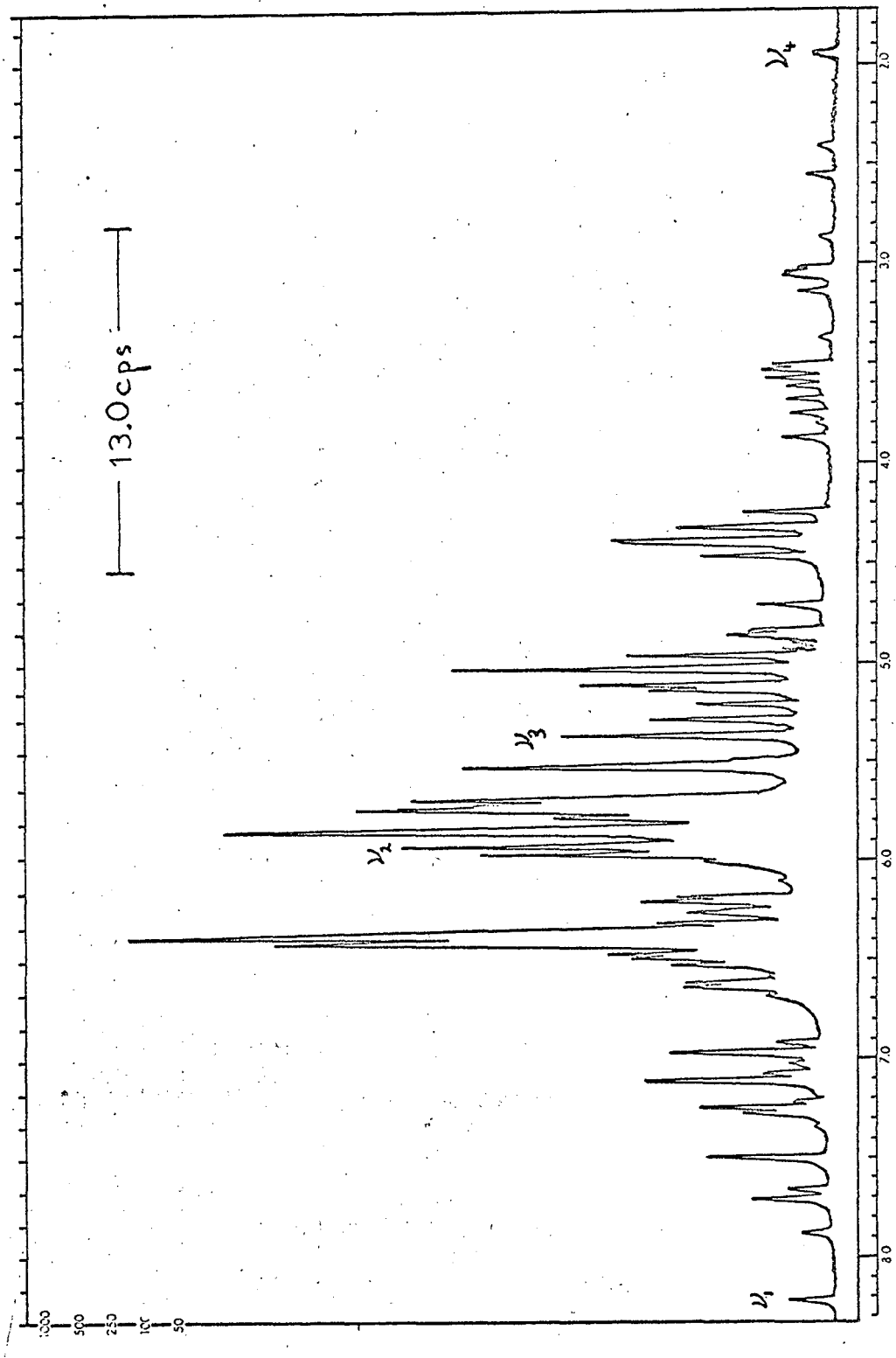

Fig. 13

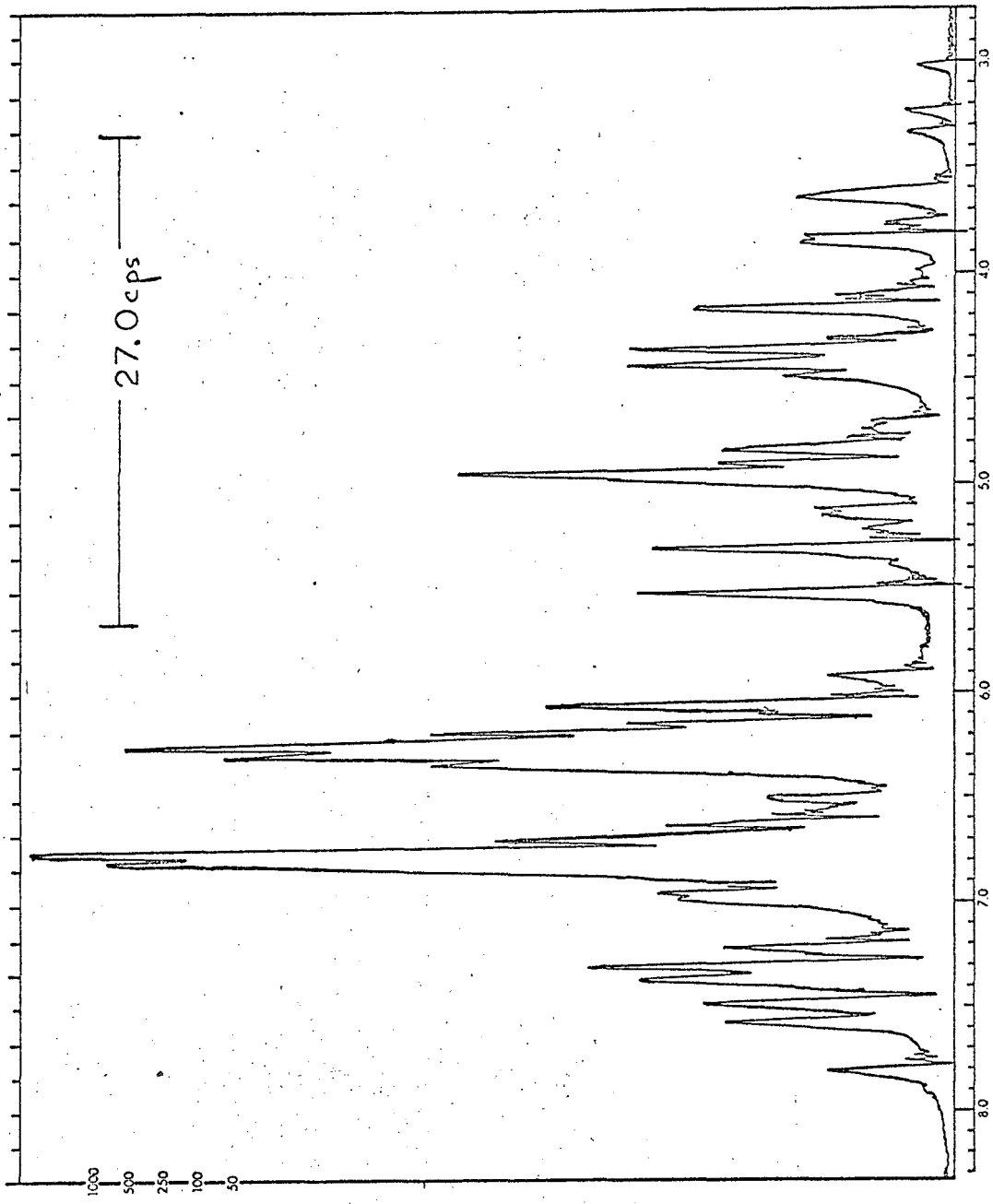

Fig. 14

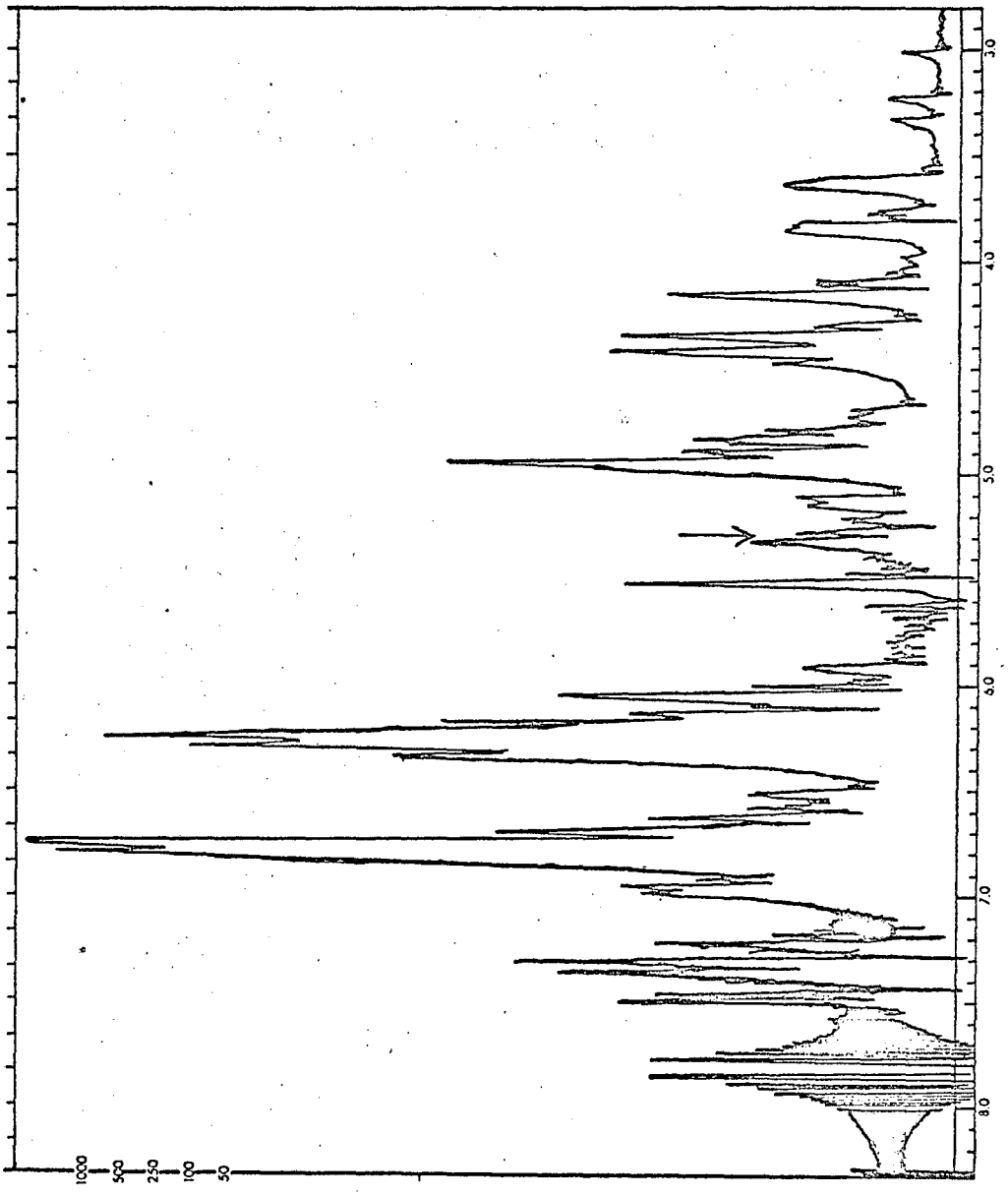

Fig. 15

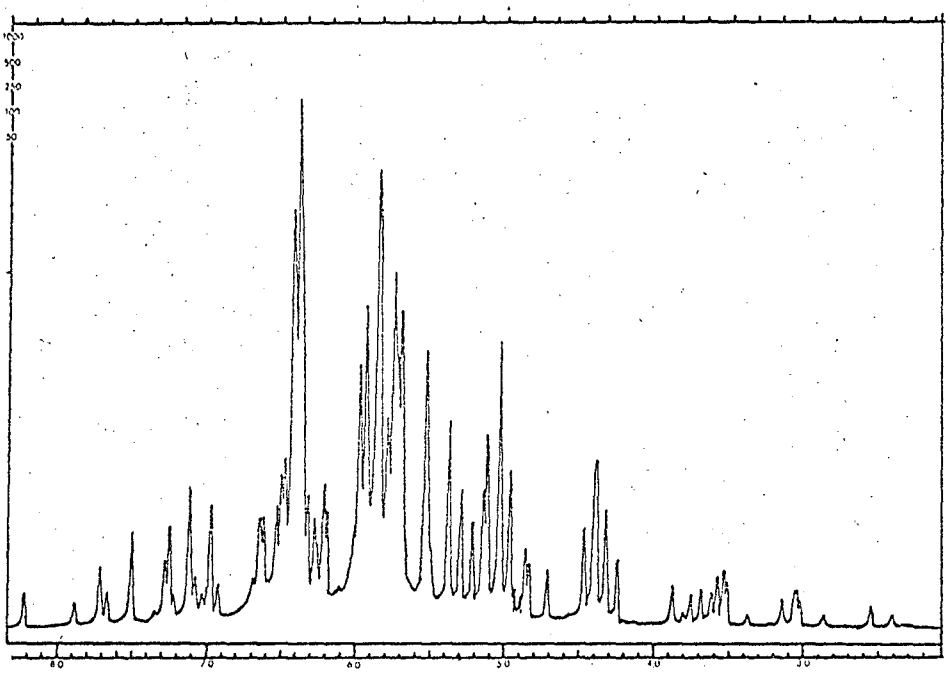

(a)

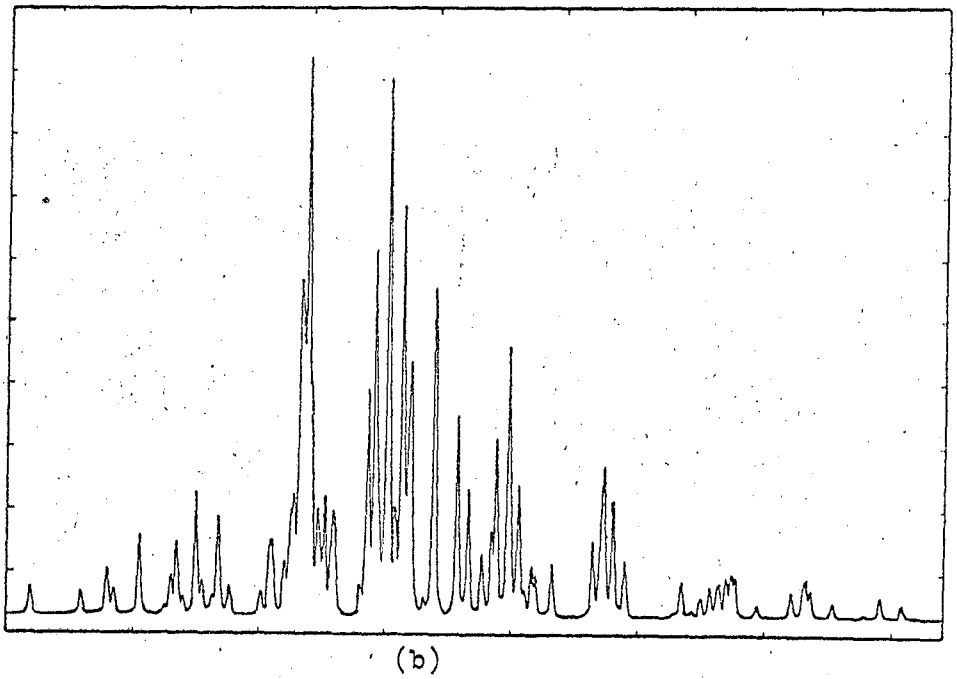

(b)

Fig. 16

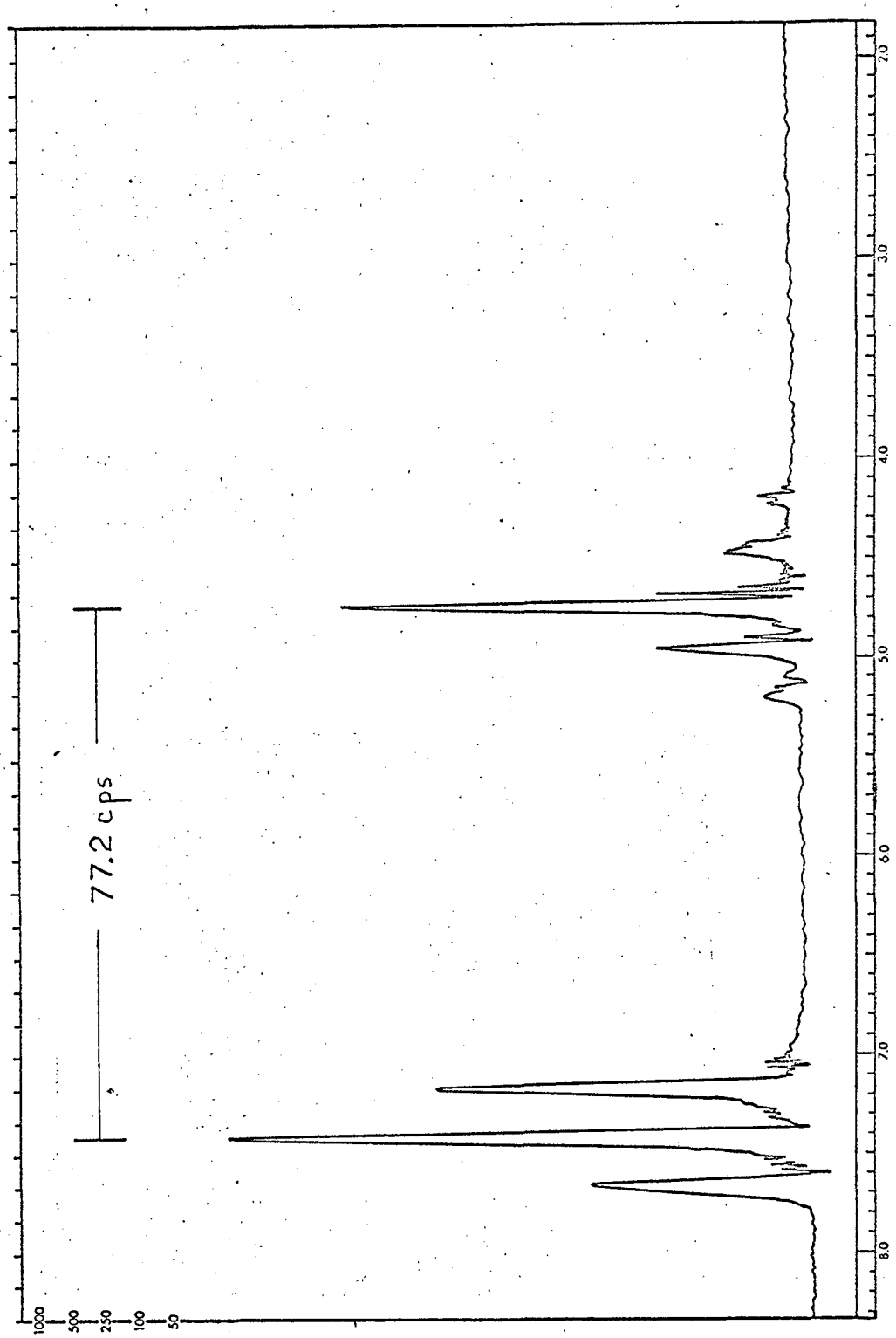

Fig. 17

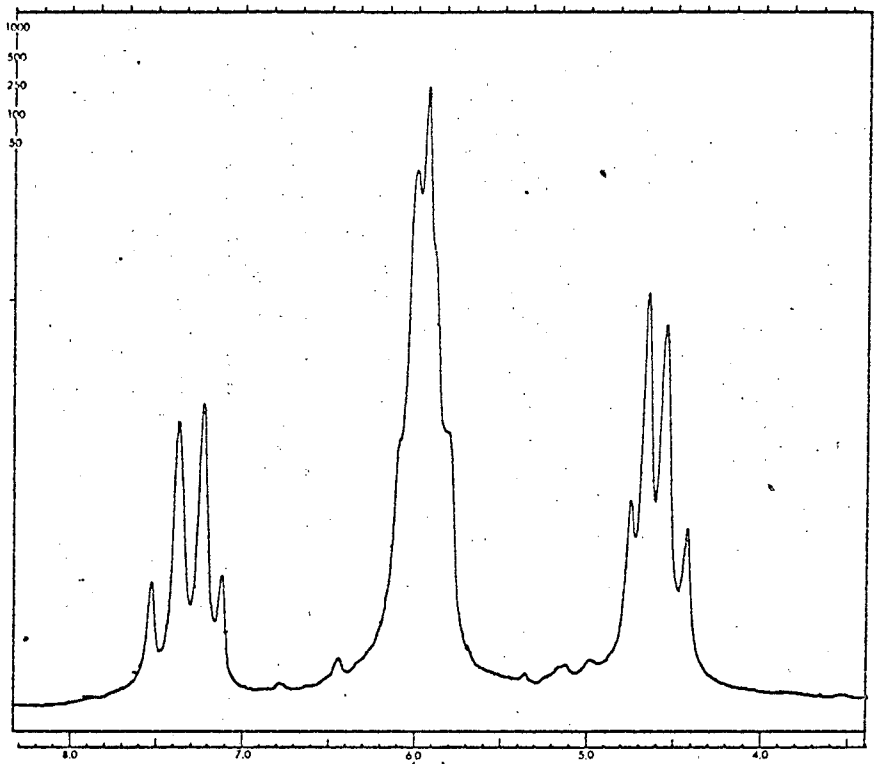

(a)

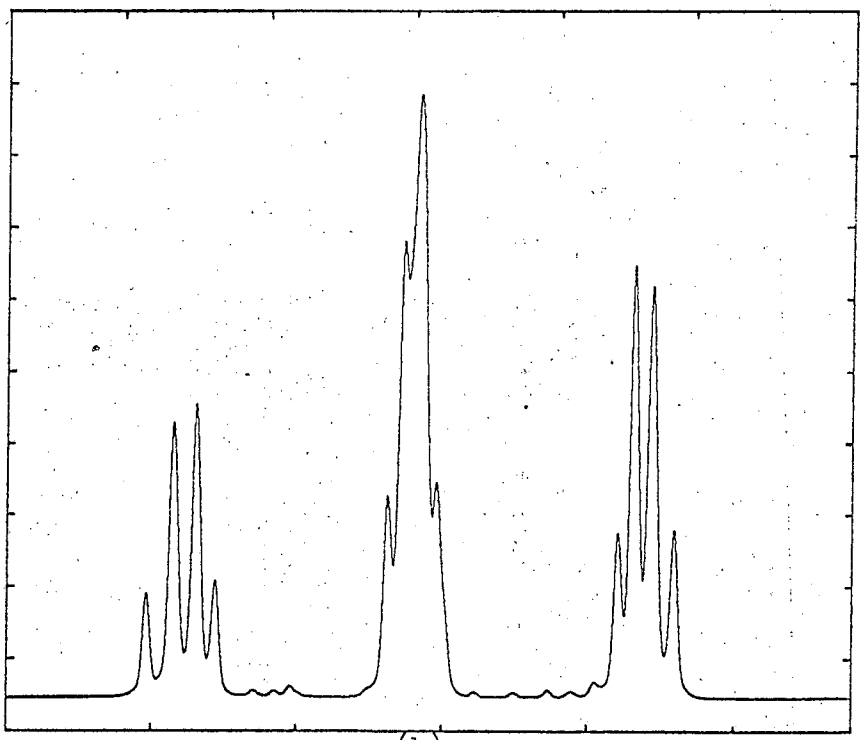

(b)

Fig. 18

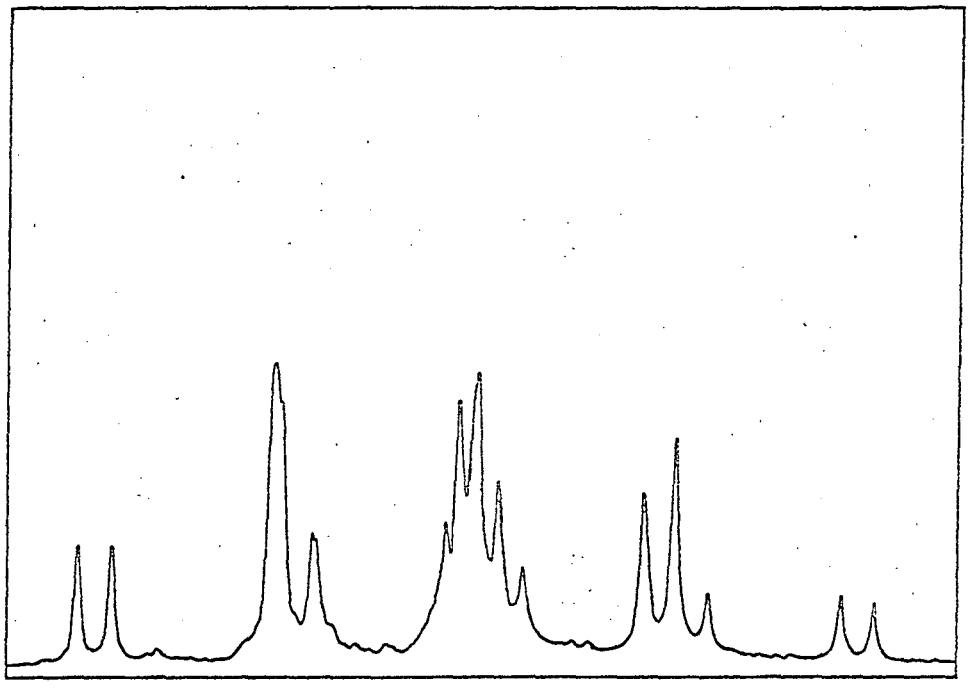

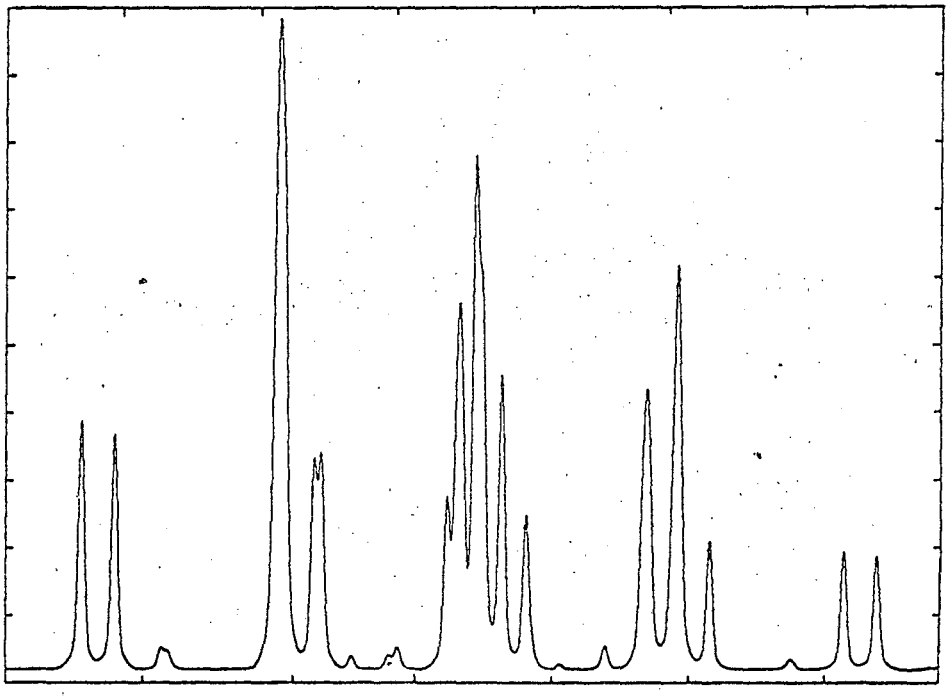

Fig. 19

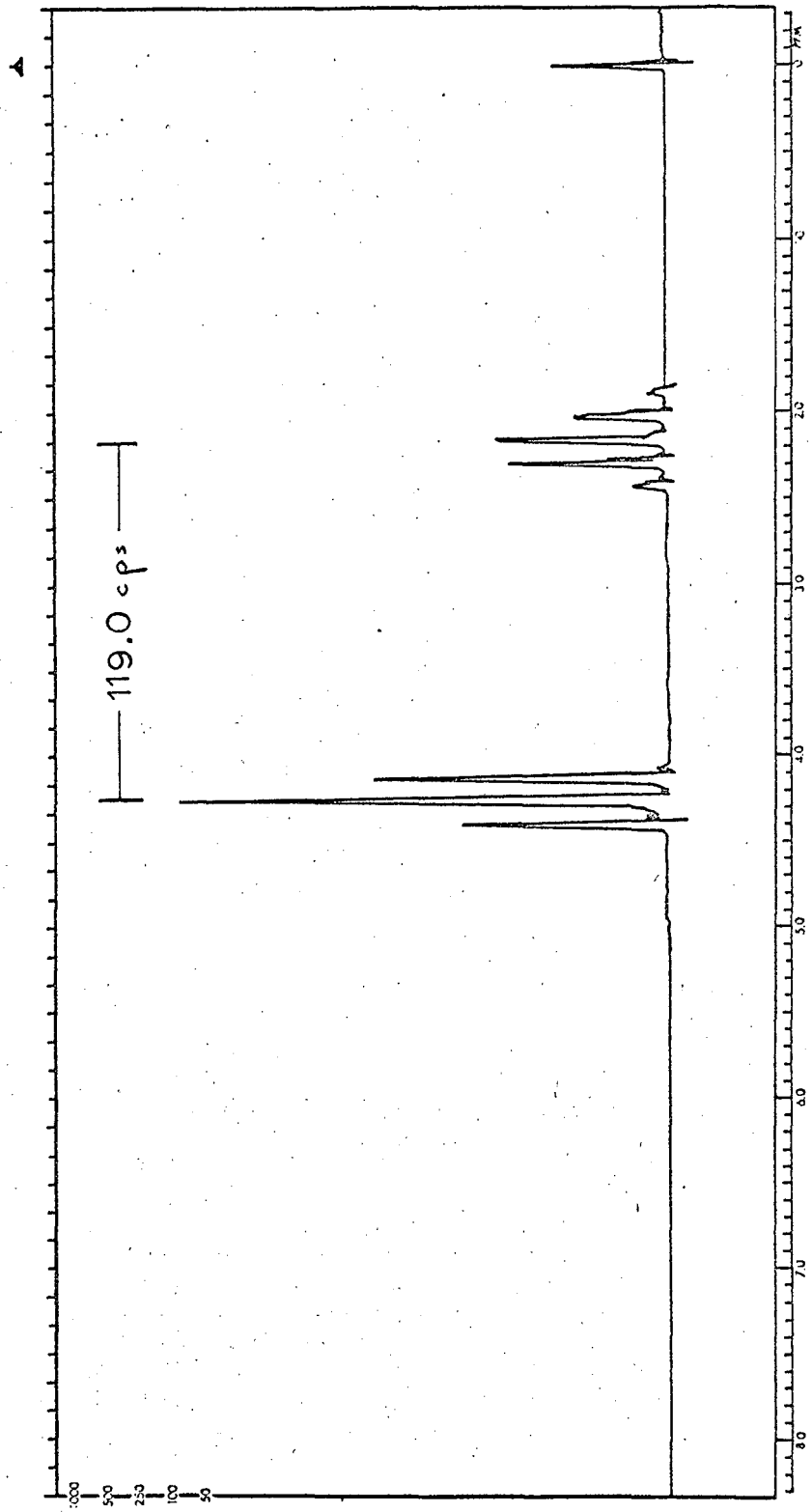

Fig. 20

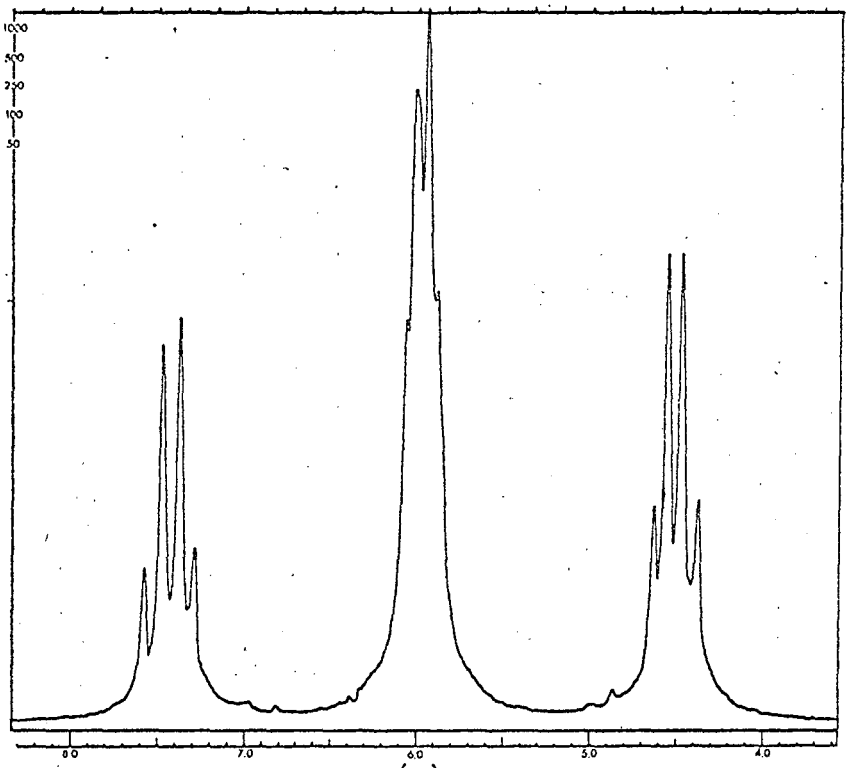

(a)

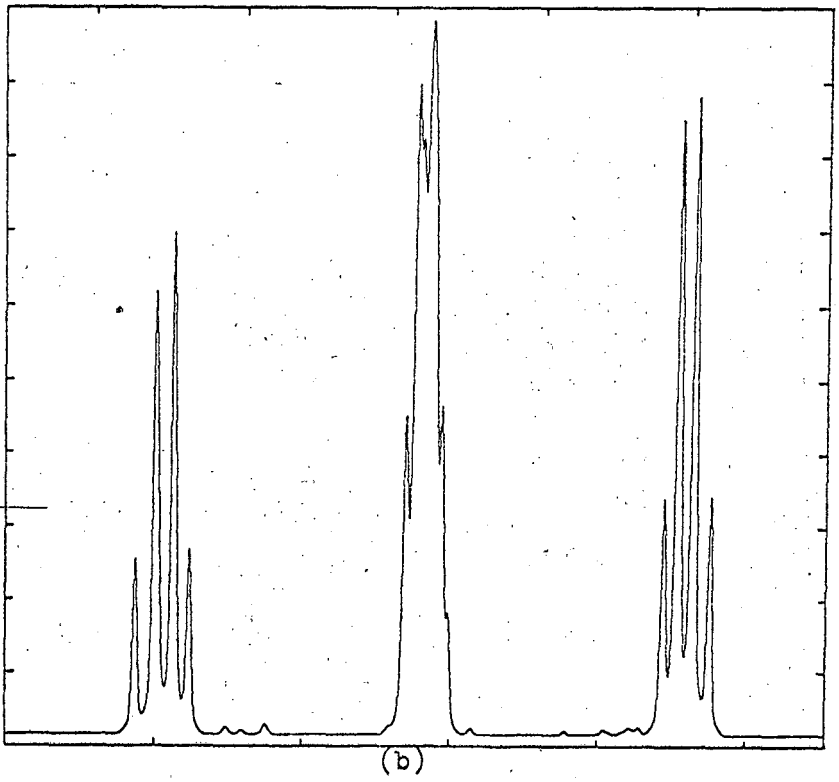

(b)

Fig. 21

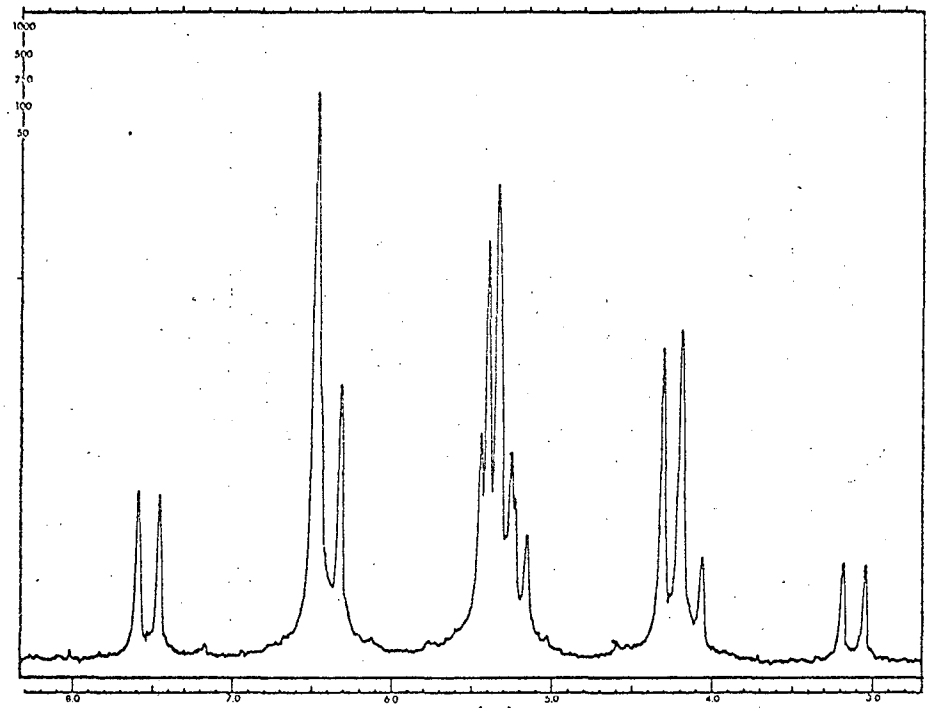

(a)

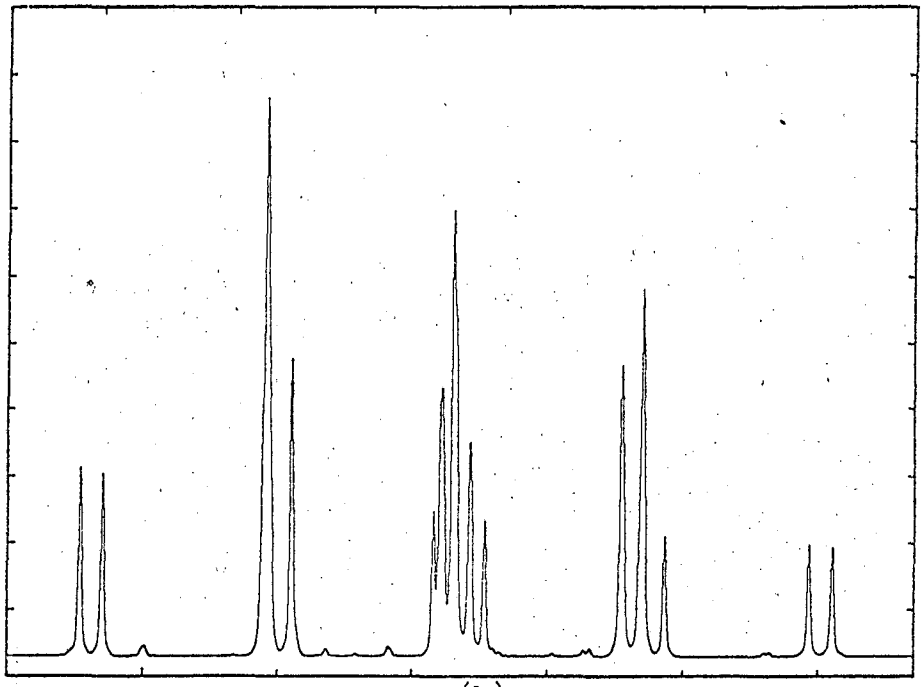

(b)

Fig. 22

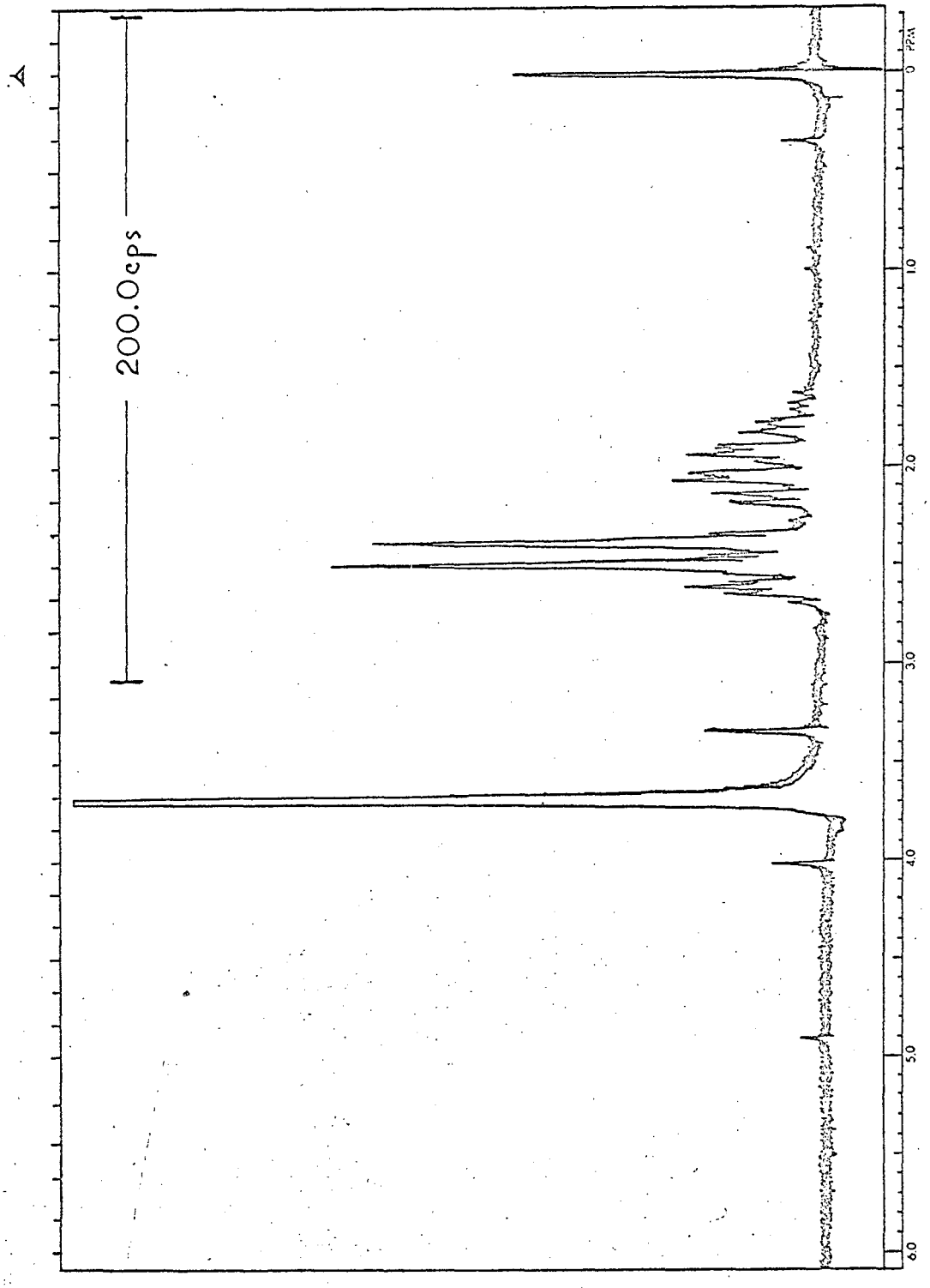

Fig. 23

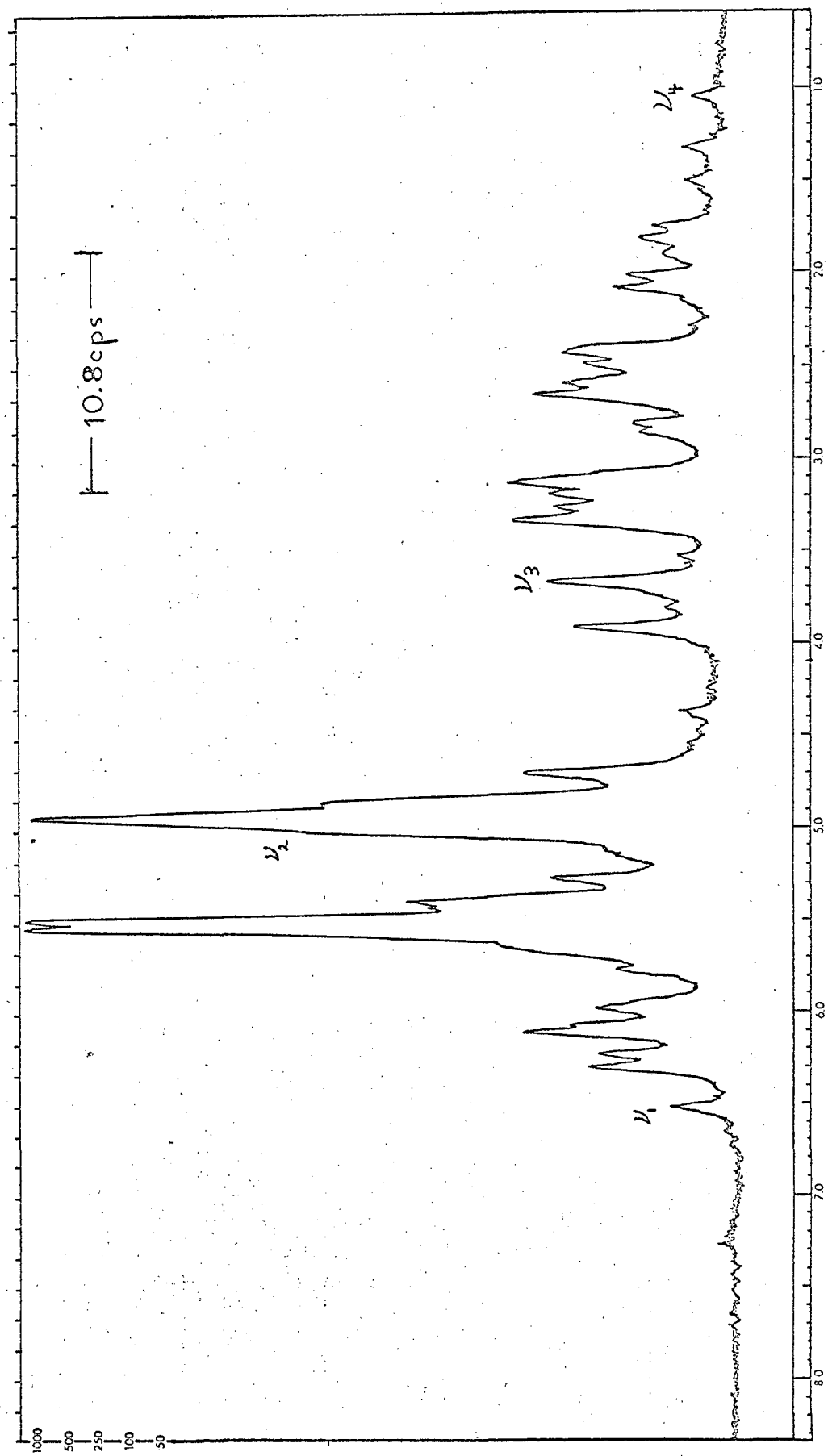

Fig. 24

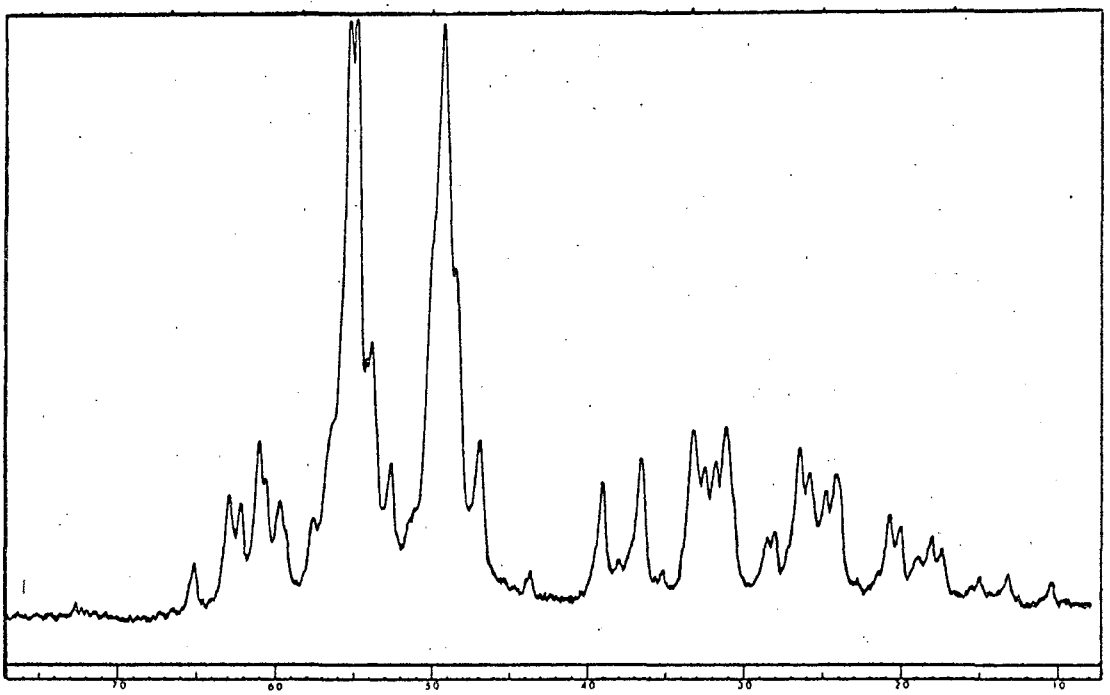

(a)

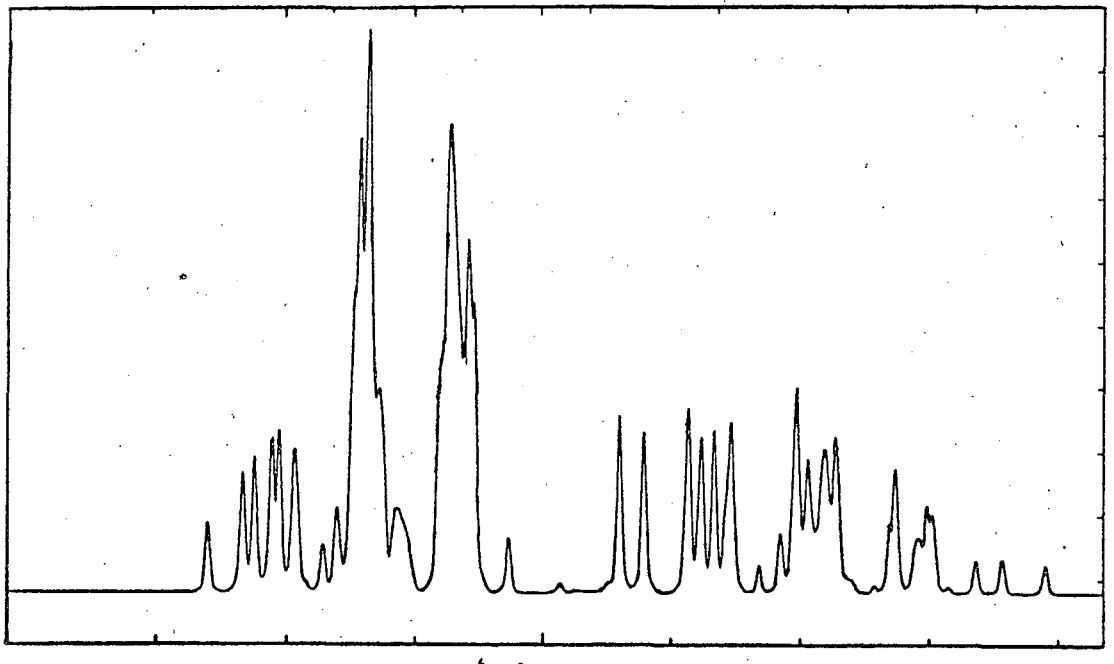

(b)

Fig. 25

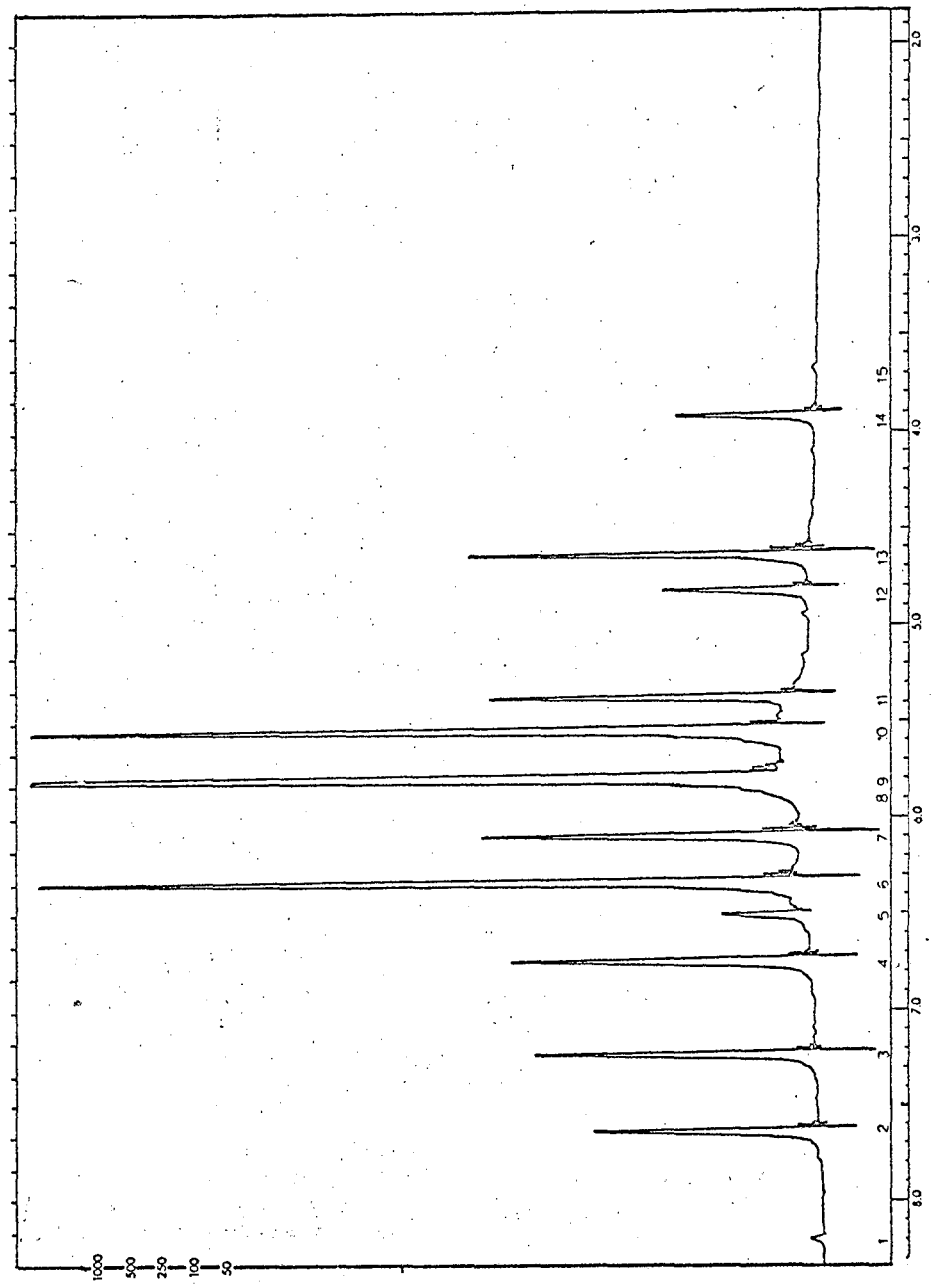

Fig. 26

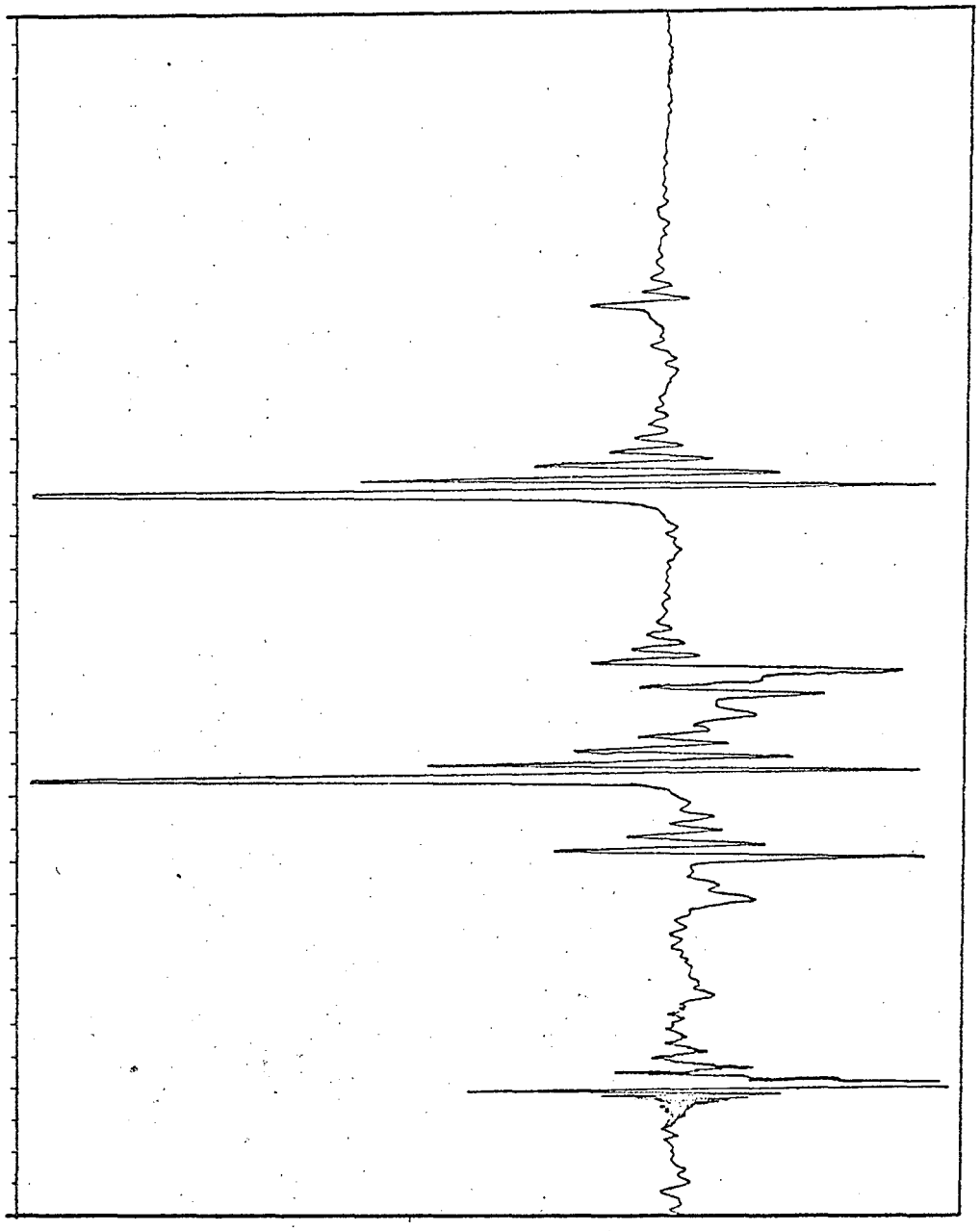

Fig. 27

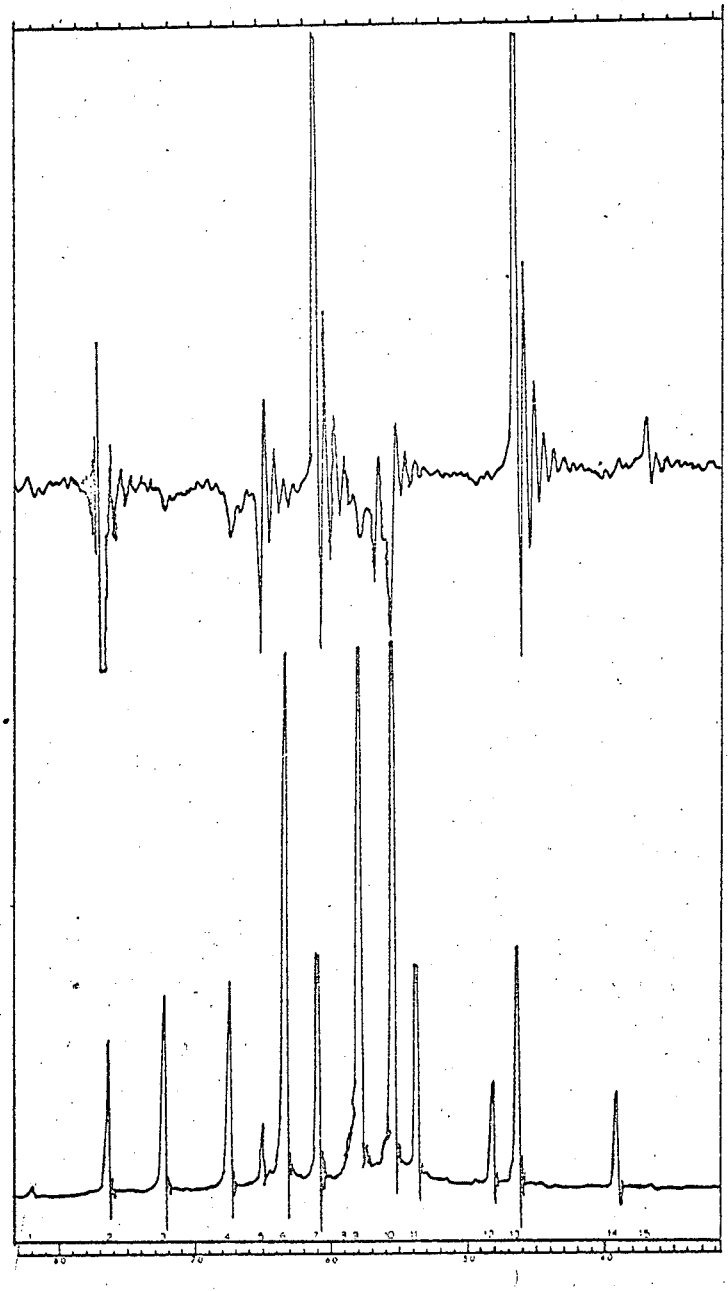

Fig. 28

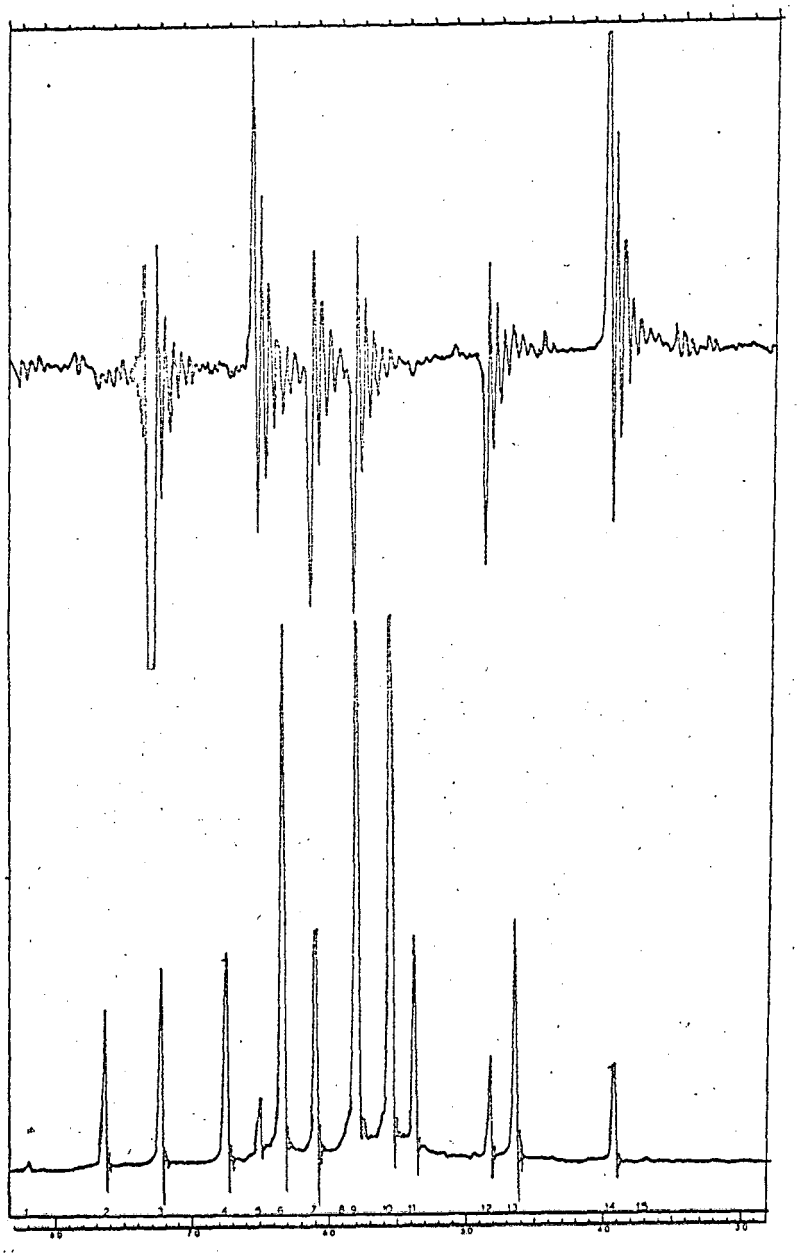

Fig. 29

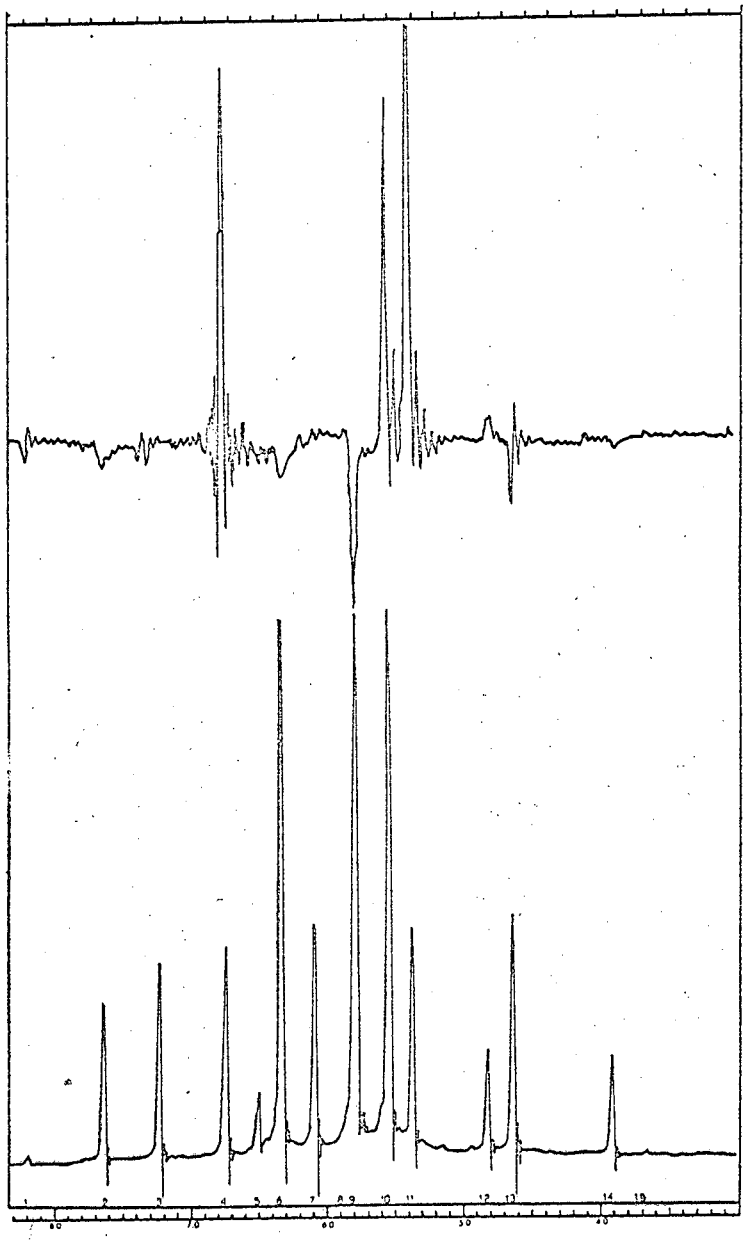

Fig. 30

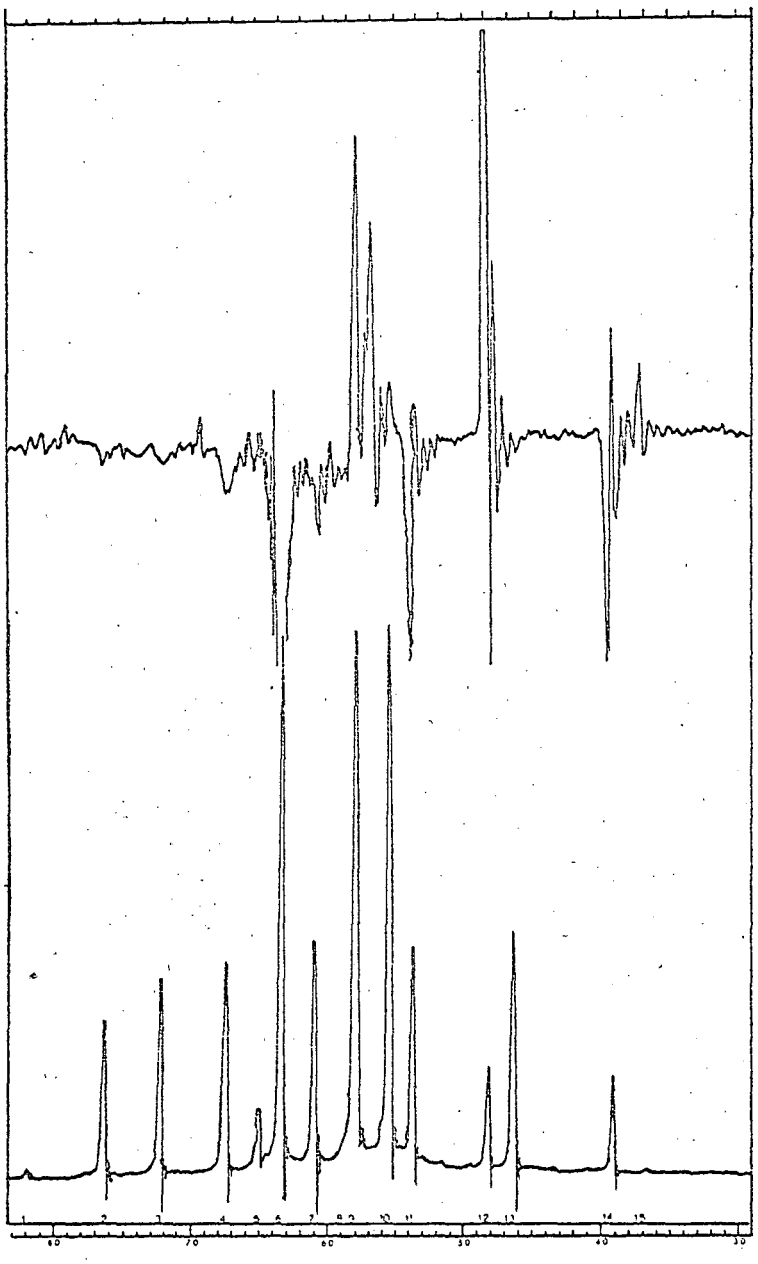

Fig. 31

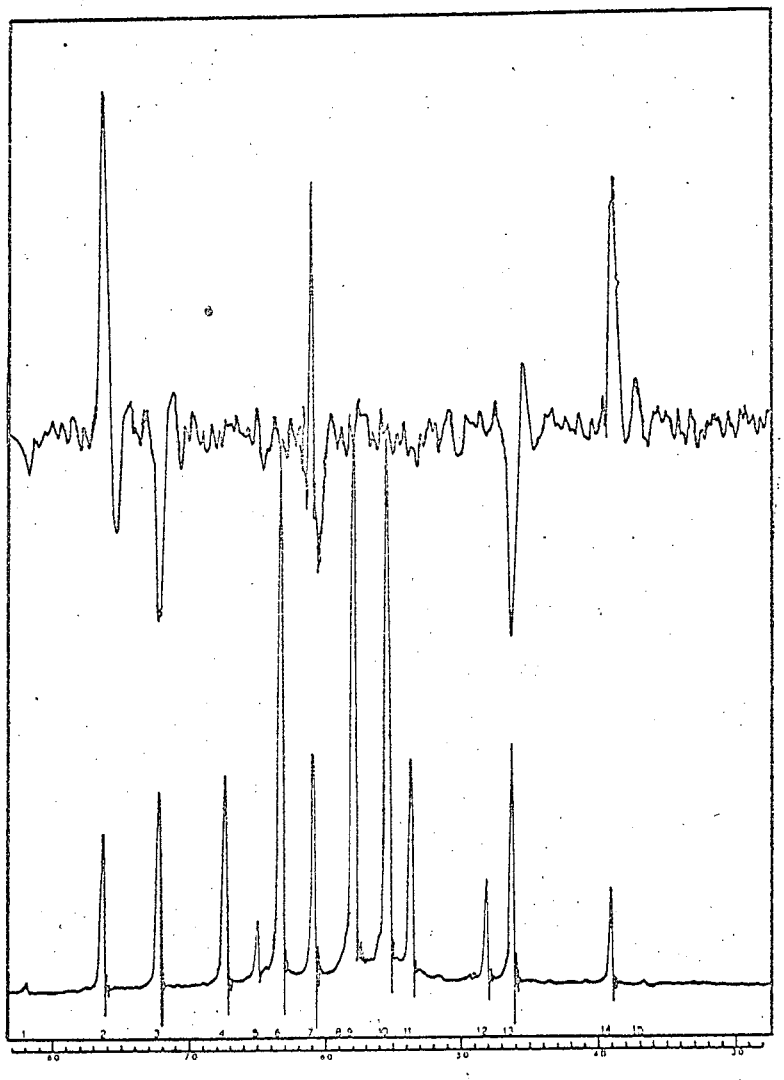

Fig. 32

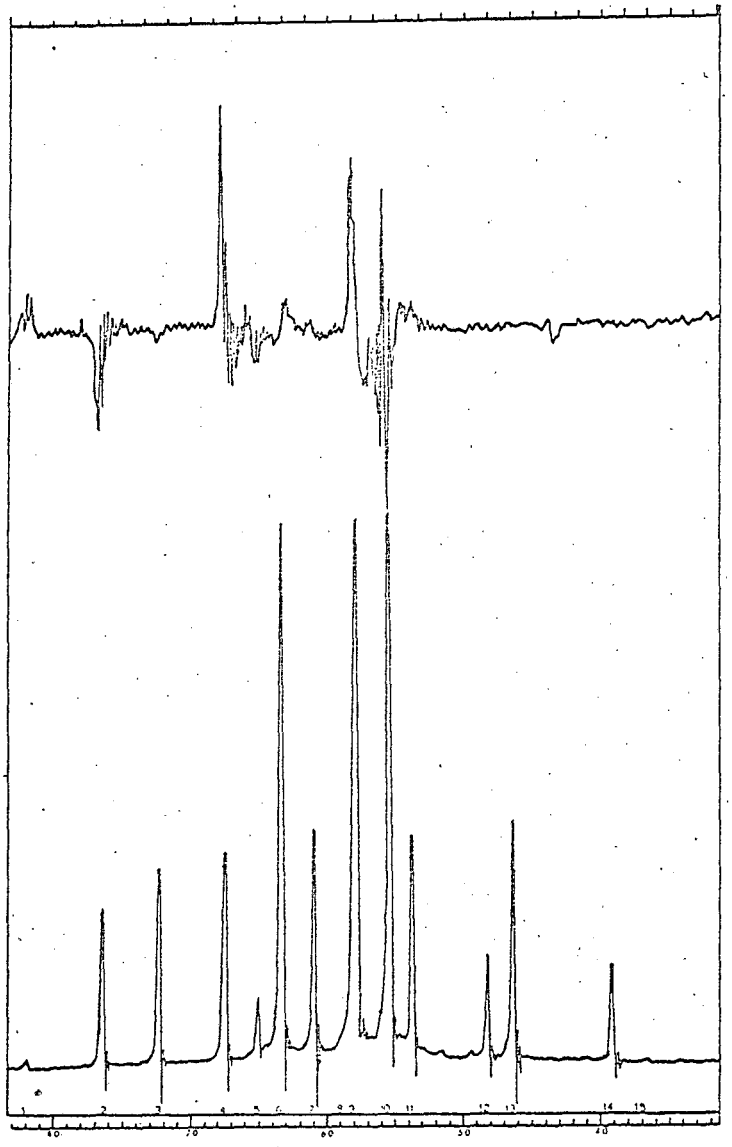

Fig. 33

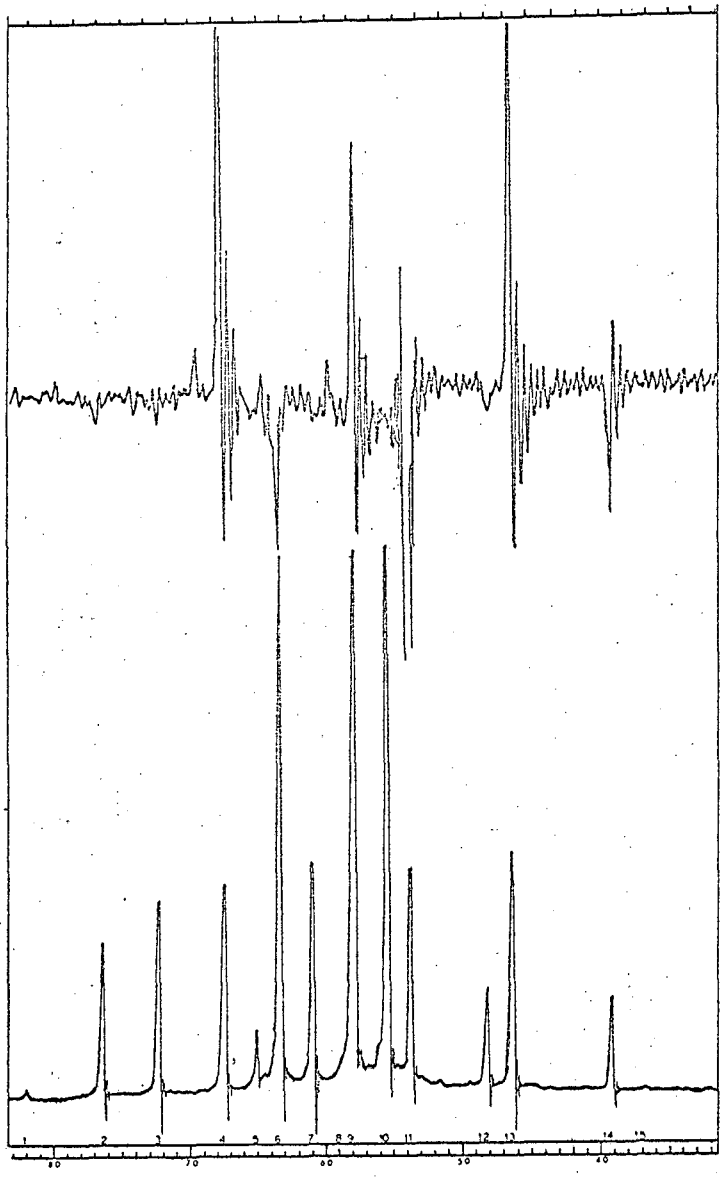

Fig. 34

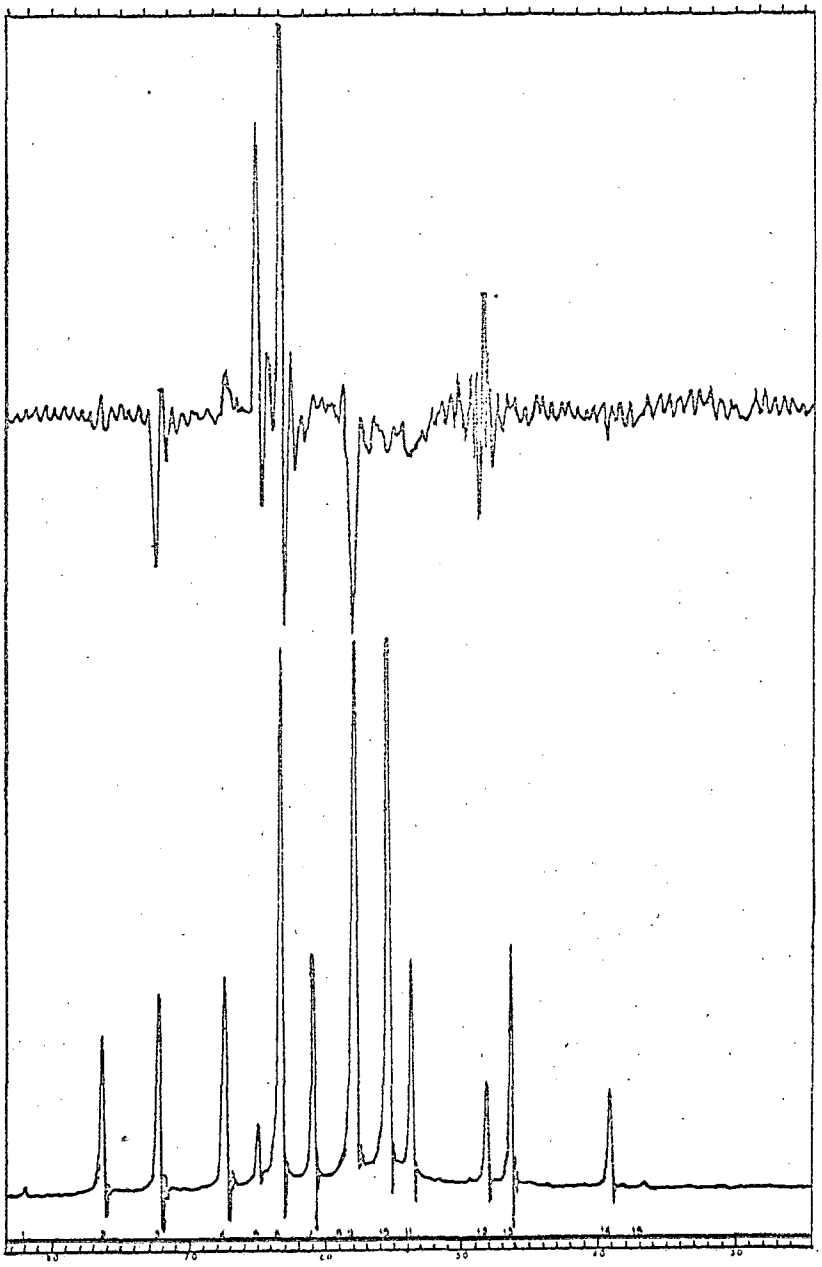

Fig. 35

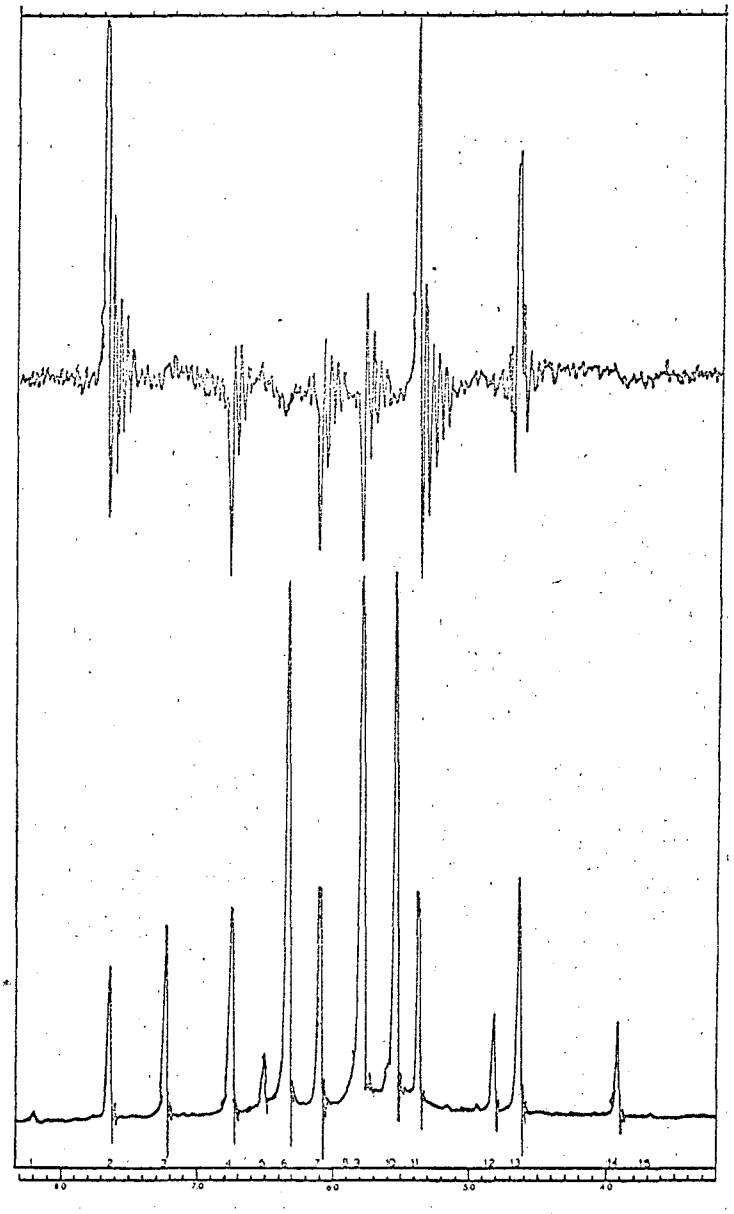

Fig. 36

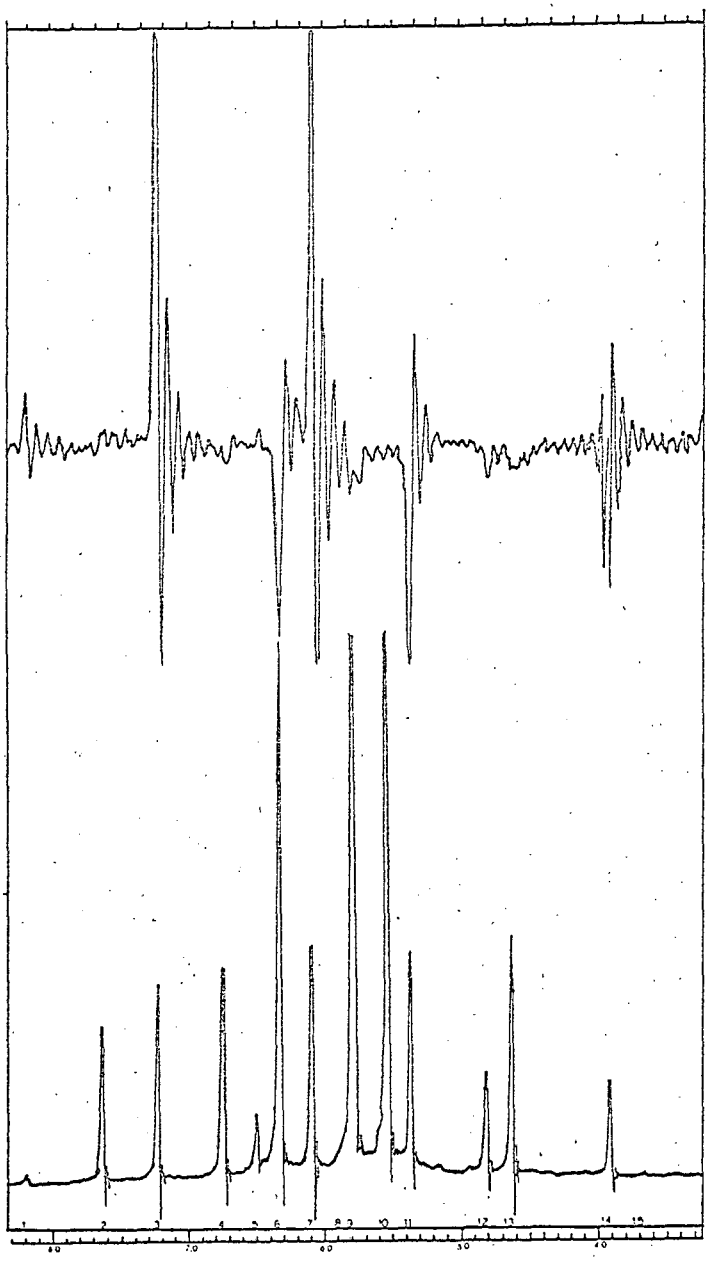

Fig. 37

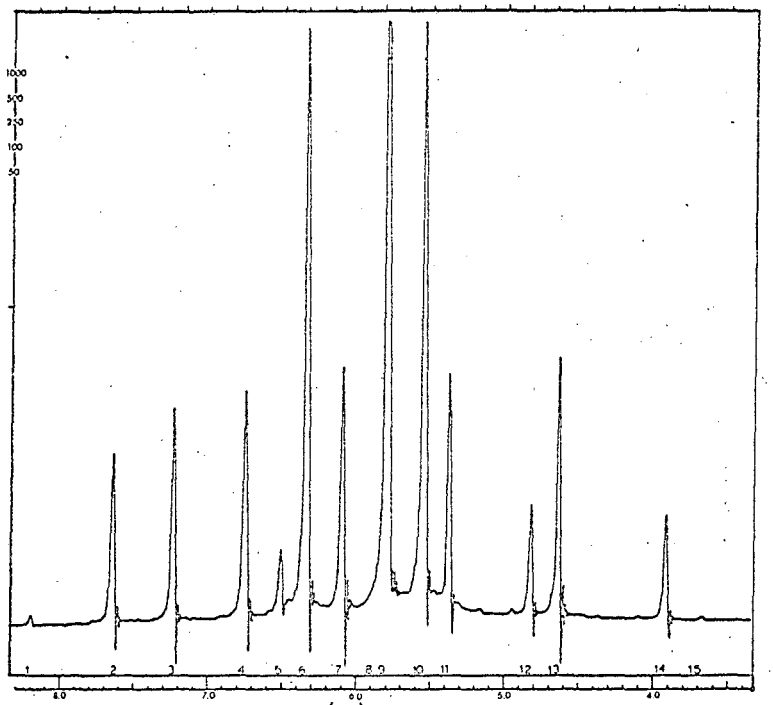

(a)

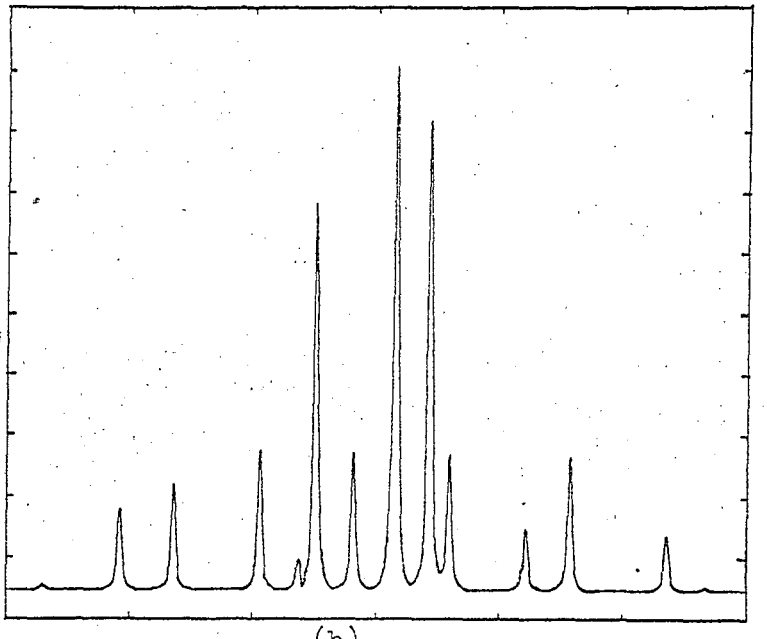

(b)

Fig. 38

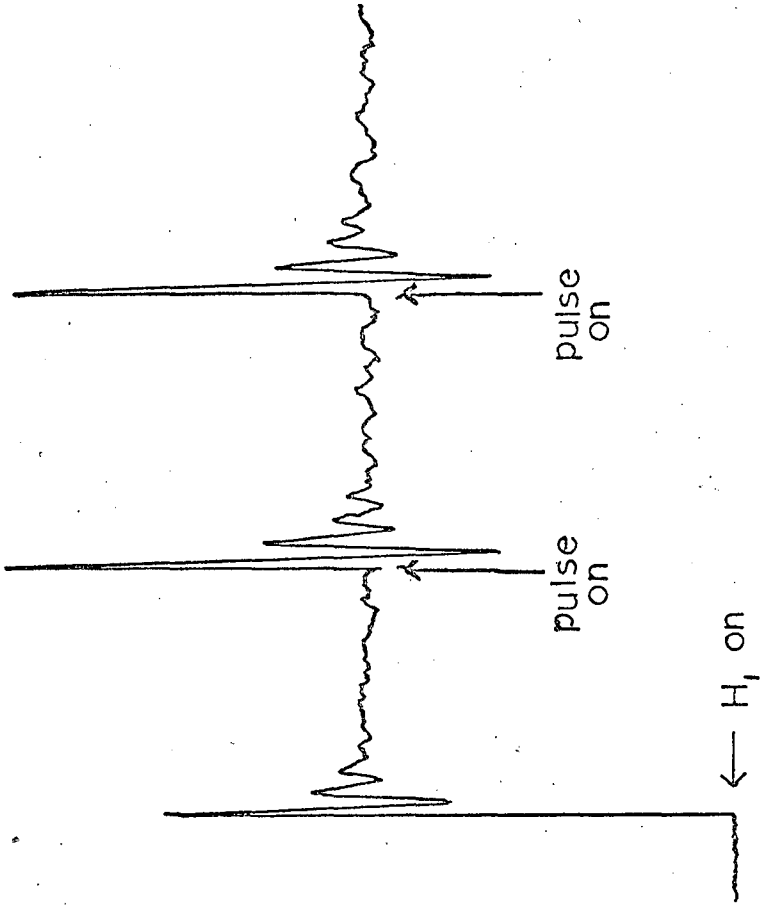

Fig. 39

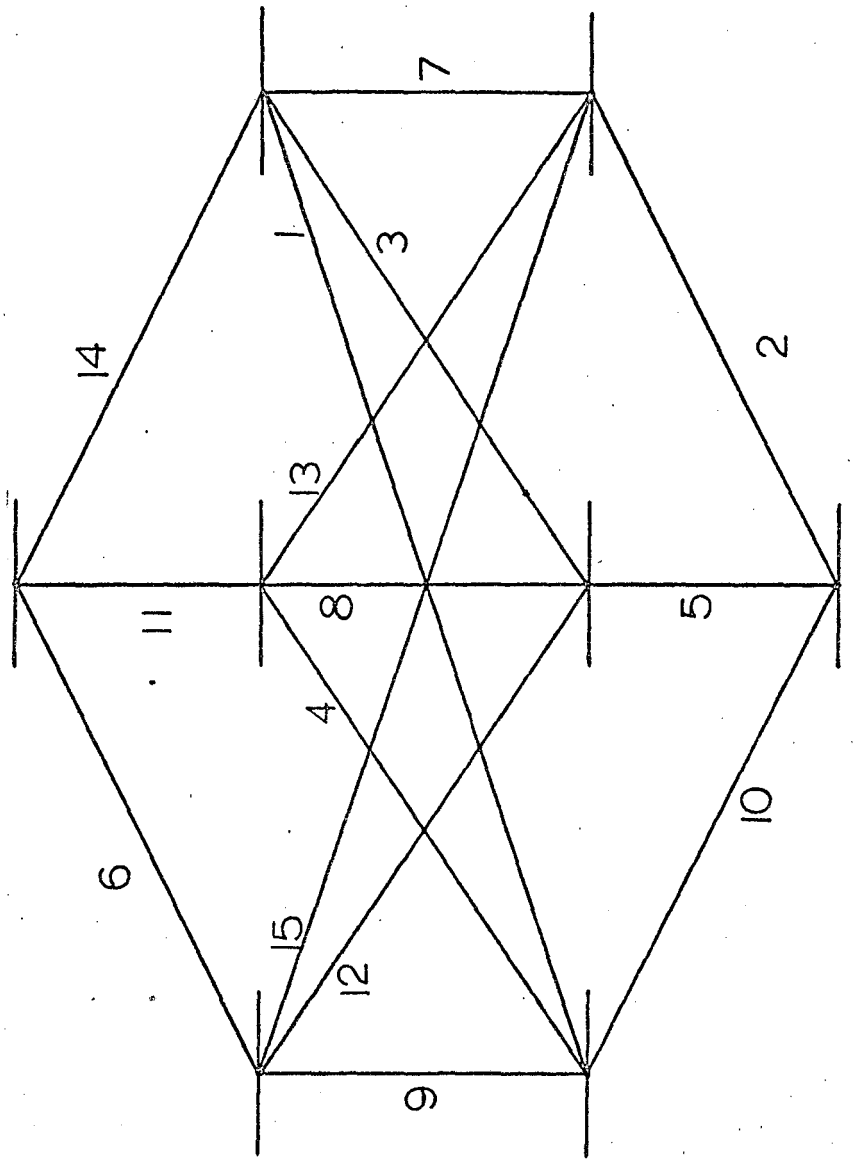

Fig. 40